

CRYSTALLIZATION OF PROTEINS
BY DYNAMIC CONTROL OF
SUPERSATURATION

A THESIS
Presented to
The Academic Faculty

by

Lori June Wilson

In Partial Fulfillment
of the Requirements for the Degree
Doctor of Philosophy
in
Chemistry

Georgia Institute of Technology
November 1990

Copyright © 1990 by Lori June Wilson

CRYSTALLIZATION OF PROTEINS
BY DYNAMIC CONTROL OF
SUPERSATURATION

APPROVED:

F.L. Suddath, Chairman

J.A. Bertrand

L.A. Bottomley

R.F. Borkman

Roger M. Wartell

Date approved by Chairman _____

If you can look into
the seeds of time
and say which grain will
grow and which will not,
Speak then to me . . .

Macbeth

ACKNOWLEDGEMENTS

This work represents the efforts of several people, many of whom deserve individual thanks. Dr. F.L. "Bud" Suddath, my advisor, deserves much of the credit for the success of this project. Many thanks also go to past and present members of his research group, Harmon Zuccola, Gretchen Meinke, Terry Bray, Jay Bertrand, Dr. Susan Phillips and Mi Li who suggested ideas, proofread manuscripts, helped prepare talks and posters, and provided friendship that made graduate school bearable.

Thanks also goes to Paula F. Turner, alias "Mom", who has provided inspiration and support. Finally, without daily encouragement from my husband, Doug Brewer, this thesis would not exist. Thank you all.

LIST OF TABLES

	Page
Table 1. Variables Influencing Macromolecule Crystallization.	11
Table 2. Salts Used in Crystallization.	13
Table 3. Organic Solvents Used in Crystallization.	13
Table 4. Proteins of Pharmacia's Broad pI Calibration Kit and their corresponding pIs.	75
Table 5. Estimation of Crystal Quality by Visual Inspection.	90
Table 6. Optimization of crystallization conditions for lysozyme at pH 4.00.	91
Table 7. Optimization of crystallization conditions for lysozyme at pH 4.70.	92
Table 8. Size and Number of Lysozyme Crystals Grown in Linbro Wells and Acetate Buffer.	98
Table 9. Size and Number of Lysozyme Crystals Grown in Linbro Wells and Citrate Buffer.	101
Table 10. Comparison of rate of pH change.	135
Table 11. Results of crystals grown with controlled evaporation following the 40 hour evaporation curve.	155
Table 12. Results of crystals grown with controlled evaporation following the 80 hour evaporation curve.	156
Table 13. Number of days before crystals were observed in drops.	169
Table 14. Volume evaporated in microliters before crystals were observed.	169
Table 15. Determination of the Limit of Detection of the Gravimetric Method.	179
Table 16. Repetitive Gravimetric Measurement of a 10 μ L Drop.	180

TABLE OF CONTENTS

	Page
ACKNOWLEDGEMENTS.....	iv
LIST OF TABLES.....	vii
LIST OF FIGURES.....	viii
SUMMARY.....	xv
 Chapter	
I. BACKGROUND.....	1
Introduction	
X-ray Diffraction Methods	
Required Properties of Protein Crystals	
Theoretical Principles of Protein Crystal Growth	
Methodological Principles of Protein Crystal Growth	
Crystallization Methods	
Lysozyme Crystal Growth	
Purpose and Scope	
II. HARDWARE AND SOFTWARE DEVELOPMENT.....	30
Introduction	
Hardware for pH Control	
Software for pH Control	
Hardware for Evaporation Control	
Software for Evaporation Control	
III. PURIFICATION OF HEN EGG WHITE LYSOZYME.....	61
Introduction	
Materials and Methods	
Results and Discussion	
Conclusions and Recommendations	
IV. HANGING DROP VAPOR DIFFUSION STUDIES ON THE CRYSTALLIZATION OF LYSOZYME.....	86
Introduction	
Materials and Methods	
Results and Discussion	
Conclusions and Recommendations	

V. pH CONTROL OF SUPERSATURATION.....	112
Introduction	
Materials and Methods	
Results and Discussion	
Conclusions and Recommendations	
VI. EVAPORATION CONTROL OF SUPERSATURATION.....	138
Introduction	
Materials and Methods	
Results and Discussion	
Conclusions and Recommendations	
Appendix	
I. ALTERNATIVE EVAPORATION MONITORING TECHNIQUES.....	174
Conductance Monitoring with a Micro Conductance Cell	
Periodic Refractive Index Measurement	
Gravimetric Analysis of Drop Volumes	
Chloride Ion-selective Electrode	
II. COMPUTER PROGRAMS.....	183
Computer Automated Crystallization Apparatus	
Humidity Reader	
Conductance Reader	
III. SILANIZATION OF COVERSLEIPS.....	196
VITA.....	197

LIST OF FIGURES

	Page
Figure 1	Schematic representation of the energetics of crystallization and of amorphous precipitation. 6
Figure 2	Hanging drop chamber. 17
Figure 3	Sitting drop chamber. 18
Figure 4	Sandwich drop chamber. 19
Figure 5	Schematic of arrangement for pH control of a hanging droplet. 32
Figure 6	Flow chart of program used to monitor pH and control solenoid valves for pH experiments. 34
Figure 7	Arrangement of components for evaporation control of supersaturation. 36
Figure 8	TCD and valve arrangement. 38
Figure 9	Top view of crystallization chamber. 40
Figure 10	Side view of crystallization chamber. 42
Figure 11	TCD, Humidity and Conductivity monitoring of evaporative water loss from drops. 44
Figure 12	Electrical signal connections for TCD, Humidity and Conductivity monitoring. 45
Figure 13	Temperature control box. 47
Figure 14	Front Panel (user interface) for the Computer Automated Crystallization Apparatus (CACA). 49
Figure 15	Flow chart of program logic used to control evaporation. 51
Figure 16	Initialization subroutine (INITVI) 53
Figure 17	Evaporation Control and Monitoring subroutine. 54
Figure 18	Sub diagram of baseline determination and subtraction. 55
Figure 19	Temperature monitoring subroutine. 57
Figure 20	Termination and File Storage subroutine. 58
Figure 21	Silver stain development procedure. 65
Figure 22	Separation of lysozyme with dialysis tubing. 67
Figure 23	SDS-PAGE on Sigma lysozyme. 69
Figure 24	Log MW-Rf plot to determine molecular weight of protein bands. 70
Figure 25	Comparison of Sigma lysozyme and Calbiochem lysozyme. 71
Figure 26	Separation of Sigma lysozyme on Mono S 5/5 cation exchange column. 72

Figure 27	Separation of Calbiochem lysozyme on Mono S 5/5 cation exchange column.	73
Figure 28	SDS-PAGE on Sigma lysozyme with different strength reducing agents.	76
Figure 29	Lysozyme activity assay on Sigma lysozyme.	77
Figure 30	Separation of Sigma lysozyme and unknowns with isoelectric focusing using the PhastSystem and PhastGel 3-9.	78
Figure 31	The pH gradient profile indicated by Pharmacia's Broad pI Calibration Kit for the gel shown in Figure 30. The gel was photographed for measurement.	79
Figure 32	SDS-PAGE on solution from outer bag and inner bag after membrane separation.	81
Figure 33	Time scale of lysozyme diffusion through membrane.	82
Figure 34	Comparison of different lot numbers of Sigma lysozyme with SDS-PAGE.	83
Figure 35	3-dimensional surface and contour of crystal appearance quality vs. salt and protein concentration at pH 4.00.	95
Figure 36	3-dimensional surface and contour of crystal appearance quality vs. salt and protein concentration at pH 4.70.	96
Figure 37	Procedure for measurement of the crystal area. Crystals were magnified and photographed. Length X and Z were measured either off of the photographs with a precision micrometer ($\pm 0.05\text{mm}$) or with a micrometer eyepiece ($\pm 0.10\text{mm}$). The area was calculated by multiplying X by Z and dividing by the magnification.	97
Figure 38	10^0 diffraction photograph of a lysozyme crystal grown in 0.1M acetate buffer, pH 4.00, at a lysozyme concentration of 25 mg/mL and salt concentration of 2.5% (w/v). From this, unit cell parameters were found to be $a=b=79.1$ and $c=37.9$.	99
Figure 39	Hen egg white lysozyme crystals grown in 0.1M acetate and 0.1M citrate buffers at equal salt and protein concentrations.	102
Figure 40	Comparison of crystals grown from purified vs. unpurified form of lysozyme in citrate buffer.	103

Figure 41	10 ⁰ diffraction photograph of a lysozyme crystal grown in 0.1M citrate buffer, pH 4.00, at a supposed purified lysozyme concentration of 25 mg/mL and salt concentration of 1.0% (w/v). From this, unit cell parameters were found to be a=b=67.54 and c=31.13.	105
Figure 42	Phase diagram of hen egg white lysozyme in acetate buffer at pH 4.00.	107
Figure 43	SDS-PAGE with silver stain development on a solution of dissolved lysozyme crystal and diluted mother liquor.	108
Figure 44	pH equilibration within a Linbro well with sodium acetate.	117
Figure 45	pH equilibration within a Linbro well with ammonium sulfate as precipitant.	118
Figure 46	Calibration of the high flow rotameter with nitrogen gas.	120
Figure 47	Calibration of the low flow rotameter with nitrogen gas.	121
Figure 48	Data output for the three calibration buffers at pH 4.00, 7.00 and 10.00.	122
Figure 49	Calibration response curve pH vs. voltage output.	123
Figure 50	Results of experiment pH1EXP. Change in pH with acetic acid valve open continuously.	124
Figure 51	Results of experiment pH2EXP. Change in pH with acetic acid valve open 10 sec; off 10 sec; dry gas on 15 sec; off 25 sec; repeat.	126
Figure 52	Results of pH3EXP. Oscillations due to removal of acetic acid with dry gas purges and incorporation of acetic acid with saturated acetic acid gas purges.	128
Figure 53	Results of pH4EXP. Dry gas purged replaced with water-saturated gas purge.	129
Figure 54	Results of PH5EXP. Duplicate of experiment pH4EXP.	130
Figure 55	Results of pH6EXP. Determination of the relative strengths of the dilution and acid addition.	132
Figure 56	Results of pH7EXP. Water-saturated gas interval reduced to 5 seconds.	133
Figure 57	Results of pH8EXP. Water-saturated gas mixed with dry gas to inhibit the dilution of the drop.	134

Figure 58	Short term evaporation curves (theoretical). The straight line equation of these curves was used by the computer program to determine the evaporation profile.	141
Figure 59	Long term evaporation curves (theoretical). The linear relationship was used to control the evaporation of the drops.	142
Figure 60	Calibration response curve for the flat conductance cell.	144
Figure 61	Evaporation to dryness of a 10 μ L drop as monitored by the TCD.	145
Figure 62	Calibration of the TCD with different volume of deionized water.	146
Figure 63	Calibration of the T-type thermocouple.	147
Figure 64	Vapor equilibration in hanging drop crystallization.	150
Figure 65	Theoretical equilibration curves used with N ₂ (g) controlled evaporation of hanging drops.	152
Figure 66	Three equilibration curves quantified with (a) thermal conductivity detector and (b) on-line conductance monitoring. The starting conditions = 20 μ L drop volume of 0.05M NaCl. Differences in conductance readings (b) are thought to be due to concentration gradients within the drop.	153
Figure 67 (a) (b)	Purified lysozyme (25.9 mg/mL), pH 4.00, 0.1M acetate buffer, 5% NaCl (a) (above) Crystals obtained with hanging drop vapor equilibration with a reservoir. Crystals seen after 2 days (b) (lower) Crystals obtained with gas evaporation of 10 μ L in 100 hours. Crystals seen after 3 days.	158
Figure 67 (c) (d)	Purified lysozyme (25.9 mg/mL), pH 4.00, 0.1M acetate buffer, 5% NaCl (c) (above) Crystals obtained with gas equilibration curve of 400 hours. Crystals seen after 4 days (d) (lower) Crystals obtained with gas evaporation of 10 μ L in 800 hours. Crystals seen after 9 days.	159

Figure 68 (a) (b)	Unpurified lysozyme (23.2 mg/mL), pH 4.00, 0.1M acetate buffer 5% NaCl. (a) (above) Crystals obtained with hanging drop vapor equilibration with a reservoir. Crystals seen after 2 days (b) (lower) Crystals obtained with gas evaporation of 10 μ L in 100 hours. Crystals seen after 3 days.	160
Figure 68 (c) (d)	Unpurified lysozyme (23.2 mg/ μ L), pH 4.00, 0.1M acetate buffer 5% NaCl. (c) (above) Crystals obtained with gas equilibration curve of 400 hours. Crystals seen after 5 days (d) (lower) Crystals obtained with gas evaporation of 10 μ L in 800 hours. Crystals seen after 7 days.	161
Figure 69	Comparison of crystal number for the different gas equilibration curves and for the control experiment (Linbro well).	162
Figure 70	Comparison of crystal area for the different gas equilibration curves and for the control experiment (Linbro well).	163
Figure 71 (a) (b)	Purified lysozyme (23.2 mg/mL), pH 4.00, 0.1M citrate buffer, 0.5 % NaCl. (a) (above) Crystals obtained with hanging drop vapor equilibration with a reservoir. Crystals seen after 4 days (b) (lower) Crystals obtained with gas evaporation of 10 μ L in 100 hours. Crystals seen after 3 days.	165
Figure 71 (c) (d)	Purified lysozyme (23.2 mg/mL), pH 4.00, 0.1M citrate buffer, 0.5 % NaCl. (c) (above) Crystals obtained with gas equilibration curve of 400 hours. Crystals seen after 5 days (d) (lower) Crystals obtained with gas evaporation of 10 μ L in 800 hours. Crystals seen after 10 days.	166
Figure 72 (a) (b)	Purified lysozyme (23.2 mg/mL), pH 4.00, 0.1M citrate buffer, 1% NaCl. (a) (above) Crystals obtained with hanging drop vapor equilibration with a reservoir. Crystals seen after 4 days (b) (lower) Crystals obtained with gas evaporation of 10 μ L in 100 hours. Crystals seen after 3 days.	167

Figure 72 (c) (d)	Purified lysozyme (23.2 mg/mL), pH 4.00, 0.1M citrate buffer, 1% NaCl. (c) (above) Crystals obtained with gas equilibration curve of 400 hours. Crystals seen after 5 days (d) (lower) Crystals obtained with gas evaporation of 10 μ L in 800 hours. Crystals seen after 11 days.	168
Figure 73	Micro-conductance cell.	175
Figure 74	Calibration response curve of the micro-conductance cell. NaCl solutions made up in 0.10M Na acetate buffer, pH 4.00.	176
Figure 75	Calibration response of refractive index vs. NaCl concentration at 20 ^o C.	177
Figure 76	Calibration response of refractive index vs. (NH ₄) ₂ SO ₄ concentration at 20 ^o C.	178
Figure 77	Calibration curve of chloride ion selective electrode.	181
Figure 78	Front panel (user interface) of Computer Automated Crystallization Apparatus.	184
Figure 79	Zero level. Initialization. Recording tick count and conversion to seconds.	185
Figure 80	First level. Main control and data recording functions. Read temperature, open valve, integrate peaks from TCD.	186
Figure 81	Breakdown of first level loops. Shown here are 0 and 1 of evaporation control sequence structure. Loop 0 closes valves for determined amount of time. Loop 1 reads TCD baseline for 4 iterations and computes average.	187
Figure 82	Break down of first level loops. Shown here are 2 and 3. Loop 2 reads analog values of peaks from the TCD controller then integrates the peaks after subtracting away the baseline determined in loop 1. If the peak is too small to be considered a response it is ignored. Loop 3 creates an array of the data collected in loop 2 and graphs the data on the front panel.	188
Figure 83	Second level. This final level makes sure the valves are closed before the program terminates and writes the arrays created in level one to the file listed on the front panel in text format.	189
Figure 84	Front panel (user interface) of Humidity Reader.	190

Figure 85	Humidity Reader Diagram. Levels 0 and 1. Level 0 opens a file on the specified volume. Level one records data from humidity indicator and writes the data to a file.	191
Figure 86	Humidity Reader Diagram. Level 2 closes the file and terminates the program.	192
Figure 87	Conductance Reader Front Panel.	193
Figure 88	Conductance Reader Diagram. Level 0 and 1. Level 0 opens a file on the specified volume while level 1 records, graphs and writes the data to a file.	194
Figure 89	Conductance Reader Diagram. Level 2. Closes the file and terminates the program.	195

SUMMARY

The growth of protein crystals is known to be the limiting factor in the determination of the three-dimensional structures of most proteins. It is expected that the kinetics of supersaturation, which is directly related to solvent evaporation, will affect protein crystal growth and nucleation and accordingly determine the quality, number, size and morphology of the crystals. With a technique that controls the evaporation of solvent from a protein solution with N_2 (g) it is possible to determine the effect of different evaporation profiles on hen egg white lysozyme crystals. Hen egg white lysozyme was chosen as the model protein because it crystallizes easily and has solubility data available for most salt, pH and temperature ranges. Commercially available lysozyme was further purified by a number of methods. Crystals grown with the purified lysozyme and with the unpurified lysozyme in citrate buffer were different shapes but were found to be of the same symmetry space group by precession photos.

Differences were seen in the lysozyme crystals grown using different evaporation rates. At three of the four initial conditions for lysozyme crystal growth longer evaporation times yielded better crystals. The evaporation times required to see a change in the appearance of the crystals was much longer than expected. The number of rates studied so far represent only a small fraction of the ones now available with the gas evaporation device. The technique

also provides for control of both solution pH and temperature which are related to the solubilities of proteins.

CHAPTER I

BACKGROUND

Introduction

While the function of biological macromolecules is determined by their molecular structure, the determination of the three-dimensional structure of these molecules by X-ray analysis relies on the availability of high quality protein crystals. The use of crystals in structural biology goes back to 1934, when the first X-ray diffraction pattern of a protein crystal was produced [1]. Since then, tremendous progress has been made in every area of X-ray crystallography except for crystallization. It is the difficulty in producing high quality protein crystals which is now delaying structural determinations of most proteins. While structure determination can be done in several weeks to a few months, the production of suitable crystals has remained an empirical process and is, therefore, time intensive. Rational approaches to protein crystallization are needed to fulfill the increasing need for three-dimensional knowledge of proteins, nucleic acids and multimolecular assemblies. This need has been increasing over recent years with the advent of techniques such as site directed mutagenesis [2] and rational drug design [3]. The work reported in this thesis has been carried out with the intention of breaking the

"bottle neck" of X-ray analysis by providing both better techniques for obtaining protein crystals as well as an increased understanding of the mechanism of protein crystallization.

X-ray Diffraction Methods

Protein crystallography plays an important role in the understanding of specific functions of biological molecules by providing the three-dimensional structures of the molecules. The entire process relies on crystals of high enough order to diffract monochromatic light producing a diffraction pattern. The electron density in the crystal is calculated by Fourier Transformation of the diffraction pattern. This requires information of the intensities and directions of the diffracted rays which are measured on photographic film or, as in the case of proteins, on an area sensitive detector. Determination of the relative phase of each ray is the most challenging task. One solution for phase determination is isomorphous replacement [4] where a heavy atom is placed within the crystal without disturbing its packing. The phases of the diffracted rays are determined by their changes in intensity with the addition of the heavy atom. Phase determination is another area that would benefit from an increased understanding of protein crystal growth processes. It is not uncommon for heavy atom derivatives of proteins to resist crystallization with traditional methods. Since isomorphous

replacement is the primary technique for phase determination, this is a major stumbling block to structure determination. However, as understanding of the mechanisms involved in crystal growth increases, so will the ability to obtain crystals of heavy atom derivatives.

Once the phase and amplitude of each diffracted ray are determined, the electron density of the protein may be calculated. The secondary structure is obtained by matching the density with the amino acid residues of the primary structure. The structure is then refined by computer methods. Knowledge of the structure of a protein can then be used to provide information about its biological function.

Required Properties of Protein Crystals

The first requirement of protein crystals for X-ray diffraction analysis is the need for single crystals and not multiple growths. These single crystals should measure at least 0.3 mm in each dimension. This size restraint results from a compromise between maximum diffraction intensity and minimum crystal absorption for copper K_α radiation. The diffraction intensity is proportional to $l^3e^{-\mu l}$, where l is the linear dimension of the crystal and μ the linear absorption coefficient. The degree of order in the crystal should be as high as possible; the crystal should at least produce diffraction to 3\AA resolution. A high degree of order is thought to be related to both

mechanical and chemical stability as well as low solvent content [5]. It is also important for the protein to be present in the crystal in its native state. Since there are only a few contacts made between protein molecules within the crystal, the proteins are mainly surrounded by solvent. Matthews [6] has compiled data on solvent content of protein crystals and has estimated that, on average, 50% of the unit cell is solvent. Normally, protein crystals are thought to range from 20%-70% solvent with some extreme cases even higher [7] [8]. The solvent in the crystal allows the protein molecules to remain in their native state. Evidence that molecules do remain in their native state arises from activity measurements on crystallized enzymes, and comparison of protein structures from different media [9] [10].

The quality of protein crystals can be evaluated in a number of ways. A qualitative analysis can be made by viewing the crystals under magnification. The number, size and morphology of the crystals can be important indicators of the crystal quality. The appearance of inclusions, imperfections and clusters are sometimes characteristic of crystals with low internal order. A more thorough analysis of the crystal order is the measurement of diffraction resolution. This provides some indication of the internal order of the crystals but can be highly subjective and is often dependent on crystal orientation. The most comprehensive analysis is to compare three-dimensional intensity data sets. These types of analyses rely on previous knowledge of the structure of the protein and require the use of an area detector for data collection. Since this type of analysis is quite

detailed only a few investigations of crystal quality have been completed [11].

Theoretical Principles

Current theories of macromolecular crystal growth generally divide the process into three steps: nucleation, post-nucleation growth, and cessation of growth[12]. These three processes are described energetically in Figure 1 [13] and are discussed in detail below.

Nucleation

There are two types of nucleation: homogeneous and heterogeneous. Homogeneous nucleation occurs in the absence of foreign particles as opposed to heterogeneous nucleation which takes place on the surface of foreign bodies. Both types of nucleation have been useful in protein crystallography.

Homogeneous Nucleation. From an entropy point of view it is unfavorable for disordered molecules to aggregate into ordered crystals. However, many favorable bonds are made within the crystal to counteract the entropy effect. Before these contacts are made it is energetically unfavorable for the molecules to aggregate (Figure 1). To overcome this energy barrier, solution conditions are adjusted to supersaturation so that protein molecules are forced to form

Figure 1. Schematic Representation of the energetics of crystallization and of amorphous precipitation.

aggregates. Basically, at supersaturated conditions there is not enough water to maintain hydration or to shield the protein molecules from neighboring protein molecules. These aggregates can then go on to form ordered nucleates or disordered amorphous precipitate. The difference in these two states can be approximated by addition of molecules only at end positions of a linear chain (amorphous conditions) or the addition of molecules in three dimensions (crystallization conditions). If the aggregation occurs too rapidly, an amorphous precipitate will often form. This is undesirable, as crystals generally do not arise out of this state. In some cases, however, crystals will form along with precipitate or form after the precipitate if the energy barrier between the two forms is low enough.

Once nuclei are formed they serve as the base for addition of more single protein molecules, or monomers [14] [15]. These monomers continue to attach to the crystal until an equilibrium has been reached between the liquid and solid phases. A more recent theory [16] suggests that the protein monomers form nucleates when concentrated enough, and these nucleates combine to form larger particles. Experimental evidence has been shown to support both of these theories, so it is possible that both processes may be occurring simultaneously.

Heterogeneous Nucleation. In the case of heterogeneous nucleates, a crystal is introduced into a supersaturated solution of a second compound. At a critical level of supersaturation, significantly lower

than that required for homogeneous nucleation, crystals of the second compound will nucleate and grow from crystal faces of the added crystal. The promotion of nucleation of the second compound is due to physical and/or chemical interactions between the two compounds. It is presumed that the second compound is concentrated on the added crystal perhaps by absorption. Heterogeneous nucleation has been used to grow crystals of several proteins [17] [18] [19]. There is one advantage to heterogeneous nucleation over homogeneous nucleation. Growth of crystals from high levels of supersaturation tend to produce crystals with defects. The ideal conditions for growth are at a much lower supersaturation level than the conditions required for homogeneous nucleation. Heterogeneous nucleation allows growth at a much lower supersaturation level thereby yielding higher quality crystals. However, heterogeneous nucleation often yields crystals of undesirable space groups.

Post-Nucleation Growth

The second step in the crystallization process is post-nucleation growth. There are two stages in the growth process: (1) the transport of material to the growing crystal surface and (2) the association of the molecules with the ordered crystal lattice. The growth rate of the crystal is believed to be limited by both of these processes. It is desirable to slow the first stage so that molecules are added to the lattice at a slow rate resulting in a higher ordered crystal.

This is difficult since nucleation, the first step, requires a high supersaturation level. A high degree of supersaturation usually leads to numerous small crystals. Crystals that grow too fast usually reach a smaller terminal size, presumably because of structural defects that have been incorporated into the lattice [20]. In order to obtain large, single crystals, the level of supersaturation must be kept low, so that molecules are not forced into the crystalline lattice in a disordered fashion.

Cessation of Growth

The final step in the protein crystallization process is the cessation of growth. After a long time interval, crystals will cease to grow, even if the level of supersaturation is increased. This phenomenon is not completely understood. It is possible that some change in the crystal surface causes further growth to be unfavorable. This could be due to the accumulation of surface defects resulting from improperly oriented protein molecules or incorporation of impurities which do not fit the lattice well. Regardless, crystals seem to reach a terminal size based on experimental conditions.

Methodological Principles

Crystallization is generally achieved by forcing protein molecules out of solution with slow approaches to insolubility. This is carried out by adjusting one or more of several solution parameters. The most common have been ionic strength (salts) [21] [22] [23], dielectric constant (polyethylene glycol (PEG), and organic solvents) [24], pH [25], counter ions [26] [27], and temperature [28]. A comprehensive list of the factors which effect protein crystals is shown in Table 1 [29]. Since proteins denature under mildly hostile conditions the only conditions that can support crystal growth are those that cause no perturbation of the molecule's properties. Thus, protein crystals are grown from solutions that maintain a tolerable range of pH, temperature, and ionic strength.

The concentrations of the macromolecule and precipitant are the most important factors affecting crystallization. These levels must be chosen so that crystallization is achieved. Highly concentrated protein solutions (10-100 mg/mL) are used. The proteins should be as pure as possible to eliminate interfering effects from contaminants. The purity of protein samples has been studied and the effect of impurities on crystal quality has been quantified [30]. The most serious effect of impurities is loss in reproducibility from one crystallization batch to another. Since several crystals of the same space group are often

Table 1. Variables Influencing Macromolecule Crystallization

Concentration of precipitant
Concentration of macromolecule
Temperature
pH
Pressure
Level of reducing agent or oxidant
Substrates, coenzymes, and ligands
Purity of protein or nucleic acid
Preparation and storage of macromolecule
Proteolysis and fragmentation
Age of macromolecule
Degree of denaturation
Vibration and sound
Volume of crystallization sample
Metal ions
Seeding
Amorphous precipitate
Buffers
Cleanliness
Organism or species from which macromolecule
was isolated
Gravity, gradients, and convection

needed to gather a complete data set the inability to reproduce crystals under the same conditions is limiting.

Temperature is another important factor since the solubility of proteins varies with temperature. Most proteins have a solubility minimum at low temperatures while others exhibit a solubility maximum at low temperatures. Extreme deviations in temperature can cause a protein to denature or form an amorphous precipitate. Unfortunately, temperature as an adjustable parameter is frequently ignored as an important variable and is most likely responsible for much of the unreliability associated with protein crystal growth. However, temperature can be used as a crystallization method, usually by slowly cooling a saturated solution to produce a supersaturated solution [31] [32].

The nature of the precipitant can greatly affect the ability to obtain crystals. There are three main varieties of precipitating agents: salts, organic solvents, and hydrophilic polymers. Salts (Table 2) [33] increase the ionic strength of the solution, which decreases the solubility of proteins. By slowly increasing the concentration of the precipitant, the protein is forced out of solution. Organic solvents interact with water molecules and decrease the ability of water to solvate the protein molecules. Organic solvents (Table 3) [34] also alter the dielectric properties of the solvent, which can decrease a protein's solubility. Hydrophilic polymers of varying sizes (1000, 4000, 6000, and 10000) are often used to crystallize proteins [35]. Though the actual mechanism which causes crystals to form in

Table 2. Salts Used in Crystallization

Ammonium or sodium sulfate
Lithium sulfate
Lithium chloride
Sodium or ammonium citrate
Sodium or potassium phosphate
Sodium or potassium or ammonium chloride
Sodium or ammonium acetate
Magnesium sulfate
Cetyltrimethyl ammonium salts
Calcium chloride
Ammonium nitrate
Sodium formate

Table 3. Organic Solvents Used in Crystallization

Ethanol
Isopropanol
2-Methyl-2,4-pentanediol (MPD)
Dioxane
Acetone
Butanol
Acetonitrile
Dimethyl sulfoxide
2,5-Hexanediol
Methanol
1,3-Propanediol
1,3-Butyrolactone

polyethylene glycol mixtures is not well understood, they are thought to function by binding to water, decreasing the solubility of the protein. They also alter the dielectric properties of the solution.

Even if suitable conditions are found which will yield crystals of a desired protein, the quality of those crystals may be poor due to the effects of gravity during the growth process. Gravity is an important non-solution factor affecting the quality of protein crystals. Ideally, one wishes crystal growth to be controlled by diffusion of protein to the growth surface. On Earth, density gradients are created as the solution surrounding a growing crystal is depleted of protein. As a crystal grows and removes solute from solution, the resulting decrease in density around the crystal causes a buoyant plume of less dense solution to rise from the growing crystal. This solutal convection was first described by Frankenheim [36] more than a hundred years ago. Solutal convection is known to influence many crystal properties, including growth kinetics, impurity incorporation, crystal composition and morphology. Schlieren images of growing protein crystals have proven the presence of a convective plume about the crystals [37] [38]. A mathematical model has been developed to describe solutal flow in protein crystal growth [39]. While this is a step forward, the role played by these hydrodynamical effects in the growth of crystals from solution is better established for small molecules than for proteins. Gravity can also cause sedimentation of crystals to the bottom of the solution in which they are growing. This can cause problems by

causing crystals to grow into each other or producing fragile crystals that break when analyzed.

One possible approach to minimizing these flows and sedimentation effects is the use of the microgravity environment. NASA, as well as other agencies [40] [41], is actively investigating protein crystal growth in microgravity as a way to obtain more ordered crystals for use in structure determination [42]. Crystallization of γ -interferon D1, porcine elastase, and isocitrate lyase in the microgravity environment has yielded crystals that are larger, exhibit more uniform morphologies and produce diffraction data to significantly higher resolutions than the best crystals of these proteins grown on Earth [43].

Crystallization Methods

Vapor Diffusion

Currently, vapor diffusion methods are the most frequently used method for growing protein crystals [44]. The basic components of vapor diffusion crystallization are a drop of protein solution, containing protein and precipitating agent, and a larger reservoir, containing only precipitating agent. The method relies on the fact that there is a higher concentration of a precipitating agent in a reservoir and, as a result, the equilibrium vapor pressure above the reservoir is lower than that of the protein drop. Since the system is sealed, water

evaporates from the drop increasing the concentration of precipitating agent and protein until the drop and reservoir have equal vapor pressures of volatile components. The shape of the equilibration curve is determined by the initial solute concentrations, the difference in the equilibrium vapor pressure of the drop and reservoir, temperature and the diffusion path of the vapor [45]. The conditions of supersaturation that result in the protein solute leaving the solution phase as a crystalline solid must be achieved during this equilibrium process: however, the optimal conditions for crystal nucleation and growth are most often not attained by this method [46]. Furthermore, since nucleation takes place at a supersaturation level which is usually much higher than the level required for sustained crystal growth, it would be desirable to lower the supersaturation after nucleation has been induced [47].

Hanging Drop. The hanging drop method [48] is the most frequently employed method for growing protein crystals. A drop (typically 10 to 50 μ L) containing the protein, buffer, and precipitating agent is hung from a silanized glass microscope coverslip over a reservoir solution in a sealed chamber (see Figure 2). The reservoir solution contains the same buffer as the protein drop, but the precipitant concentration is higher (typically twice that of the drop). This difference in precipitant concentration causes volatile components to diffuse from the drop to the reservoir solution.

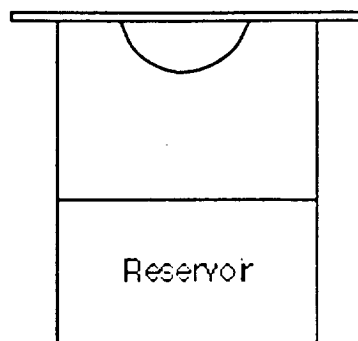


Figure 2. Hanging Drop Chamber.

This occurs until the vapor pressure is equal in the drop and reservoir. Since the volume of the reservoir is large compared to the drop, there is little dilution effect in the reservoir due to the water added from the drop. The precipitant concentration of the reservoir can be varied so that any final volume in the drop can be achieved. The time required for equilibration varies with the factors mentioned above.

Another important variable which is controlled in a similar manner is pH. If the pH of the drop is significantly different than the pH of the reservoir, volatile acids and bases will diffuse from the reservoir to the drop until the pH of the drop reaches the pH of the reservoir.

Sitting Drop. The sitting drop method [49] is another frequently used procedure for growing protein crystals. The protein drop is placed on a platform which sits above a reservoir solution. The chamber is sealed with a glass coverslip and is shown in Figure 3. The concentration procedure is similar to the hanging drop method with

reservoir solution. Volatile components diffuse from the protein drop to the more concentrated reservoir solution. Larger amounts of protein solution (up to 100 μL) may be used than with the hanging

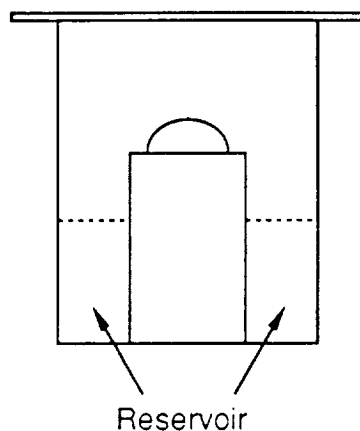


Figure 3. Sitting Drop Chamber.

drop method. The time for evaporation of sitting drops has been found to increase with increased drop volume [50].

Sandwich Drop Method. A variation to the sitting drop method involves lowering the glass coverslip until it touches the top of the drop, forming a "sandwich" between the platform and the coverslip (see Figure 4). This procedure [51] reduces the exposed surface area of the protein solution, so equilibration between the protein and reservoir solutions occurs at a slower rate than in other methods. This arrangement is more suitable for optical viewing as the protein drop is situated between two flat, transparent surfaces. There is more

contact with surfaces which can lead to multiple nucleation sites on the glass.

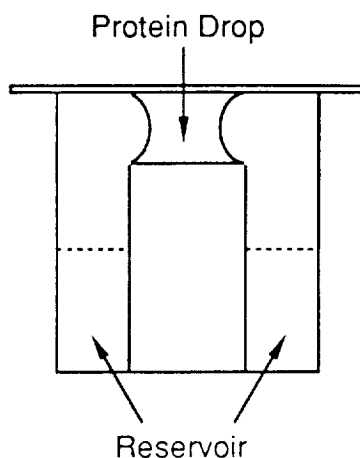


Figure 4. Sandwich Drop Chamber.

Liquid/Liquid Diffusion

These methods allow protein and precipitating solutions to come in contact with each other, either directly or separated by a semi-permeable membrane. Crystallizations are usually affected by varying the solution concentrations until conditions are found which are suitable for crystal growth. When in direct contact, the two solutions diffuse into one another. When separated by a membrane, water and salts permeable to the membrane diffuse from the protein solution to the precipitating solution.

Batch Method. This is perhaps the simplest of the liquid/liquid diffusion methods [52]. This method mixes the protein and precipitant together and lets the resulting solution sit undisturbed. Hopefully, the precipitant will force the protein out of solution as large, single crystals, although an amorphous precipitate or micro-crystals may form. Often, varying the level of precipitant only slightly will give a very different result. Thus, this method is not very reproducible.

Dialysis Method. A widely used method involves liquid diffusion across a membrane between two solutions [53]. One solution contains the protein and precipitating agent. The other solution contains precipitating agent at a higher level than in the protein solution. The two solutions are separated by a dialysis membrane that does not allow protein to pass through it. Water and salts can diffuse through the dialysis membrane between the two solutions. Protein is forced out of solution either by water or salt equilibrating across the membrane. The equilibration rate can be varied by changing the relative concentrations of precipitating agent in each solution.

Gel Methods. A less commonly used method which shows some promise for minimizing the effects of gravity involves the growth of crystals in gels [54]. Two types of gels are used, physical gels and chemical gels. Physical gels consist of polymeric chains entangled

together and held by non-covalent bonds. These gels are typically made of gelatin or agarose. Chemical gels consist of polymeric chains which are covalently cross-linked with each other. Silica or polyacrylamide is usually used for making these types of gels.

Crystals grown in gels are suspended in the bulk, not on the bottom of the cell, unless that is where nucleation occurred. The crystal is supported by the gel network, but can continue to grow as this network is not rigid. This network provides the most desired feature of a gel, the minimization of convective flow due to density gradients produced by a growing crystal. This property allows the growth process to be dominated by diffusional mass transfer, not convective flow to the growth surface.

The use of gels to grow crystals is currently limited by the small terminal size the crystals reach. This problem may be due to mechanical restraints induced by the gel network, or possibly by slow diffusion of protein monomers through the network.

Automated Systems

There are several systems, both commercial and research, which can be used for screening crystal growth conditions with minimal human intervention. These systems typically incorporate robotics and computer control for deploying solutions and monitoring the growth process [55] [56]. Most of these devices are based on the hanging drop vapor diffusion technique, using a liquid reservoir to affect the

evaporation of a protein solution. Though these devices greatly reduce the need for human intervention, they still take a trial and error approach to finding suitable crystallization conditions. There has been an attempt to use these systems to converge on suitable conditions based on prior experiments [57]. A basic statistical design approach has also been developed to attempt to predict conditions suitable for crystal growth [58]. All of these approaches still do not allow the conditions of an experiment to be dynamically modified while crystal growth is in progress.

Lysozyme Crystal Growth

Lysozyme catalyzes the hydrolysis of a polysaccharide that is the major constituent of the cell wall of certain bacteria. The solution of the structure of lysozyme is one of the triumphs of X-ray crystallography [59] [60] [61]. The mechanism of the enzyme, which was previously unknown, was determined by examination of the structure of lysozyme and its complexes with inhibitors [62]. Because lysozyme crystallizes easily it has been the protein of choice for most protein crystal growth studies [63] [64] [65] [66] [67] [68] [69]. Lysozyme also has readily available solubility data for most salt, pH and temperature ranges [70]. The mechanisms for the crystal growth of lysozyme have been studied with electron microscopy. The growth mechanism was found to be a lattice defect mechanism at low supersaturation and two-dimensional nucleation at high

supersaturation [71]. From studies on lysozyme it is hoped that general theories can be developed for protein crystal growth.

Purpose and Scope

Analyzing protein structures by crystallography can be a slow and difficult undertaking since the first, and possibly hardest task, involves growing X-ray quality grade crystals, which have to be well ordered to give rise to good diffraction spots.

Gronenborn and Clore [72]
Analytical Chemistry
January 1, 1990

The growth of protein crystals has been shown to be the limiting factor in the determination of the three-dimensional structures of most proteins. Current systems, although useful for screening a large number of conditions, do not have the capability to grow crystals by changing the solution parameters while an experiment is in progress. There is a need for techniques to allow crystal growth without the exhaustive screening process. This need is particularly critical in the cases of hard to obtain proteins, where numerous trials are not possible due to lack of material. The difficulty in development of new techniques has been the nature of the proteins, need for a dust free environment, and micro size requirements. Despite these difficulties, this thesis reports a technique which employs $N_2(g)$ to control the evaporation of a hanging drop. The kinetics of water evaporation will determine the kinetics of supersaturation and accordingly influence

the number and size of crystals. With this technique it was possible to determine the effect of different evaporation rates on protein crystals. It also provides for control of both solution pH and temperature which are related to the solubilities of proteins. With this added control it is possible to provide different supersaturation levels for the nucleation and growth levels.

In order to develop the technique it was first necessary to quantify the evaporation and pH equilibration within a hanging drop vapor diffusion crystallization experiment. This technique has been of interest to NASA because it allows computer control of solution conditions thereby eliminating the need for interaction with the mission specialist on board the U.S. Space Shuttle. Current plans are to incorporate a flight version of this technique on the U.S. Space Station, Freedom, in 1992. Although the advantage of automating the crystal growth processes was the main driving force in developing the technique, the added control provided a tool to probe the nucleation and growth supersaturation regions which has led to an increased understanding of each step.

SELECTED REFERENCES

- [1] Bernal, J.D. and Crowfoot, D. (1934) *Nature*, **133**, 794-795.
- [2] Oxender, Dale L. and C. Fred Fox (1987) *Protein Engineering*, (Alan R. Liss, Inc., New York) 51-63.
- [3] Voet, Donald and Judith G. Voet (1990) *Biochemistry* (John Wiley & Sons) 755-757.
- [4] Green, D.W., Ingram, V. and Perutz, M.F. (1954) *Proc. R. Soc.*, **A225**, 287.
- [5] Smit, J.D.G. (1979) , *Journal de chimie physique*, **76**, 805-810.
- [6] Matthew, B.W. (1968) *J. Mol Biol.*, **33**, 491.
- [7] Higashi, J.R., L.C. Sieker, L.H. Jensen and W.Lovenberg (1970) *J. Mol. Biol.*, **50**, 391-406.
- [8] Longley, W. (1967) *J. Mol. Biol.*, **30**, 323.
- [9] Matthews, B.W. (1977) *The Proteins*, Vol. III, 3rd edition, Academic Press, New York.
- [10] Drenth, J. (1972) *Enzymes: Structure and Function*, Eight FEBS Meeting, North Holland, Amsterdam, p.1.
- [11] DeLucas, L.J. et al (1989) *Protein Crystal Growth in Microgravity*, *Science*, **246**, 651-654.
- [12] Feher, G. (1986) *Journal of Crystal Growth*, **76**, 545-546.
- [13] Wycoff, Harold W. C.H. Hirs and Serge N.Timasheff (1985) *Methods in Enzymology*, **114**, p.81.
- [14] J. Schlichtkrull (1967) *Acta Chem. Scand.*, **10**, 1455 and 1459: 11, 291, 299, 439, 484, and 1248.
- [15] Kam, Z. , H. B. Shore, and G. Feher (1978), *J. Mol. Biol.*, **123**, 539.
- [16] Pusey, M.L. (1990) *J. Crystal Growth*, in press.

- [17] McPherson, Alexander and P. Schlichta (1988) J. Crystal Growth **90**, 47-50.
- [18] McPherson, Alexander and Paul Schlichta (1987) Science, **239**, 385-387.
- [19] McPherson, Alexander and Paul J. Schlichta (1987) J. Crystal Growth, **85**, 206-214.
- [20] Feher, G. and Kam, Z. (1985) Methods in Enzymology, **114**, 101.
- [21] Green, Arda (1931) , J. Biological Chemistry, **XCIII**, 2, 495-515.
- [22] Melander, Wayne and Horvath, Csaba (1977) Archives of Biochemistry and Biophysics, **183**, 200-215.
- [23] von Hippel, Peter H. and Schleich, Thomas (1969) Accounts of Chemical Research, **2**, 9, 257-265.
- [24] McPherson, Alexander, Jr. (1976) Journal of Biological Chemistry, **251**, 20, 6300-6303.
- [25] McPherson, A., Jr., *Preparation and Analysis of Protein Crystals* (Wiley, New York, 1982) pp. 82-123.
- [26] Reis-Kautt, Madeline M. and Arnaud F. Ducruix (1989) Journal of Biological Chemistry, **264**, 2, 745-748.
- [27] Arakawa, Isutomu and Serge N. Timasheff (1982) Biochemistry, **21**, 6545-6552.
- [28] Rosenberger, Franz and Meehan, Edward J. (1988) J. Crystal Growth, **90**, 74-78.
- [29] Reference 25.
- [30] Abergel, C. and J.C. Fontecilla-Camps (1989) Proc. Third International Conference on the Crystallization of Biological Macromolecules, **P33**, 105.
- [31] Osborne, T.B. (1892) Am. Chem. J., **14**, 662.
- [32] Rosenberger, F. , E.J. Meehan (1988) J. Crystal Growth, **90**, 74.

- [33] Reference 25.
- [34] Reference 25.
- [35] McPherson, A. Jr. (1976) J. Biol. Chem., **251**, 20, 6300.
- [36] Frankenheim, L. (1860) Poggendorfs Ann. Physik, **111**, 1.
- [37] Broom, Beth M., William K. Witherow, Robert S. Snyder and Daniel C. Carter (1988) J. Crystal Growth, **90**, 130-135.
- [38] Pusey, Marc, William Witherow and Robert Nauman (1988) J. Crystal Growth, **90**, 105-111.
- [39] Baird, J.K., E.J. Meehan, A.L. Xidis, S.B. Howard (1986) J. Crystal Growth, **76**, 694.
- [40] Trakhanov, S.D. (1989) Proc. 3rd International Conference on the Crystallization of Biological Macromolecules, **L33**, 47.
- [41] Plaas-Link, Andreas (1989) Proc. 3rd International Conference on the Crystallization of Biological Macromolecules, **L34**, 48.
- [42] DeLucas, L.J. et al. (1986) J. Crystal Growth, **76**, 681.
- [43] DeLucas, L.J. et al. (1989) Science, **246**, 651.
- [44] Reference 25.
- [45] Fowlis, W.W., L.J. DeLucas, P.J. Twigg, S.B. Howard, E.J. Meehan, J.K. Baird (1988) J. Crystal Growth, **90**, 117.
- [46] Gernert, Kim M., Robert Smith and Daniel C. Carter (1988) Anal. Biochem., **168**, 141-147.
- [47] Rosenberger, F. (1986) J. Crystal Growth, **76**, 618-636.
- [48] Reference 25, p. 96.
- [49] Reference 25, p. 94.
- [50] Mikol, Vincent, Jean-Luc Rodeau, Marc Ruff and Richard Giefe. Institut de Biologie Molculaire et Cellulaire, CNRS, 15 rue Rene Descartes, 67084 Strasbourg Cedex, France. Unpublished work.

- [51] Reference 25, p. 95.
- [52] Reference 25, p. 87.
- [53] Reference 25, p. 88.
- [54] Robert, M.C. and F. Lefauchaux (1988) J. Crystal Growth, **90**, 358.
- [55] Cox, M.J. and P.C. Weber (1987) J. Appl. Cryst., **20**, 366.
- [56] Ward, K.B., M.A. Perozzo, W.M. Zuk (1988) J. Crystal Growth, **90**, 325.
- [57] Cox, M.J. and P.C. Weber (1988) J. Crystal Growth, **90**, 318.
- [58] Carter, C.W. Jr., E.T. Baldwin, L. Frick (1988) J. Crystal Growth, **90**, 60.
- [59] Blake, C.C. F., D.F. Koenig, G.A. Mair, A.C.T. North, D.C. Phillips, and V.R. Sarma (1965) Nature, **206**, 757.
- [60] Phillips, D.C. (1967) Proc. Natn. Acad. Sci., **57**, 484.
- [61] Blake, C.C.F., L.N. Johnson, G.A. Mair, A.C.T. North, D.C. phillips and V.R. Sarma (1967) Proc. R. Soc., **B167**, 378.
- [62] Phillips, D.C. (1967) Proc. Natn. Acad. Sci., **57**, 484.
- [63] Durbin, S. D. and G. Feher (1986) J. Crystal Growth, **76**, 583-592.
- [64] Fusey, M. (1986) J. Crystal Growth, **76**, 593-599.
- [65] Fies Drautt, Madeleine M. and Arnaud Ducruix (1989) J. Biol. Chem., **264**, 2, 745-748.
- [66] Fusey, Marc, Robert Snyder and Robert Nauman (1986) J. Biol. Chem., **261**, 14, 6524-6529.
- [67] Ataka, Mitsuo and Michihiko Asai (1988) J. Crystal Growth, **90**, 86-88.
- [68] Cwen, Jeffery D., Edward M. Eyring and David L. Cole (1969) J. Physical Chemistry, **73**, 11, 3918-3921.

- [69] Ataka, Mitsuo (1986) Biopolymers, **25**, 337-350.
- [70] Marc Pusey (1990) J. Crystal Growth, in press.
- [71] Durbin, S. D. and G. Feher (1990) J. Mol. Biol., **212**, 763-774.
- [72] Gronenbore, Angela M. and G. Marius Clore (1990) Analytical Chemistry, **62**, 1. 2-15.

CHAPTER II

HARDWARE AND SOFTWARE

Introduction

Development of instrumentation to control the evaporation and pH of a 10 - 20 μ L drop was not an easy task. The most difficult challenge was to design and build a monitoring system that allowed closed-loop control of the evaporation process. It was desirable to have complete computer control and monitoring of several parameters including pH, temperature, and ionic strength. All of these must be monitored in a non-invasive manner in order to protect the delicate protein crystals. The materials that came in contact with the crystallization solution were chosen carefully so that they did not induce nucleation or contaminate the crystals. Other important considerations in the development were the retrieval of the crystals for X-ray analysis, the purity of the gas stream, moisture leakage, the number and size of cells. In order to develop the system in as little time as possible, commercial products were used if they were available. Otherwise, the components were built in-house. In the same manner, the software

programs were custom designed using commercially available data acquisition and control programming languages.

Hardware for pH Control

The pH of a hanging drop was controlled using acidic or alkaline vapor transfer. A 30 μ L drop was suspended from a solid state micro pH electrode (Lazar Research Laboratories, Model PHR-146 Combination) with a flat tip (Figure 5). This electrode is ideal for pH measurements of micro samples due to its low output impedance as compared to a glass electrode with the same sensor size. The low output impedance yields a stable signal with little noise interference. The pH electrode was housed in a glass cell with a septum for introducing the drop onto the electrode. The electrode was connected to an Orion Research 501 digital ionanalyzer with a U.S. standard connection. The pH meter was interfaced to an AT&T PC 6300 personal computer through a Keithly Series 500 Scientific Workstation which included 3 boards: (1) AMM1 Master Analog Measurement Module (2) AIM7 Thermocouple Input Module (3) DIO1 Digital Input/Output Module. Since the signal from the pH meter was on the order of 10-100 mV it was amplified with a x100 narrow bandwidth amplifier on the Keithly AIM7 Board. N₂(g) was bubbled through either solutions of acetic acid or water, or allowed to pass to the cell dry for evaporation. The gas was routed to the cell with microbore autoanalysis tubing (Cole Palmer #N-07626-84).

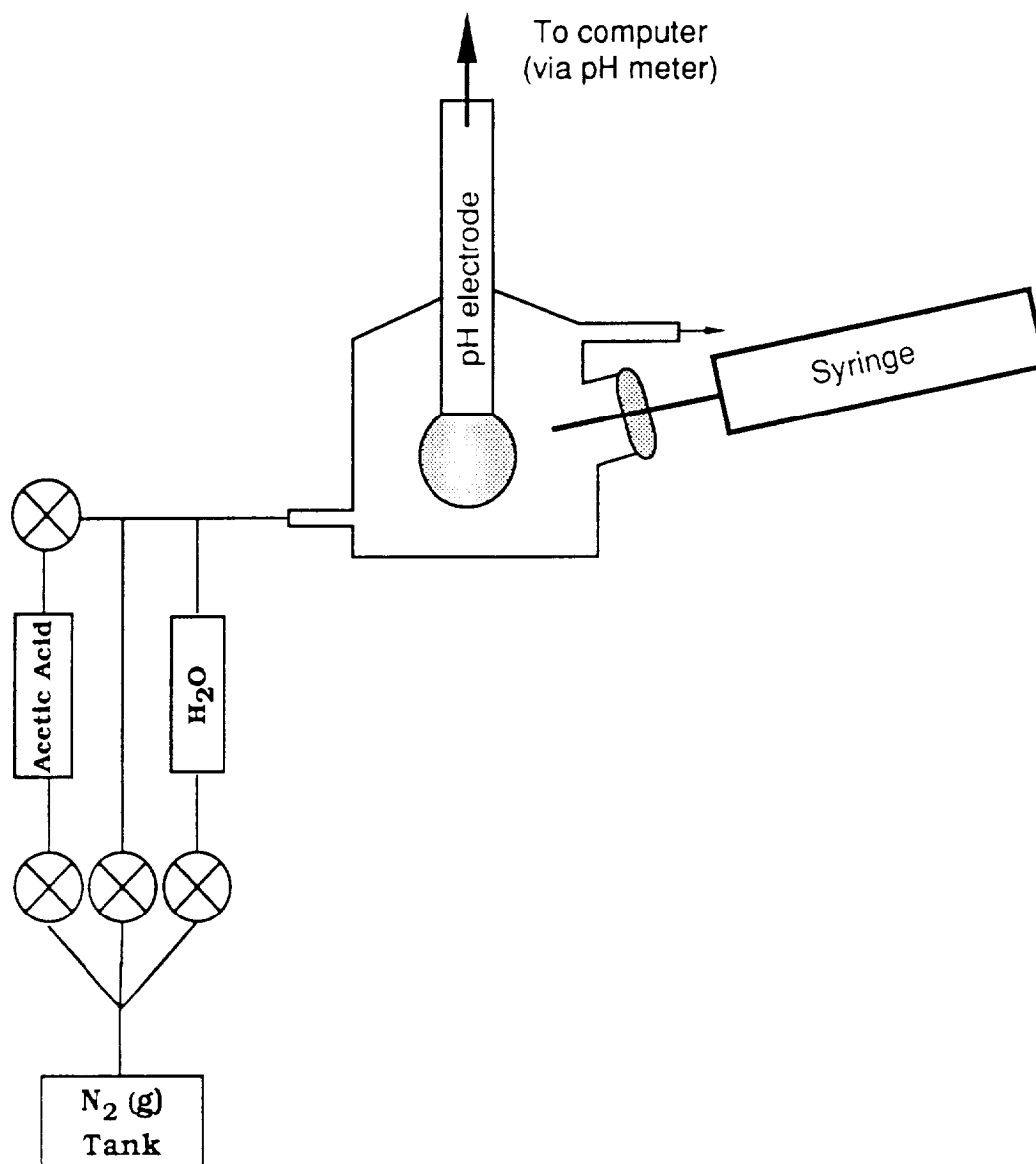
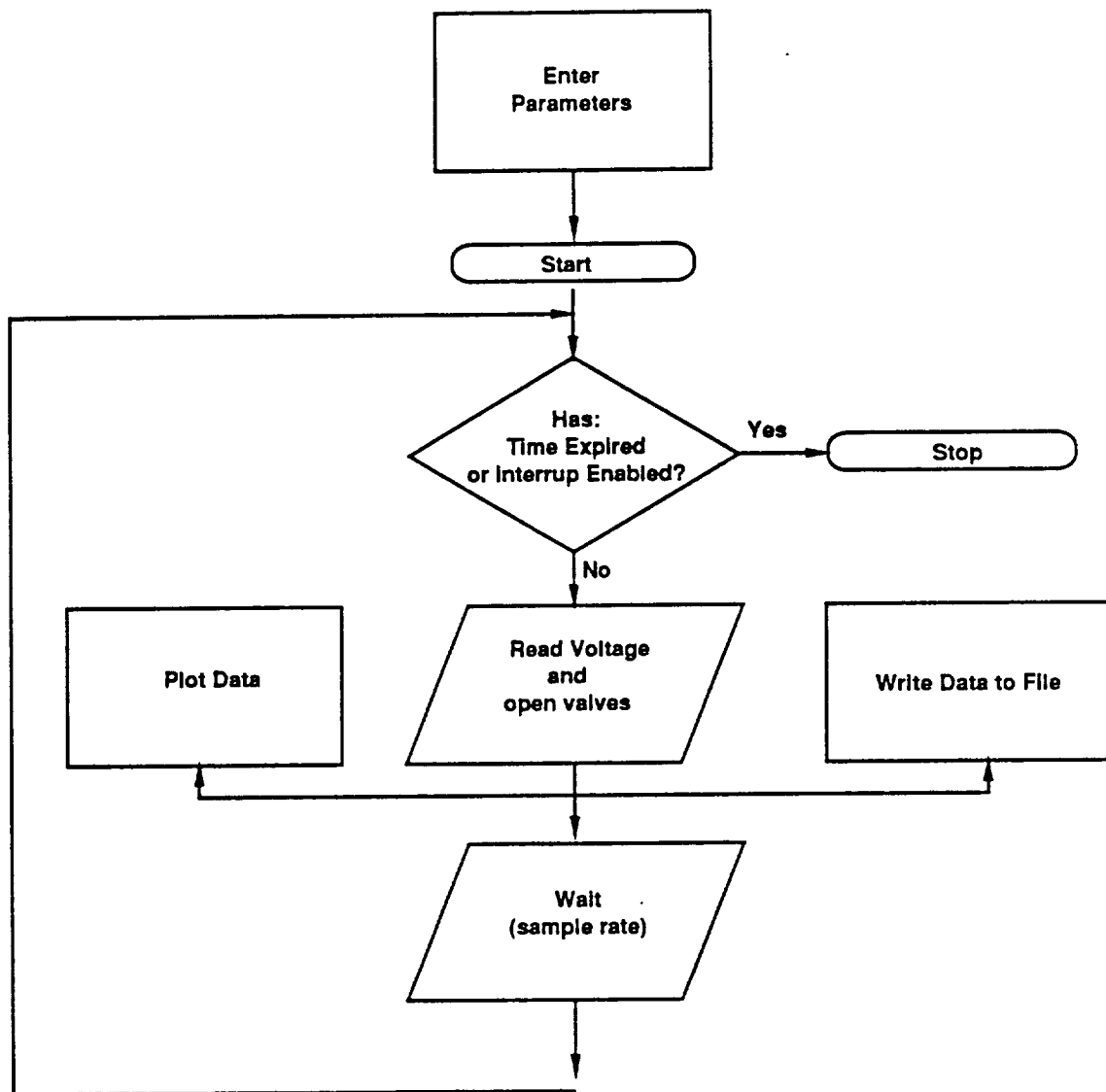


Figure 5. Schematic of arrangement for pH control of a hanging droplet.

The micro solenoid valves (LEE INSTAC, 2-way and 3-way normally closed) were computer controlled with digital output signals from the DIO1 to an Opto 22 PB16A Solid State Relay Board which converts digital signal to voltages for activation/deactivation of the solenoid valves.

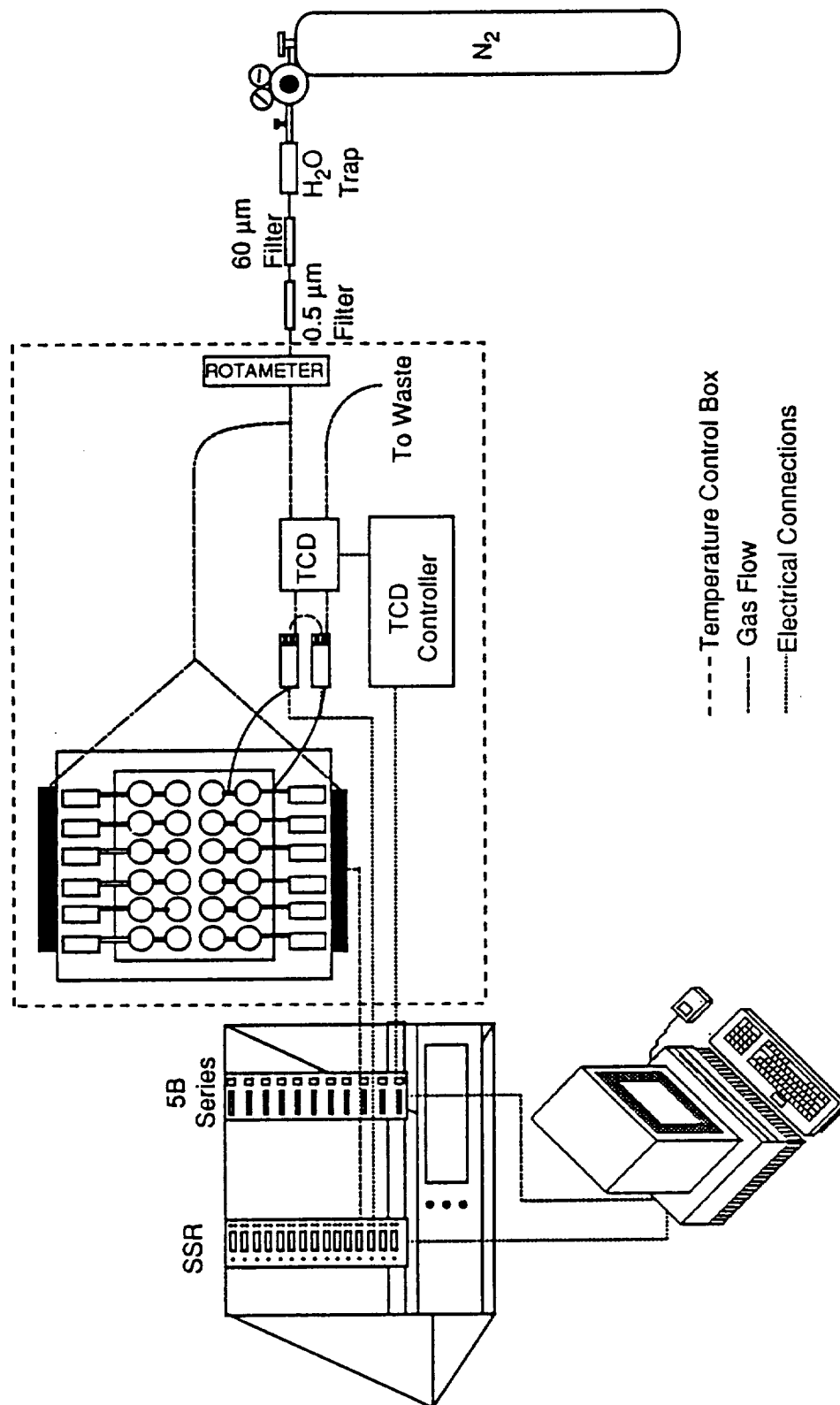
Software for pH Control

The software was developed with LabTECH Notebook, by Laboratory Technologies Corporation. A flow chart of the program logic is shown in Figure 6. One channel of analog input was set up to monitor the signal from the pH electrode. This analog signal was converted to pH using the calibration relationship shown in Chapter 5. The valves were controlled through a channel of digital output. The opening/closing sequence was determined by a waveform file of code developed prior to running the particular experiment. Thus, there was open loop control of the experiment. The experiment was either terminated manually or by time out. Upon termination of an experiment, a file with ASCII file format was created containing the data in single column format. This ASCII file was then able to be read in Lotus 1-2-3 for analysis and graphing. LabTECH Notebook was found to be limiting because of its channel structure. It was not flexible enough to have several decision making routines or set-point checks necessary for closed-loop control.



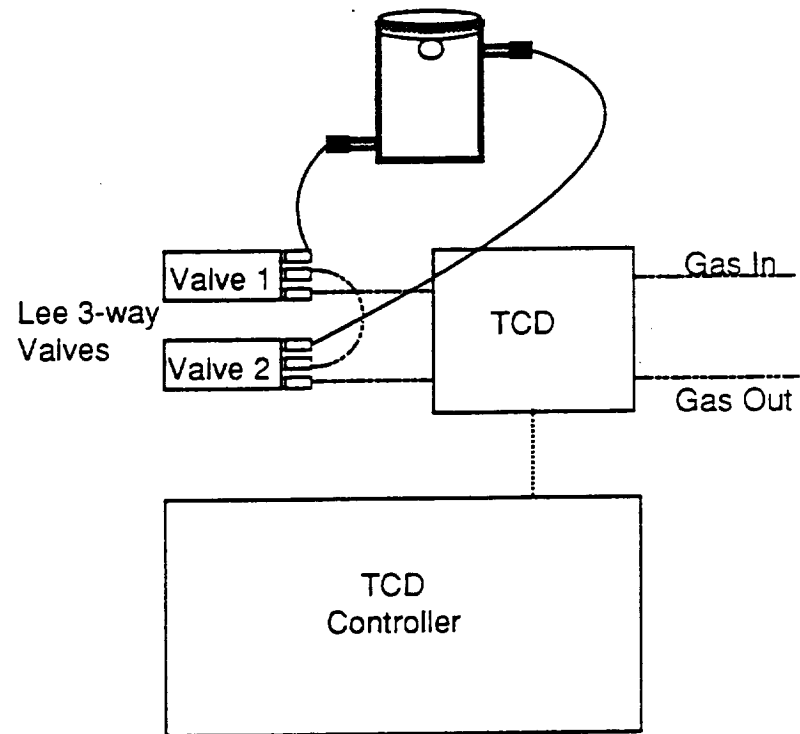
Hardware for Evaporation Control

The hardware for evaporation control went through a year of evolution before it was found to be satisfactory. Because of the rigidity of LabTECH Notebook, it was necessary to change to LabVIEW by National Instruments (Austin, Texas) [1] [2] [3]. This data acquisition language provided complete programing and supported Macintosh systems. There are five main parts to the device: (1) Gas Handling (2) Crystallization Chambers (3) Evaporation Control (4) Evaporation Monitoring and (5) Temperature Control and Monitoring. These individual components are described below in detail. Briefly, their arrangement is shown in Figure 7. A Macintosh II microcomputer was interfaced with a 5B Series Signal Conditioning Module (National Instruments) and an SSR Series PB24 Relay I/O Board (National Instruments). This provided for reading and conditioning of analog and digital input/output signals. The crystallization chamber was built in-house and allows 12 crystallization experiments to be individually controlled by the computer. The volume of water evaporated from the drop is determined by a microvolume thermal conductivity detector (TCD) (Gow-Mac Model 133 Bridge Water). The entire system is placed in a temperature control box that was also built in-house.



Gas Handling and Evaporation Control

Dry nitrogen gas was passed through three filters prior to entering the TCD or the crystallization chamber. The first filter contained CaCl_2 to absorb water. This was to ensure that the gas was dry before purging the chamber. There were two other filters in the gas line for removing particles. The first was a 60 μm filter (Nupro Company), followed by a 5 μm filter (Nupro Company). This ensured that no particulate matter which may be in the gas stream (greater than 5 μm) reached any of the system components or the protein drop. The flow rate was measured with a system of two rotameters one which measured flow rates from 0 to 1.5 mL/sec (Omega Engineering) and one that measured higher flow rates from 0 to 8.0 mL/sec (Omega Engineering). There was a constant flow of gas through the thermal conductivity detector in order to maintain a constant baseline when not in purge mode and to cool the filaments in the detector. The gas passed through the reference side of the detector to a three-way Lee valve (valve 1, Figure 8). Valve 1 allowed the gas to be directed to another valve (valve 2, Figure 8) or diverted to the chamber. Figure 8 shows the arrangement which allowed the gas to be diverted to the crystallization chamber. When valve 2 was activated, the gas was diverted through the crystallization chamber and the gas in the chamber (which contains water vapor) was directed through the sample side of the TCD. Since the thermal conductivity of

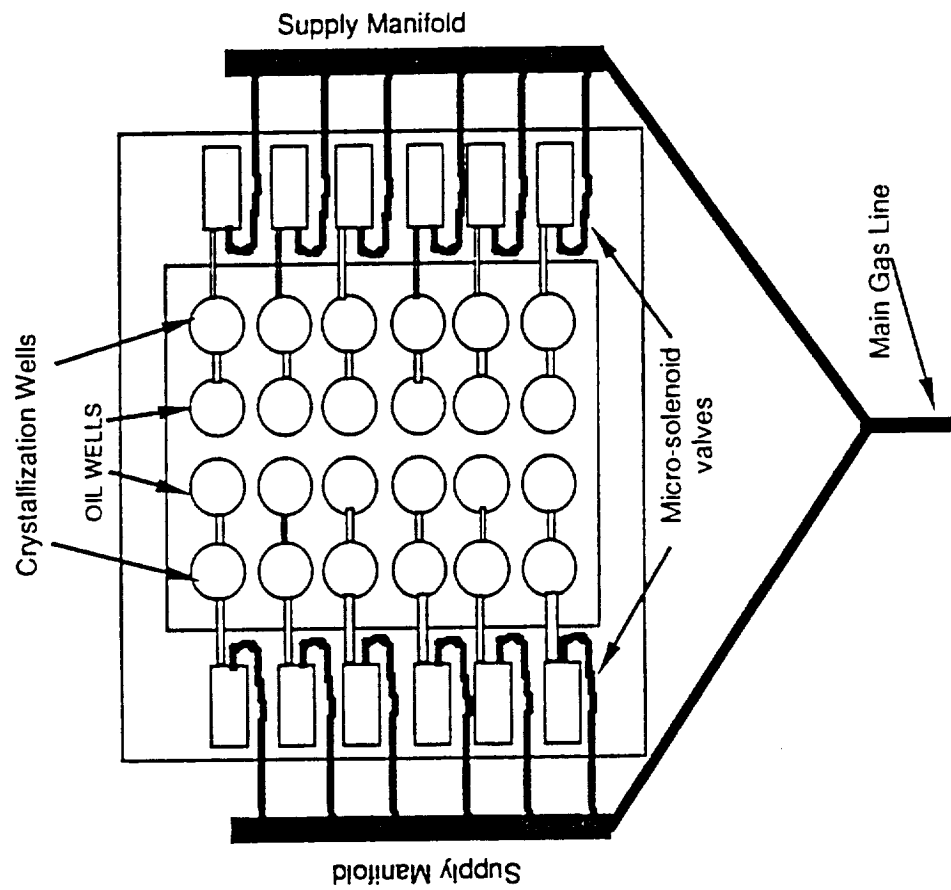


water-saturated gas is significantly different than the thermal conductivity of dry gas the wheatstone bridge in the detector is unbalanced. The amount of imbalance is proportional to the amount of water in the gas stream. This can be calibrated back to the amount of water that has been evaporated from the drop. For a review of the quantitative use of a thermal conductivity detector see [4]. The TCD was connected to only one of the 12 crystallization cells. Since the flow rate was found to be equal ($\pm 1.3\%$) in each cell the evaporation of a drop within each cell will be equal.

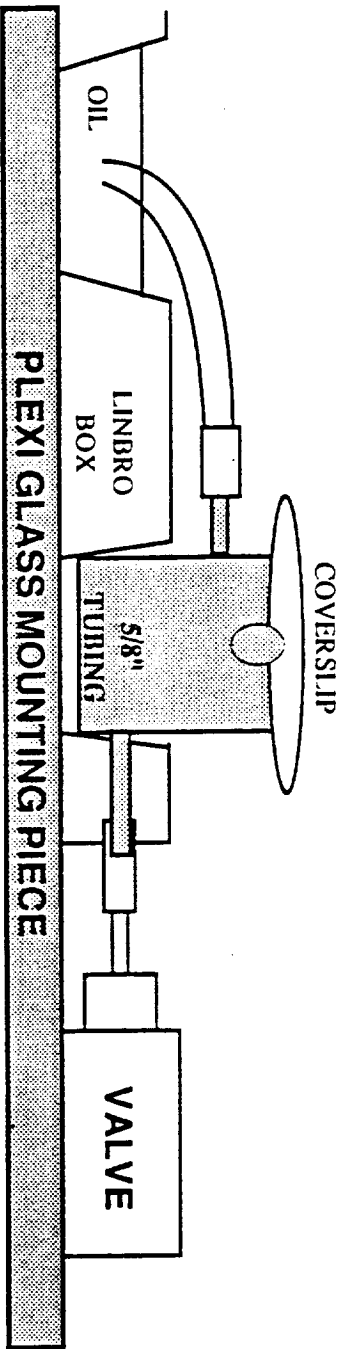
Each valve was electrically connected to a relay on the SSR Series Relay Board which was in turn connected to the NB-DIO-24 Board (National Instruments) inside the computer (Figure 12). In a similar manner, the thermal conductivity detector was connected to a 5B40-02 module on the CB5 Board where its 0-40mV signal was amplified to a 0-5 V signal before A/D conversion on the NB-MIO-16 Board (National Instruments). This set-up provides the most protection from noise interference.

Crystallization Chambers

Initial attempts to build a chamber that was air and moisture tight failed. The first chambers were machined out of plastic materials (lexane, plexiglass and polystyrene). Leak tests were run on each prototype by measuring the conductivity of a NaCl drop before and



after it was allowed to sit for an extended time period. Water vapor was found to permeate, adsorb and/or absorb with most of the plastics that were used. This was found to be in agreement with reports in the literature [5] [6]. Not until a glass cell was made were any of the leak tests successful. The final version is shown in Figure 9. It is an adaptation of a Linbro Tissue Culture Plate. The plate is made of polyethylene and has 24 wells. Glass inserts were made out of 5/8" Pyrex glass tubing. These glass inserts friction fit into one of the Linbro wells. Thus, the Linbro box only served to support the glass cells. Gas inlet and outlet tubings (2mm glass tubing) were attached so that the gas flowed in at the bottom of a cell and out at the top. This geometry assured that the gas would fill the cell and flush it out most efficiently. The outer wells of the Linbro plate were modified to hold the glass cells (Figure 10). Microbore tygon tubing was used to connect the inlet tube to the solenoid valve and the outlet tube to the oil well. The oil prevented the atmosphere from entering the cells. Solenoid valves on the exit tube were tried but it was found it was difficult to synchronize opening and closing of the valves which caused back pressure problems. To do a crystallization experiment a protein drop is placed on a silanized microscope cover slip and sealed to the cell with Dow Corning vacuum grease or other low vapor pressure greases.

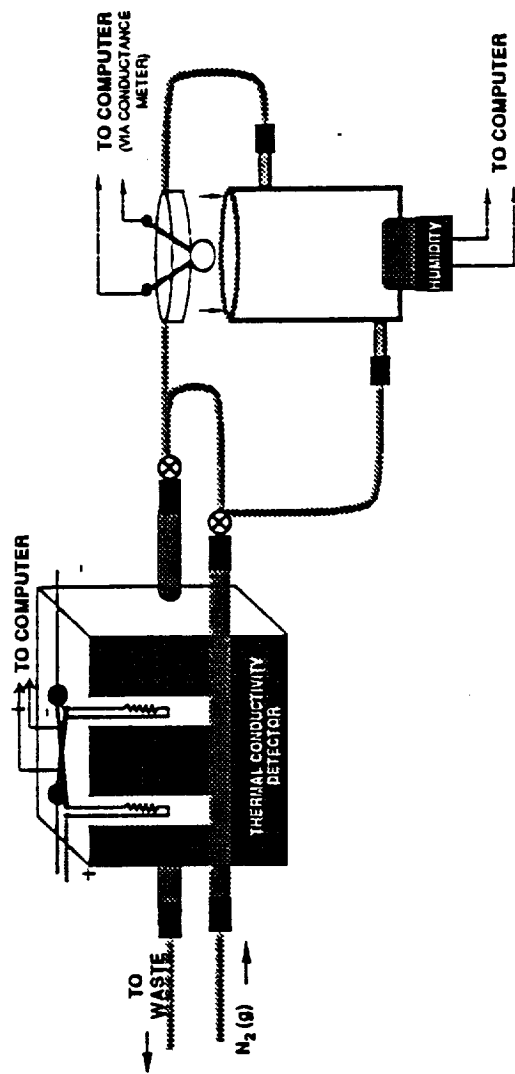


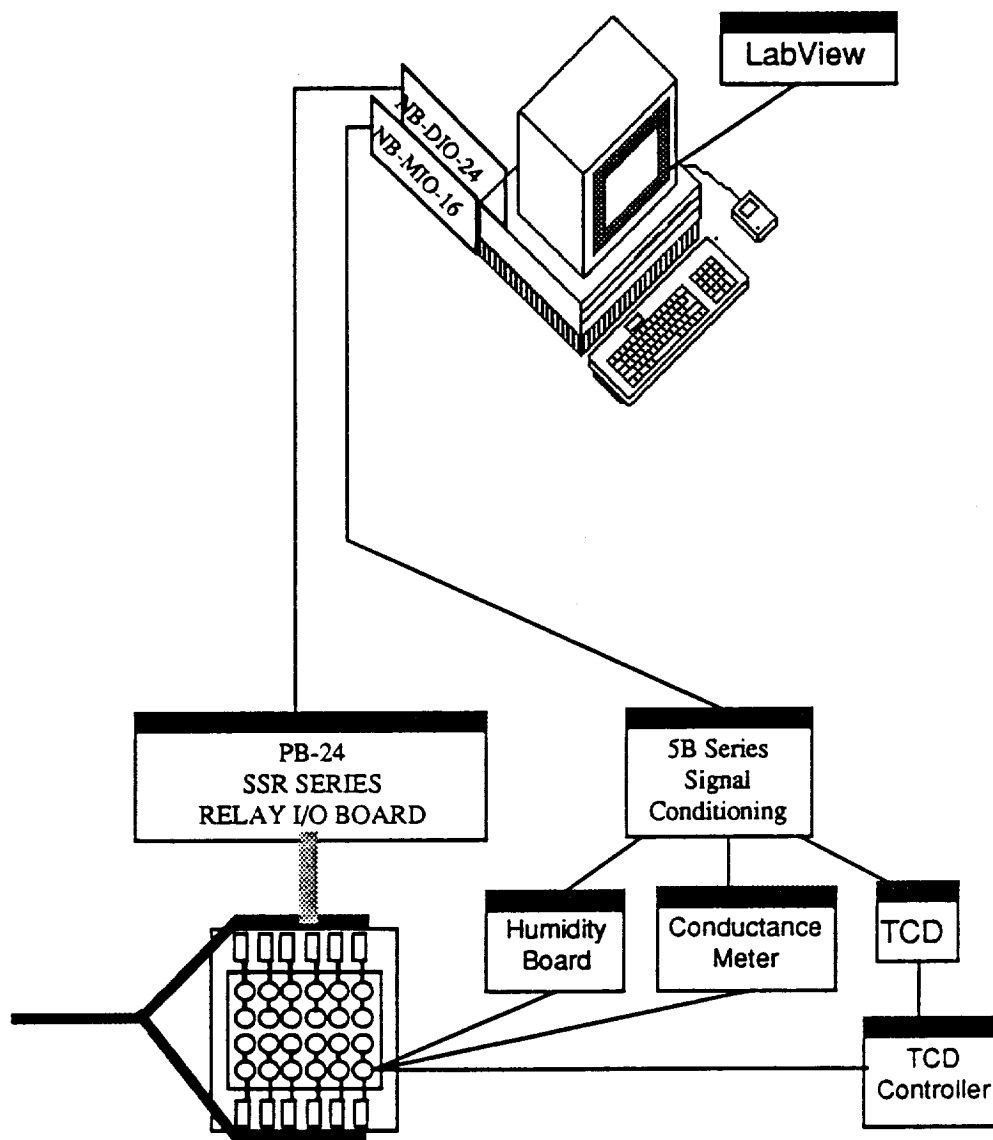
Evaporation Monitoring

Several different approaches were taken to monitor the evaporation of solvent from the drop. The most successful techniques are discussed here while the less successful attempts are discussed with limited detail in Appendix 1.

- (1) Thermal Conductivity Monitoring of Gas Stream (above)
- (2) Relative Humidity Monitoring Inside Chamber
- (3) Continuous Monitoring of Solution Conductance
- (4) Periodic Conductance Measurements with
Micro Conductance Cell (Appendix 1A).
- (5) Periodic Refractive Index Measurement (Appendix 1B).
- (6) Gravimetric Analysis of Drop Volumes (Appendix 1C).
- (7) Chloride Ion-selective Electrode (Appendix 1D).

Relative Humidity Monitoring Inside Chamber. The relative humidity of the air inside the crystallization chamber was measured with a miniature humidity indicator (Thunder Scientific, Model XX) that was epoxied to the bottom of the glass cell (Figure 11). The humidity indicator was connected to its circuit board whose signal was then passed to a 5B41-05 \pm 5V signal conditioning module where the voltage was amplified before A/D conversion with the NB-MIO-16 Board (Figure 12).





Continuous Monitoring of Conductance. The concentration of salt in the protein solution was determined by measuring the conductivity of the solution. Since the protein and salts in solution were non-volatile, the conductance of the salts in solution could be used to determine the concentration of salt in solution and changes in concentration can be related to the amount of water evaporated from the drop. A Plexiglass disc (1/4 inch thick, 1 inch diameter) was modified by adding two 24 gauge platinum wire electrodes 2 mm apart. A drop containing the protein and precipitant was suspended from the Plexiglass coverslip making sure that both electrodes were covered with solution. The Plexiglass disc with electrodes is also shown in Figure 11. A YSI conductance meter was connected to the electrodes and to the 5B40-02 on the signal conditioning board (through the recorder output) and then to the computer through the NB-MIO-16 multipurpose board (Figure 12). This signal was related to a previous calibration (Figure 60, Chapter 6).

Temperature Control and Monitoring

The temperature of both the TCD and the crystallization chamber was controlled with a temperature control box (Figure 13). The box was made of 1" plywood and used thermostated water from a Lauda Water Circulator to control the temperature. The water was circulated through a car radiator while air was forced over the radiator. When

the circulator was set at room temperature (23°C) the temperature remained constant in the box to ± 0.2 °C. The temperature was monitored at several locations in the box with T-type thermocouples. The thermocouple was connected to a 5B37-T-03 Module which provided linearized cold junction compensated responses to the computer.

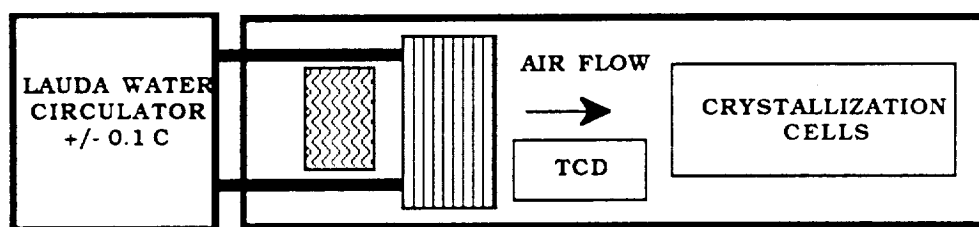


Figure 13. Temperature control box.

Software for Evaporation Control

The software used in this system was written using the graphical programming language LabVIEW. This language uses graphical icons representing subroutines which are linked together to form higher level routines. The library of subroutines includes the fundamental functions needed in the course of programming. Any needed routine that is not already available can be created from existing routines.

Structures also exist for performing repetitive operations such as for/next, while, and sequence loops.

This particular programming language has several inherent features which makes it useful in a research environment. The logic of the programming itself is much easier to devise and follow than text based languages. As a result of these advantages, the time required to write an extensive program is greatly reduced. For this system, the time required to get the software up and running was only a few weeks. Another useful feature of LabVIEW is the ease with which the program can be modified to meet the newest needs of the user. Any newly required functions can be written as a subroutine and then inserted into the code wherever it is needed. The software written for this system went through several evolutions as new features to the system were added.

Front Panel

The language is divided into two parts. The outermost level, called the Front Panel, is the user interface. This level allows the user to enter the experimental conditions prior to running the program. The specific evaporation method to be used is specified in this level and the appropriate software subroutines are enabled. This level also has real time displays for monitoring the progress of the experiment. These include the evaporation profile that the experiment is following, the total amount of water evaporated from the protein solution at any

INPUT PARAMETERS

Final Unit: 10.0000
 DESIGNED RUN TIME (HRS): 500.000
 VALUE CLOSE TIME (SEC): 75.000
 VALUE OPEN TIME (SEC): 10.000

EQUATION

$N = .000227m$

EVAPORATION CURVE

FILE STORAGE

PROG DISK: CACA.DAT
 FILES: 10/12.mml

FILE NAME

PROG DISK
 VALUE NAME

CURRENT CACA Panel

CA CA

OUTPUT PARAMETERS

computed
 and uncalculated
 crystallization
 appeared as



REMARKS

IN PAPER MODE

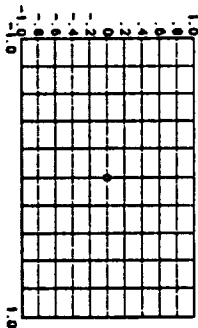
PAPER TIME (days): 000.000

TIME (SEC) TIME (MIN): 0079 0079

TIMING:



Evaporation Curve



WHEEL LINE

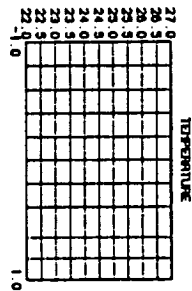
VALUE TIME

TEMPERATURE LOOP

TEMPERATURE OUTPUT (W)

ERROR(S)

FILE WRITE ERROR

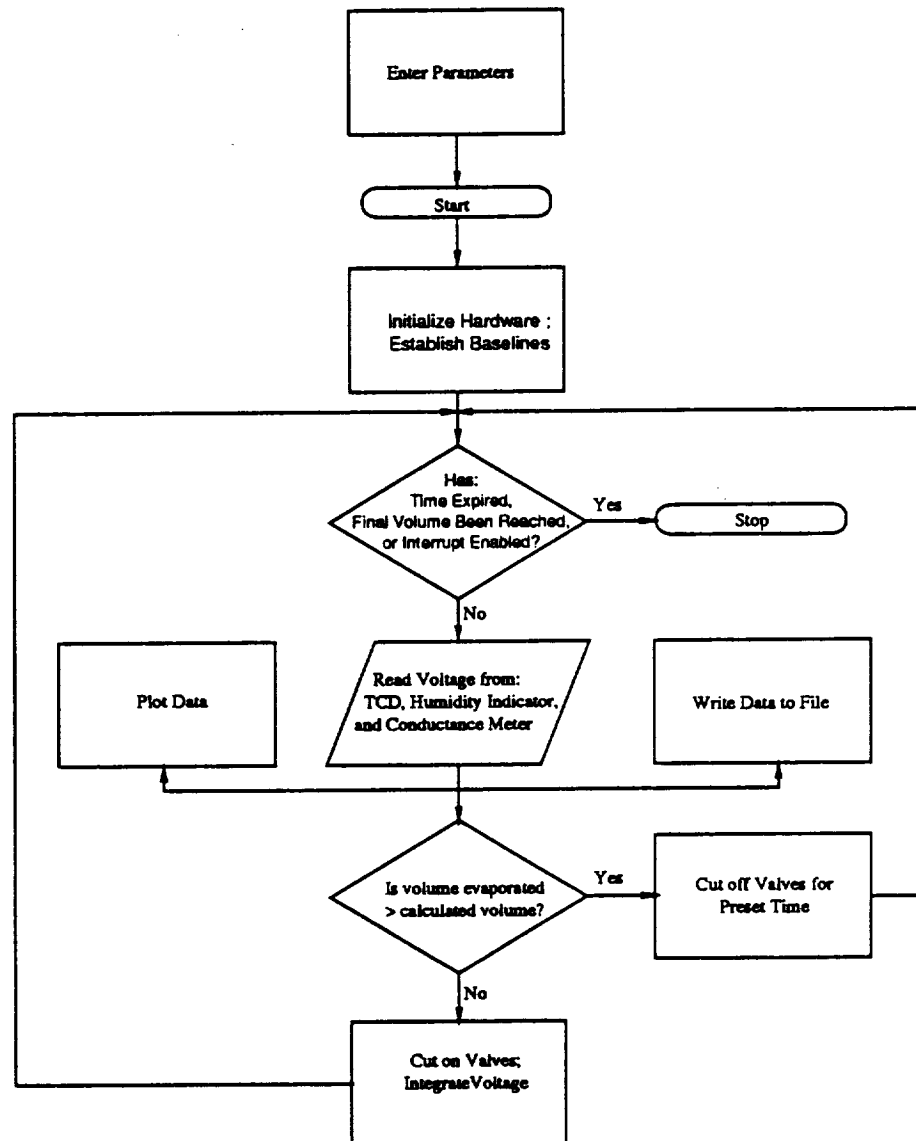


given time, temperature and any errors that may have occurred. The Front Panel used in this system is shown in Figure 14. As mentioned earlier, this level is where the user can interact with the software and is the only level one ever needs to see. It was set up to allow someone with only minimal knowledge of computers to enter parameters and perform experiments using this system.

Diagram

The second part of the software is the Diagram. The diagram is where the program is coded and is normally invisible to the user. The code itself looks very similar to a flow chart which is useful in programming. The individual subroutines are obtained from a library, which contains the basic functions typically used in programming, or are custom written by the programmer. These routines are linked together with "wires," which direct the logical flow of data from one routine to the next. Errors in the course of programming are corrected through an interactive debugger. The language returns any error with a "broken wire." This designation indicates that an improper connection has been made. The program actually will not execute until all broken wires have been removed or repaired.

The software used in this system was divided into several individual functions and coded through a sequence structure so that the routines would be executed in a specific order. A description of these functions, their individual operation, and a diagram of each routine are given below. A flow chart of the logic of the entire program is shown

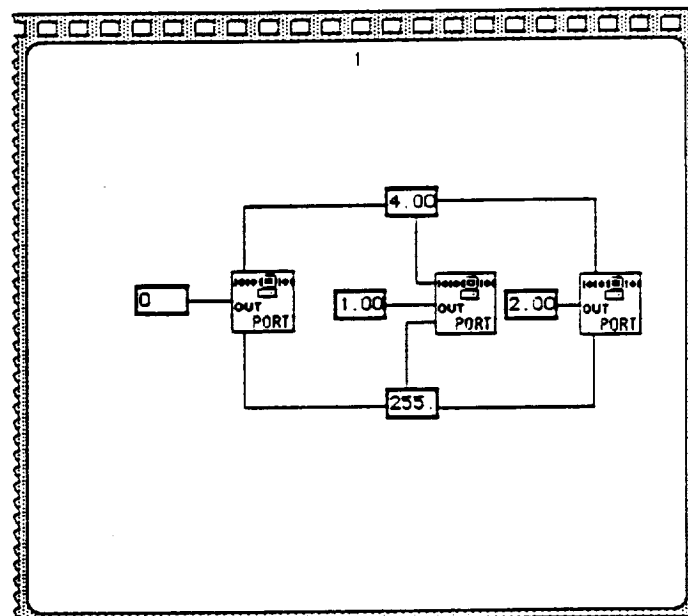
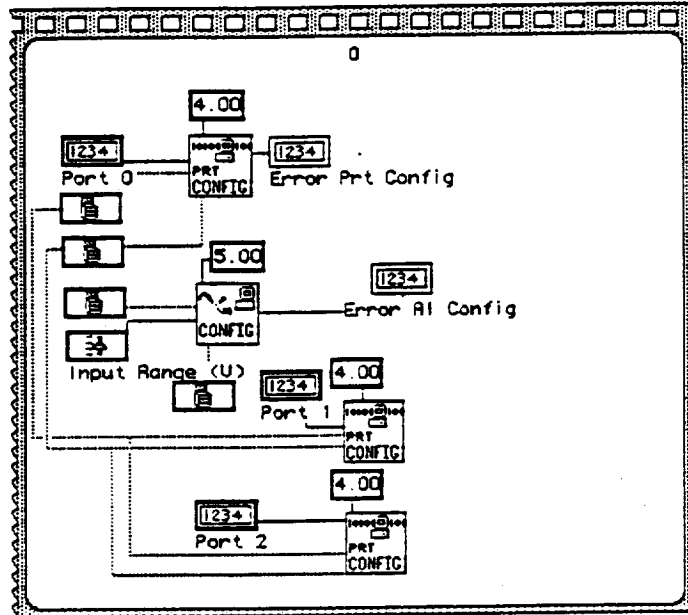


in Figure 15. The entire working code of the program is listed in Appendix 2.

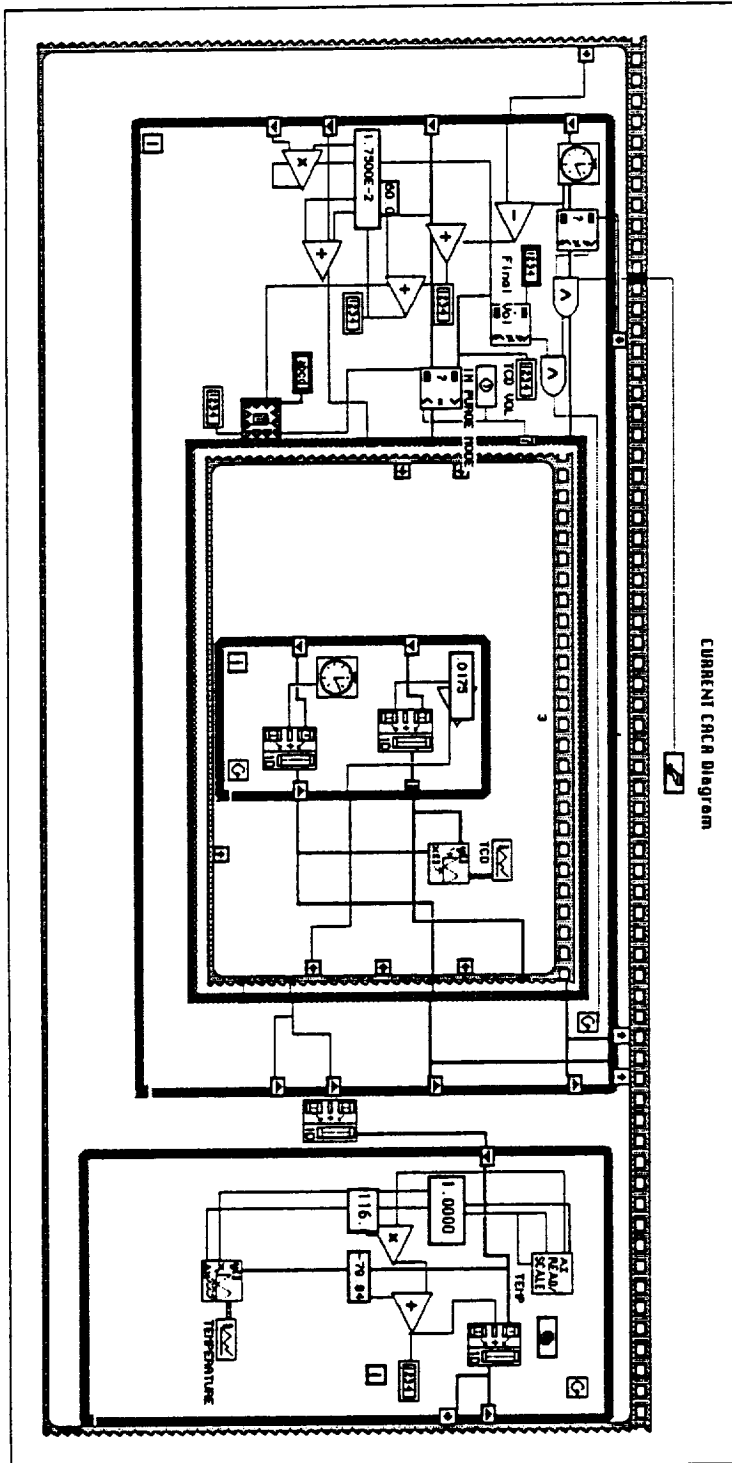
Initialization. The first operation performed by the software was to initialize all of the internal and external hardware. This routine was necessary to ensure that all of the hardware was in its starting configuration. The code for performing this operation is shown in Figure 16. The multifunction board inside the computer was configured to allow analog inputs and outputs. The three ports on the digital board inside the computer were configured as outputs. The starting time is recorded in computer tick counts and converted to seconds (60 ticks/second).

Evaporation Control and Monitoring. The evaporation while loop executes only if the time limit of the program has not been exceeded (Figure 17). The program compares the length of time the experiment is set to run with the time elapsed since the program was started. If the time the experiment has run has not exceeded the total time, then a true output is sent to a logical "and" function. If the length of the experiment has been exceeded, then this routine terminated and the data arrays which were accumulated were sent to the next subroutine which writes the data to file.

The next function accumulates a baseline reading from the TCD which is used in the first iteration of the while loop (Figure 18). Establishment of the baseline in each iteration was done to



CURRENT CRCA Diagram



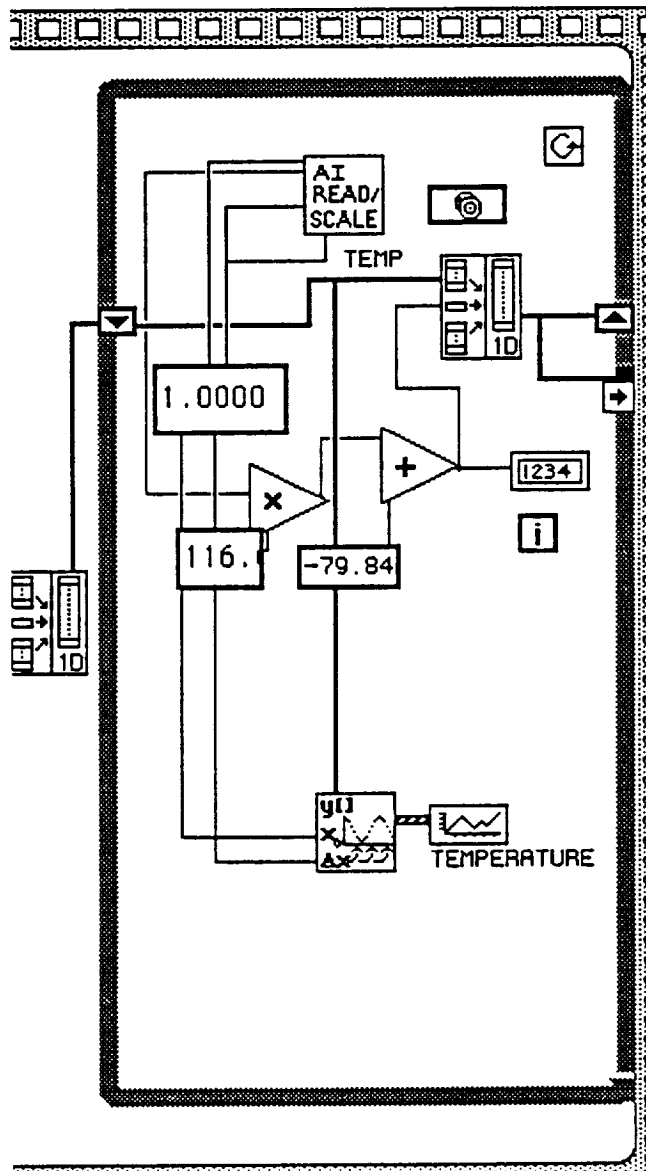
compensate for any drift in the TCD baseline. Then, a comparison is made on the total integrated voltage read from the TCD, converted to volume from a previous calibration, with the desired volume determined from the evaporation profile equation from the Front Panel. If the total volume evaporated is greater than the equation output, then the valves remained closed for a set period of time determined from the Front Panel. If the total volume evaporated is less than the equation output, then a baseline reading is obtained before the chamber is purged. The chamber was purged for a preset time that depended on the volume of the cell to be purged and the flow rate of the gas. This loop was repeated until the final volume to be evaporated was reached or the time expired.

Temperature Monitoring. Simultaneously with the evaporation loop, the temperature within the control box was recorded with the while loop in Figure 19.

Humidity monitoring. When appropriate, humidity was monitored using the humidity reader subroutine shown in Appendix 2.

Conductance monitoring. A similar subroutine was used to monitor conductance and is also listed in Appendix 2.

Termination and File Storage. The final function that the software performed was to write the accumulated data to a file (code shown in



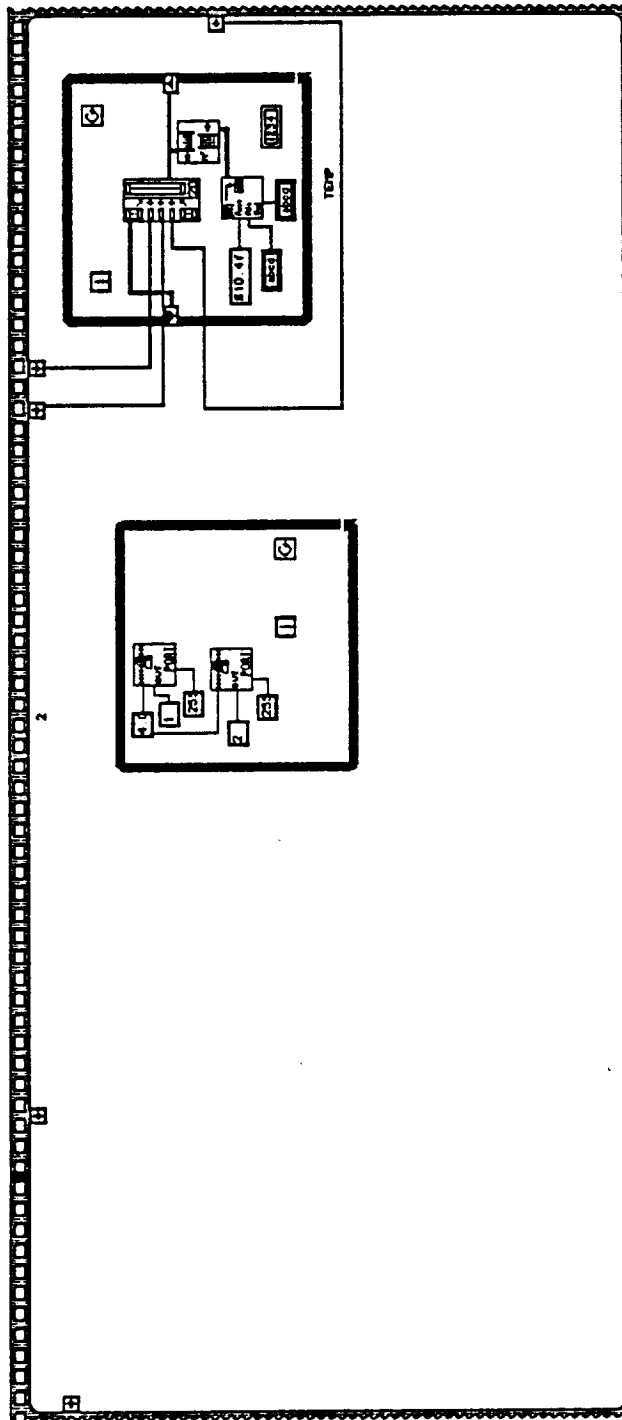


Figure 20). The data, which had been accumulated in arrays, was combined into a matrix, transposed, and saved as a spreadsheet file. This allowed the data to be accessed with Cricket Graph or Microsoft Excel for graphing and data manipulation.

SELECTED REFERENCES

- [1] Graham, Glen (1989) In Tech, September, 40-43.
- [2] Wolfe, Ron (1988), Electronic Products, February Edition, 27-32.
- [3] Dehne, Tim (1989) Electronics Test, September, 19-26.
- [4] Lawson, Alexander and James M. Miller (1966) J. of G.C., August Edition, 273-284.
- [5] Doty, Paul M, W.H. Aiken and H. Mark (1946) Journal of Industrial and Engineering Chemistry, **38**, 8, 788-791.
- [6] Rodriquez, Ferdinand (1989) *Principles of Polymer Systems*. (Hemisphere Publishing Corporation, NY) 404-403.

CHAPTER III

PURIFICATION OF HEN EGG WHITE LYSOZYME

Introduction

The importance of protein purity in crystal growth studies cannot be understated. The problem lies not in reproducing crystallization conditions but in isolating a protein preparation whose composition is uniform each time. While the actual preparation of a protein for crystallization is simple once the conditions are known, isolation and purification procedures are difficult to reproduce. It is not uncommon that one preparation will yield crystals over a wide range of conditions while other preparations will not. Commercial preparations frequently contain salts, preservatives and other additives that are not specifically stated. Furthermore, the composition of the desired protein and protein impurities will vary with different batches. However, commercial preparations are a convenient source of protein. For this reason, hen egg white lysozyme was purchased from Sigma Chemical Company and Calbiochem Corporation. It was further purified by a number of techniques. This approach allowed pure protein to be obtained from a commercial source.

Materials and Methods

Hen egg white lysozyme was purchased from Sigma Chemical Company (Grade I, Lot 46F-80602 and Lot 46F-8060) and Calbiochem (Lot 901411). *Micrococcus Luteus* was from Calbiochem. Spectra/Por dialysis membranes were purchased from Spectrum Medical Industries with molecular weight cutoff (MWCO) of 15,000 (wet tubing #132121) and 6,000-8,000 MWCO (dry tubing #132660). Buffer reagents were Fisher Certified ACS. NaCl was Baker Analyzed Reagent grade. Deionized water (Barnstead Nanopure II), 0.2 μm filtered, was used for all solutions. Samples were also filtered with Gelman Sciences Acrodisc disposable filter assembly (0.2 μm). Electrophoresis reagents were Pharmacia. Precast gels (PhastGel Gradient 8-25 and PhastGel IEF 3-9) with 6-8 lanes were purchased from Pharmacia along with the SDS Buffer Strips. Pharmacia's Electrophoresis Low Molecular Weight Calibration Kit was used for protein standards. Comassie blue development of the gels used PhastGel Blue R tablets from Pharmacia. Silver stain development used silver nitrate and reagents from Fisher.

SDS-PAGE

Sodium dodecyl sulfate-polyacrylamide gel electrophoresis (SDS-PAGE) was performed with the PhastSystem (Pharmacia LKB Biotechnology AB) according to the manufacturer's recommendation.

Samples were dissolved in a buffer containing 10mM Tris (HCL), pH 8.0, with 1mM EDTA, 2.5% (w/v) SDS and 2.5% 1,4 dithiothreitol. Comassie Blue staining of the gels was performed in the Development Unit of the PhastSystem. The silver stain development procedure used is shown in Figure 21. Dilutions were made from a purified lysozyme solution to determine the detection limit of the silver stain technique for lysozyme.

Isoelectric Focusing

To separate the proteins in the Sigma lysozyme according to their isoelectric points isoelectric focusing (IEF) with the Phast System was used according to the manufacturer's recommendations. Samples were dissolved in a 0.01M phosphate buffer at pH 8.00 to a total protein concentration of 2.0 mg/mL. Comassie Blue staining of the gels was performed in the Development Unit of PhastSystem.

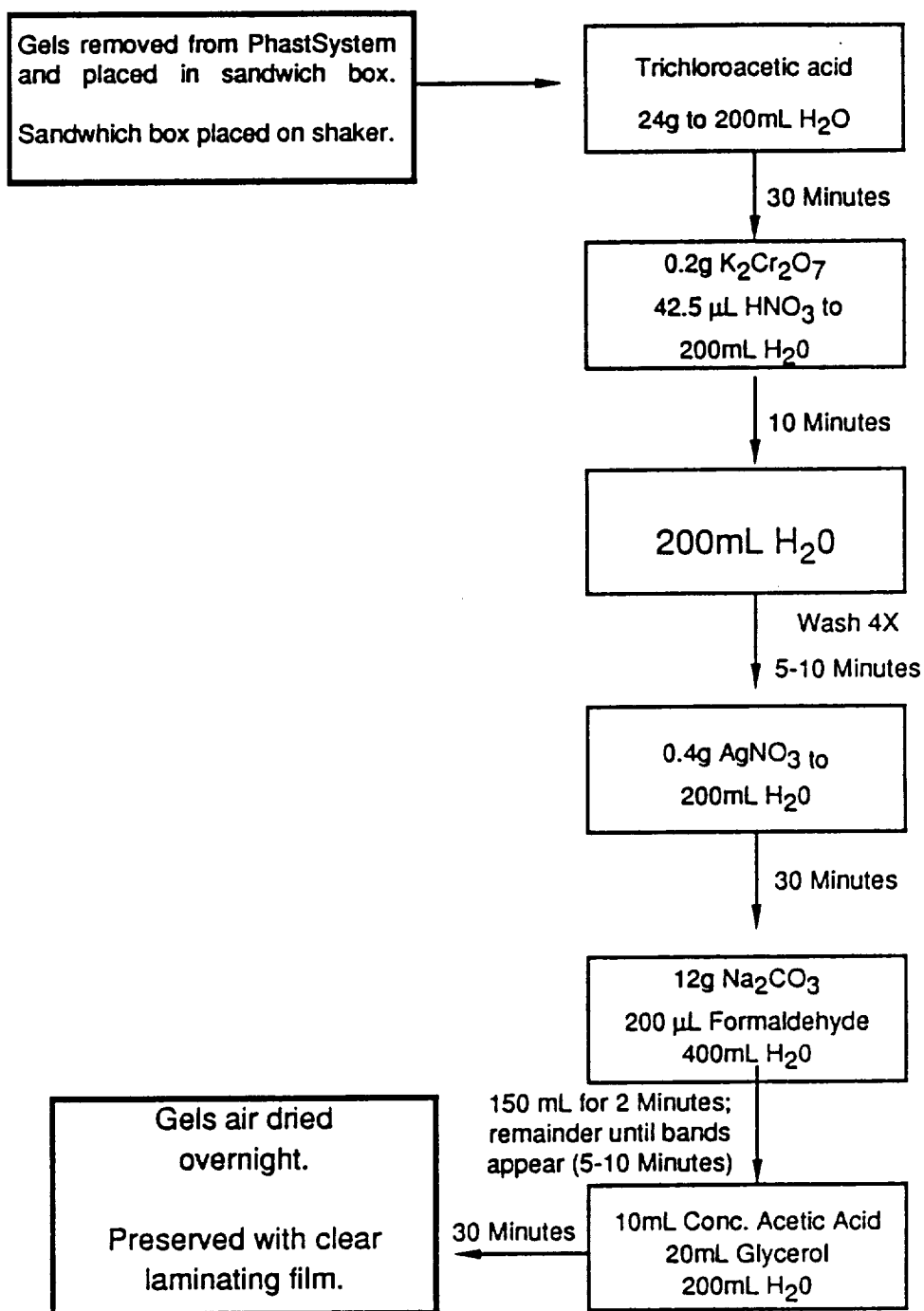
Lysozyme Activity Assay

To analyze the purity of a lysozyme solution the relative activity of the solution was measured against a pure lysozyme solution. Since lysozyme is known to lyse micrococcus luteus cells its activity on these cells can be used to assay the purity of a protein solution. The concentration of a micrococcus luteus suspension was adjusted by dilution with 0.01M phosphate buffer pH 8.00 until the A_{450} was

approximately 0.100. 3.0mL of this solution was placed into a disposable polystyrene cuvette and the signal allowed to stabilize. The purified lyophilized solids (standard) and the unknown lyophilized solids were made to a concentration of total protein of 2.5 mg/mL in 0.01M phosphate buffer pH 8.00. 210 μ L of the standard and unknown were added to separate cuvettes containing the *Micrococcus luteus* suspension and the cell was mixed by inversion. The absorbance of the mixture was monitored for several hours and the rate of decrease in the absorbance was calculated from the slope. Comparison of the two slopes yielded an estimation of the purity of the unknown sample.

Ion Exchange Separation

Fast Protein Liquid Chromatography (FPLC) was used to separate the Sigma and Calbiochem lysozyme from protein impurities. The components of the HPLC system were all purchased from Pharmacia LKB. They are: (1) LKB 2152 HPLC controller (2) LKB 2151 Variable Wavelength Monitor (3) LKB 2156 Solvent Conditioner (4) LKB 2150 HPLC Pump (5) LKB 2210 Recorder. A 2.0 mL sample loop was used giving sample volumes from 0-2.0 mL. A Mono S HR 5/5 and a HR 10/10 pre-packed strong cation exchange column (Pharmacia) was used for the separation. Initial experiments were performed on the Mono S HR 5/5 column with scale up procedures on the HR 10/10.

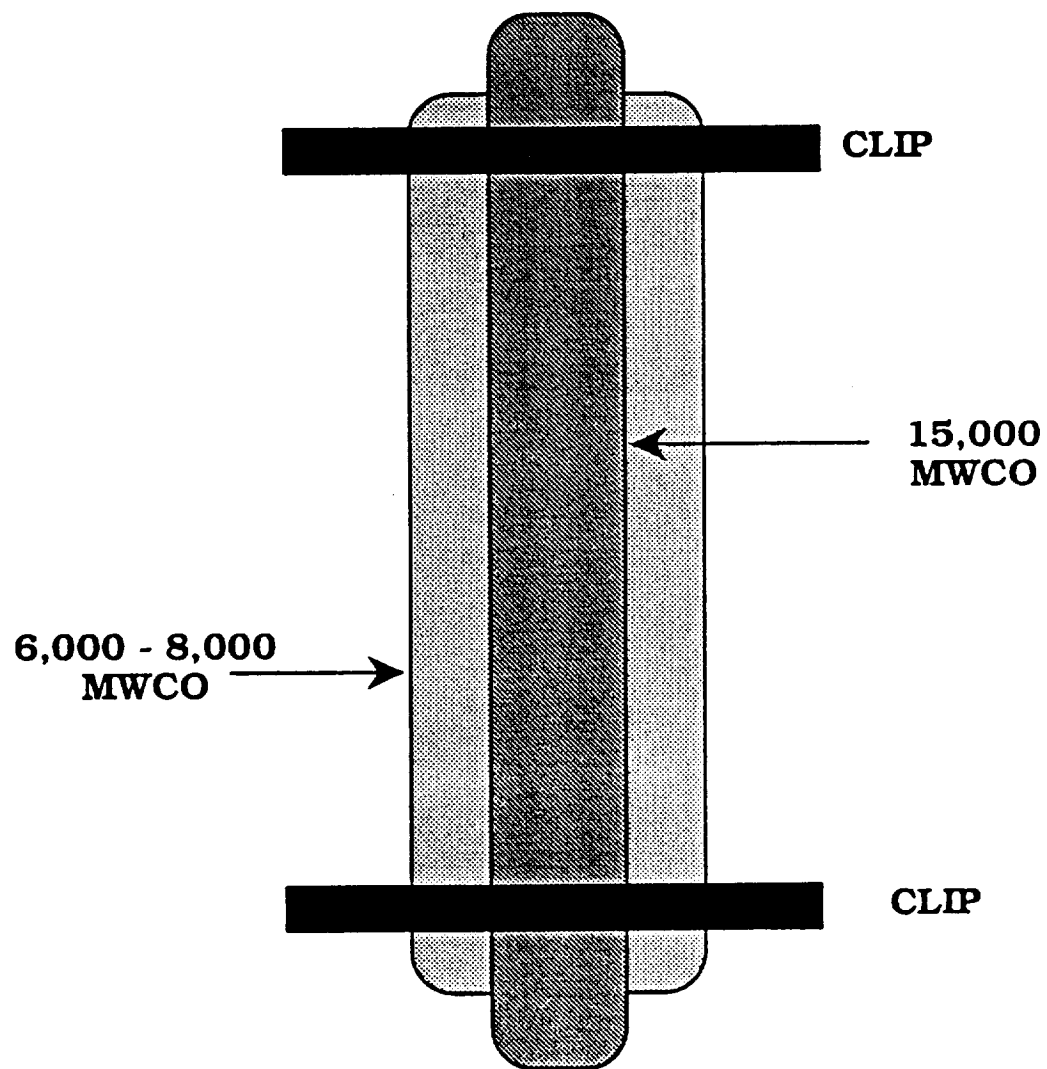


Solvents were A: 0.01M Phosphate pH 7.10 B: A+1.0M NaCl. Heart cuts of the individual peaks were analyzed with SDS-PAGE to determine their molecular weight.

Membrane Separation

Proteins can be separated from small molecules by dialysis through a semipermeable membrane, in which the protein is retained inside a dialysis bag while the smaller molecules and ions diffuse through the pores and emerge outside the bag. This technique is used most frequently to remove salts and buffers from protein solutions. Membranes can also be used to separate proteins of significantly different molecular weight. Impurities were separated from lysozyme (MW=14,400 daltons) using two dialysis bags (Figure 22). Five milliliters of an 80 mg/mL sample was placed into a 32 cm bag of 15,000 MWCO dialysis tubing. The tubing was sealed with knots and inserted into the 6,000-8,000 MWCO tubing. Deionized water was added to the outer bag so that the level was approximately 3/4 of the length of the bag. The outer bag was sealed with closures so it could be reopened to remove fractions. The double bag was then placed in 4 L of deionized water and allowed to stir at 8-10°C. The deionized water was replaced daily.

The amount of lysozyme in the outer bag was monitored daily by measuring the absorbance of the solution at 280 nm using an absorption coefficient ($A^{1\%1cm}$) of 26.5 [1]. The volume of solution

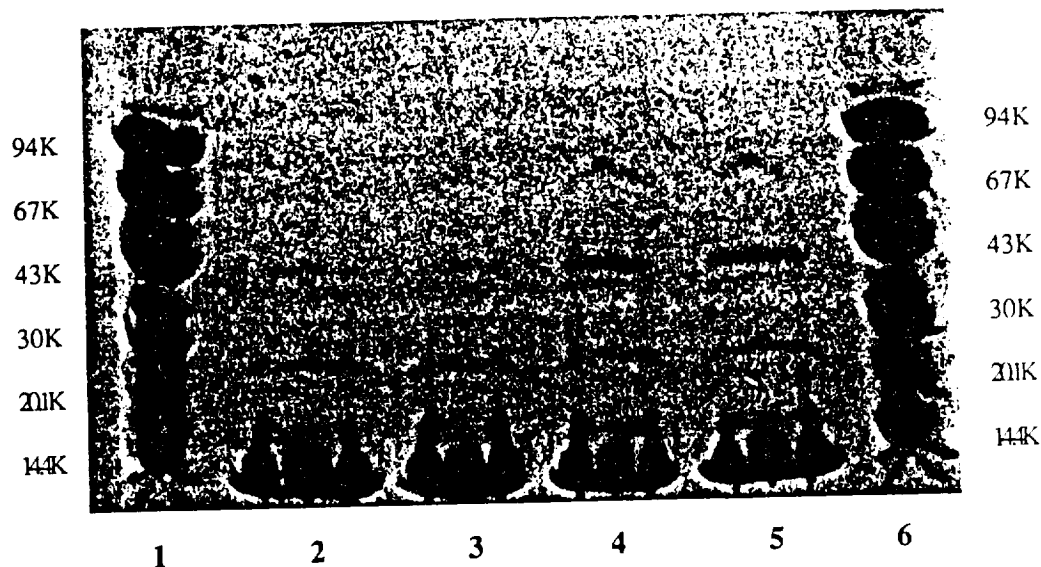


in the outer bag was estimated by measuring the length of the liquid column in the bag and multiplying this by the capacity rating of the bag (0.32mL/cm). SDS-PAGE with silver staining development was used to check the protein composition of the solutions in the inner and outer bags. Before SDS-PAGE the samples were lyophilized with a LabConoco bench top lyophilizer and weighed to ensure equal concentration of total protein.

Results and Discussion

SDS-PAGE on the unpurified lysozyme from Sigma revealed a total of five bands (Figure 23). The molecular weights of the bands were determined using a log MW versus R_f plot (Figure 24). They were found to be 14.6K (lysozyme), 17.5K, 27.8K, 46.8K and 77.9K. Calbiochem lysozyme was analyzed using the same procedure and was found to contain only the 17.8K and 14.4K bands (Figure 25). Both Sigma and Calbiochem samples were separated on the Mono S HR 5/5 column with a step-wise gradient (Figure 26 and 27).

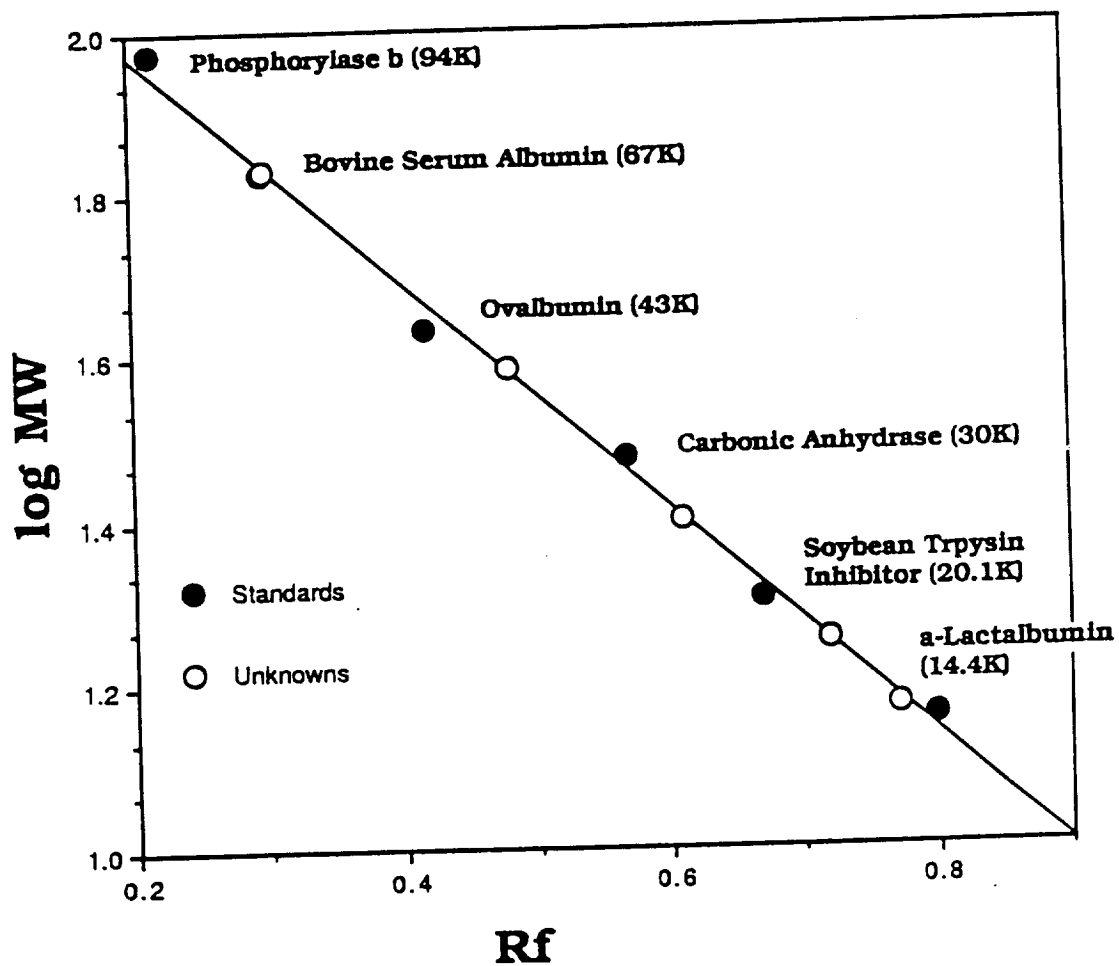
Fractions of the Sigma chromatogram were collected and run on the PhastSystem to determine their molecular weights. The samples were too dilute to be seen by the comassie or silver stain development. A concentration step was added and four of the peaks were able to be identified. The 3rd peak was found to be the 17.8K impurity. The 4th and 5th peaks were both lysozyme and the 6th peak was the 25K protein. Peaks 1 and 2 were too dilute to be identified and efforts to

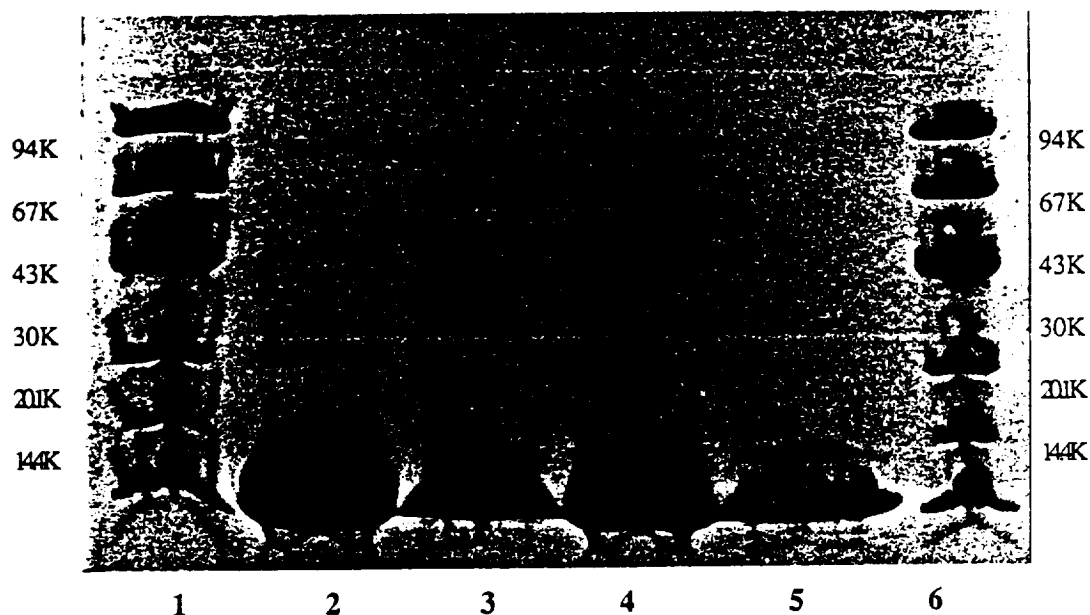


SDS-PAGE. Samples dissolved in 10mM Tris (HCl), pH 8.00, with 1mM EDTA, 2.5% (w/v) SDS and 2.5% 1,4 dithiothreitol. Heated at 100 °C for 5 minutes. Coomassie Blue Development.

(1) Pharmacia Low MW Standards (2) Sigma Lysozyme Lot 46F-8060 ~ 12,000ng (3) Sigma Lysozyme Lot 46F-8060 ~ 6,000ng (4) Sigma Lysozyme Lot 46F-80602 ~ 12,000ng (5) Sigma Lysozyme Lot 46F-80602 ~ 6,000ng (6) Pharmacia Low MW Standards.

Figure 23. SDS-PAGE on Sigma lysozyme.



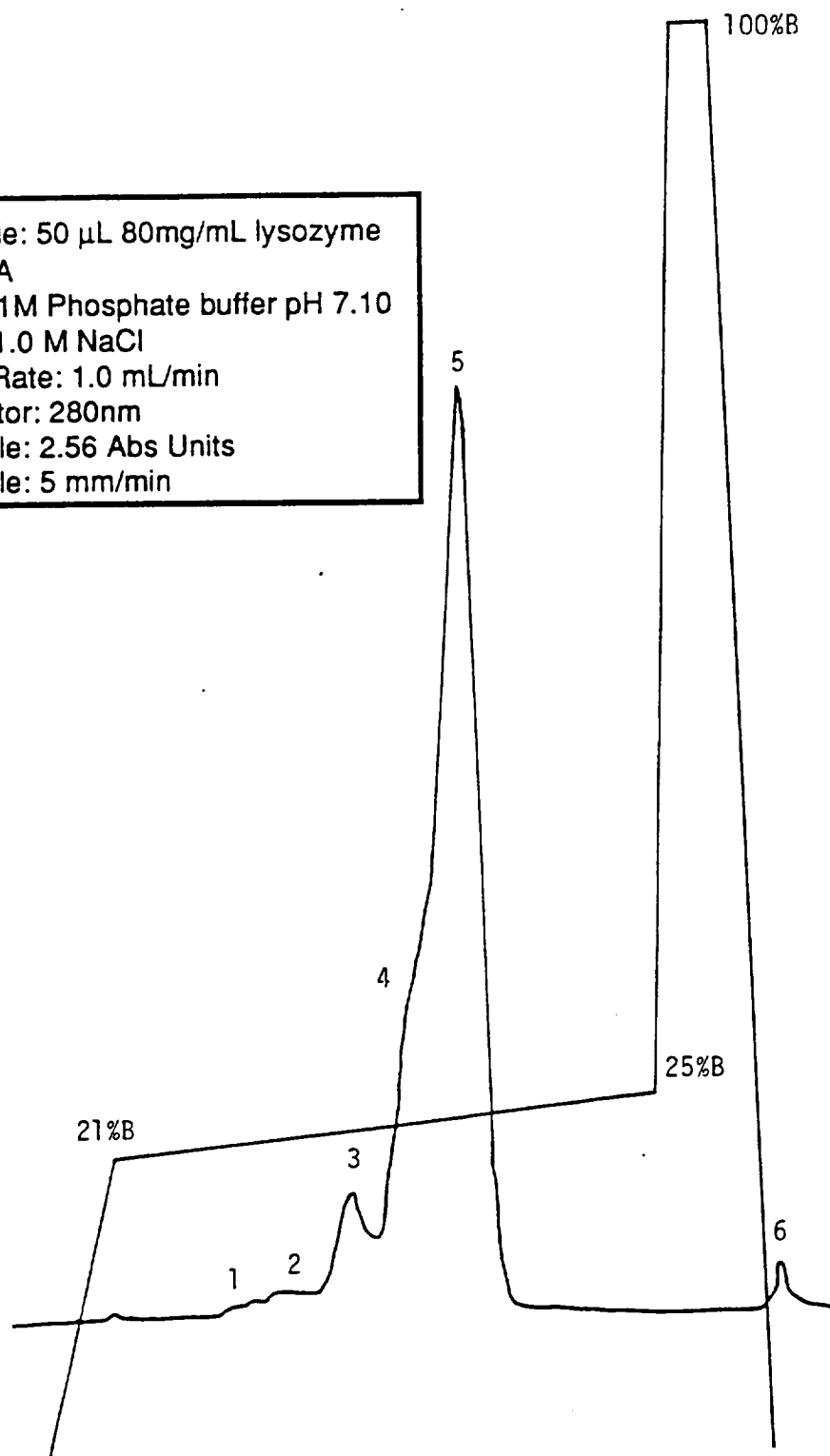


SDS-PAGE. Samples dissolved in 10mM Tris (HCl), pH 8.00, with 1mM EDTA, 2.5% (w/v) SDS and 2.5% 1,4 dithiothreitol. Heated at 100 °C for 5 minutes. Comassie Blue Development.

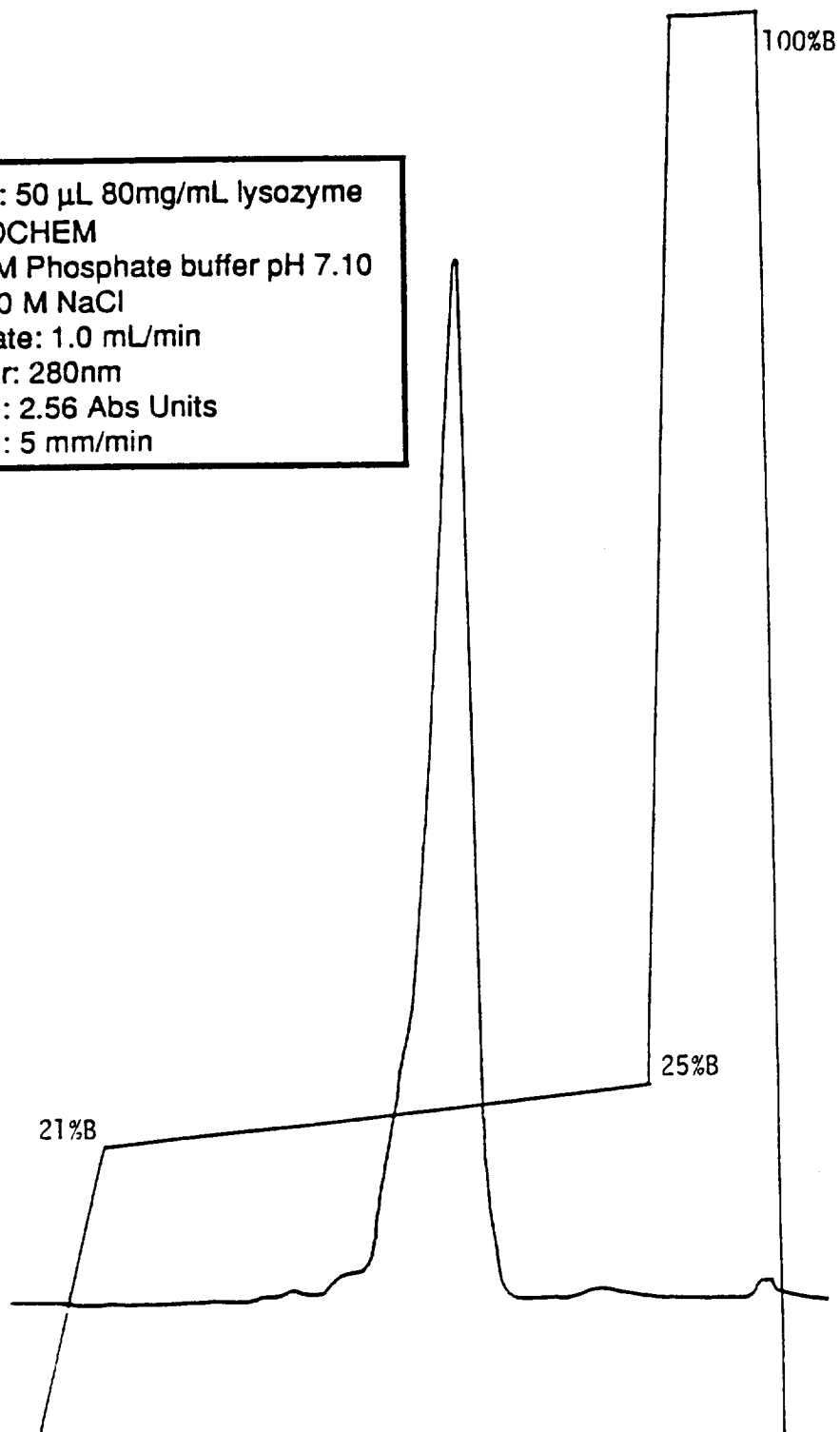
(1) Pharmacia Low MW Standards (2) Sigma Lysozyme Lot 46F-8060 ~ 12,000ng (3) Calbiochem Lysozyme ~ 6,000ng (4) Sigma Lysozyme Lot 46F-8060 ~ 12,000ng (5) Calbiochem Lysozyme ~ 6,000ng (6) Pharmacia Low MW Standards.

Figure 25. Comparison of Sigma lysozyme and Calbiochem lysozyme.

Sample: 50 μ L 80mg/mL lysozyme
SIGMA
A: 0.01M Phosphate buffer pH 7.10
B: A+1.0 M NaCl
Flow Rate: 1.0 mL/min
Detector: 280nm
Y Scale: 2.56 Abs Units
X Scale: 5 mm/min



Sample: 50 μ L 80mg/mL lysozyme
CALBIOCHEM
A: 0.01M Phosphate buffer pH 7.10
B: A+1.0 M NaCl
Flow Rate: 1.0 mL/min
Detector: 280nm
Y Scale: 2.56 Abs Units
X Scale: 5 mm/min



concentrate them were unsuccessful. By elimination, they are the 38.6K and 67K proteins. The lysozyme peak was distorted from a flow rate that was too high.

The high molecular weight components found in the Sigma lysozyme could be from either of two sources: (1) They could be lysozyme molecules connected by intermolecular disulfide bonds, or other intermolecular cross-links, created during the isolation process. (2) They could be protein impurities also found in hen egg whites. Tests were run to try and characterize the proteins. A comparison of the ratio of molecular weights of the unknown impurities to the known molecular weight of lysozyme supported the j-mer theory since all ratios were close to whole numbers. These ratios are 5.3, 3.2 and 1.9 for the bands 77.8K, 46.8K and 27.8K respectively. To test if intermolecular disulfide bonds were being reduced, protein samples were dissolved in SDS buffers containing 2.5% DTT, 8.4% DTT and 5% B-mercaptoethanol. If the disulfide bond were not being reduced with the 2.5% DTT they should be reduced with either the 8.4% DTT or the 5% B-mercaptoethanol. However, it was found that the high molecular weight bands were still present even in the presence of these harsh reducing agents (Figure 28). Therefore, it follows that the high molecular weight components are not lysozyme molecules connected by intermolecular disulfide bonds but could be cross-linked lysozyme molecules..

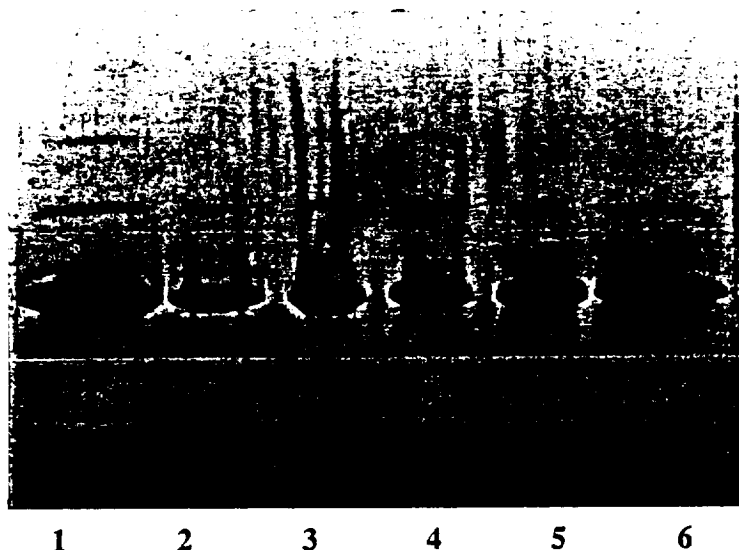
The catalytic activity of the lysozyme solutions containing the high molecular weight components was measured. First, the high

molecular weight components were separated with the membrane method. SDS-PAGE was run to determine the composition of the inner bag. It was found to contain lysozyme and the higher molecular weight bands. However, the high molecular weight bands were concentrated with respect to the lysozyme band. The catalytic activity of the solutions in the inner bag was compared to that of a pure lysozyme solution. The activity of the solution containing the high MW proteins was determined to be approximately half that of a pure solution of lysozyme with equal concentration (Figure 29). This seems to suggest that the unknown bands do not contribute to the lysozyme activity. To further support these results, the same solutions

Table 4. Proteins of Pharmacia's Broad pI Calibration Kit and their corresponding pIs.

Sample	pI
lentil lectin (basic)	8.65
lentil lectin (middle)	8.45
lentil lectin (acidic)	8.15
horse myoglobin (basic)	7.35
horse myoglobin (acidic)	6.85
human carbonic anhydraseB	6.55
bovine carbonic anhydrase B	5.85
B-lactoglobulin A	5.20
soybean trypsin inhibitor	4.55
amyloglucosidase	3.50

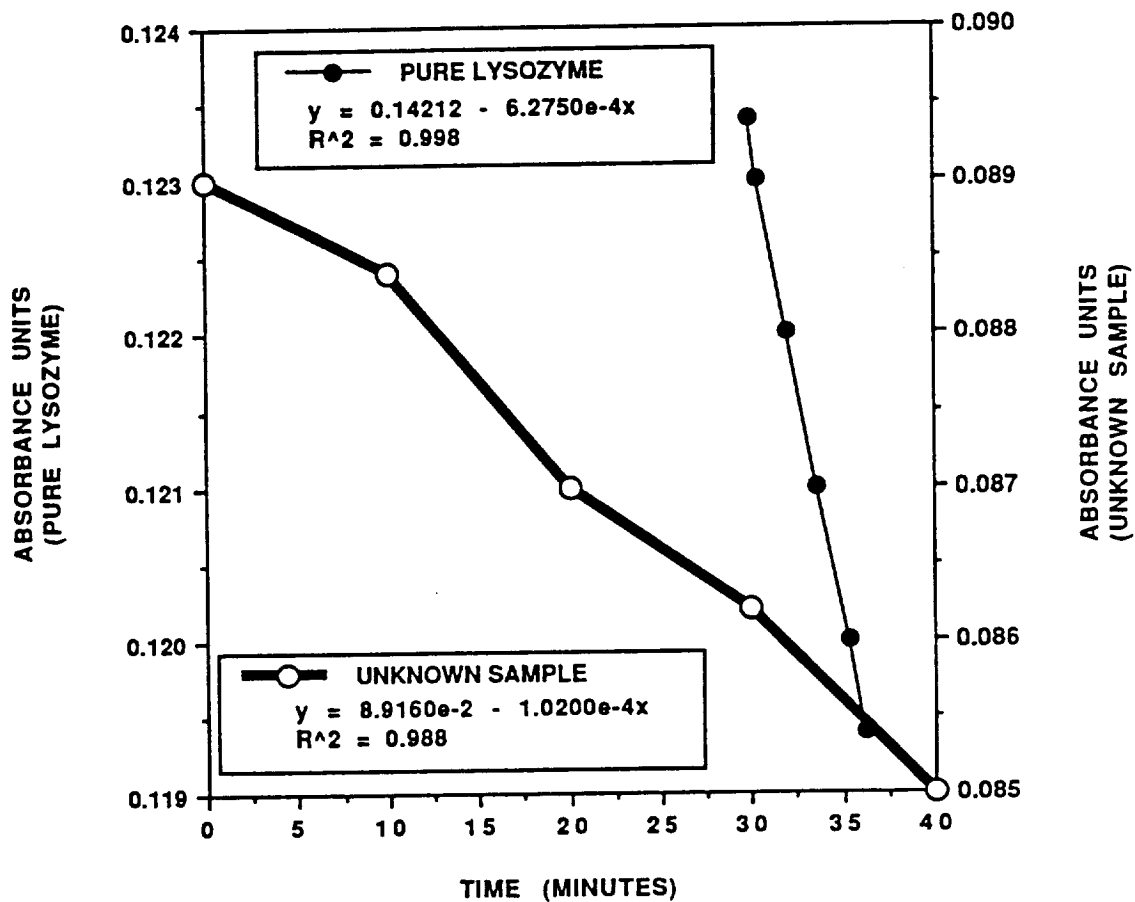
were separated by isoelectric focusing. Since lysozyme has an isoelectric pH of 11.00 and the only ampholytes (aliphatic polyamino-polycarboxylic acids) available were in the pH range 3-9 (Table 4) it was not possible to measure the isoelectric pH of lysozyme with the

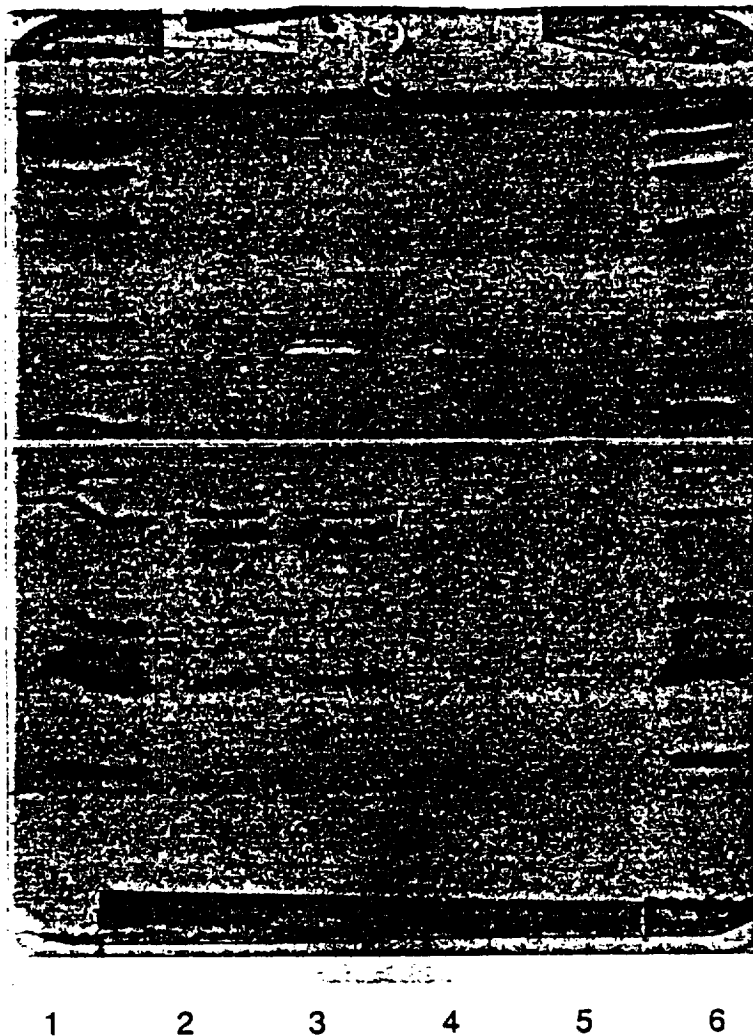


SDS-PAGE. Samples dissolved in 10mM Tris (HCl), pH 8.00, with 1mM EDTA, 2.5% (w/v) SDS and 2.5% 1,4 dithiothreitol (DTT), 8.4% DTT or 5% β -mercaptoethanol. Heated at 100 °C for 10 minutes. Comassie Blue Development.

(1) Sigma lysozyme in 2.5% DTT ~ 1mg/mL
(2) Sigma lysozyme in 2.5% DTT ~ 0.5mg/mL
(3) Sigma lysozyme in 8.4% DTT ~ 1mg/mL
(4) Sigma lysozyme in 8.4% DTT ~ 0.5 mg/mL
(5) Sigma lysozyme in 5.0% β -mercaptoethanol ~ 1mg/mL
(6) Sigma lysozyme in 5.0% β -mercaptoethanol ~ 0.5 mg/mL.

Figure 28. SDS-PAGE on Sigma lysozyme with different strength reducing agents.

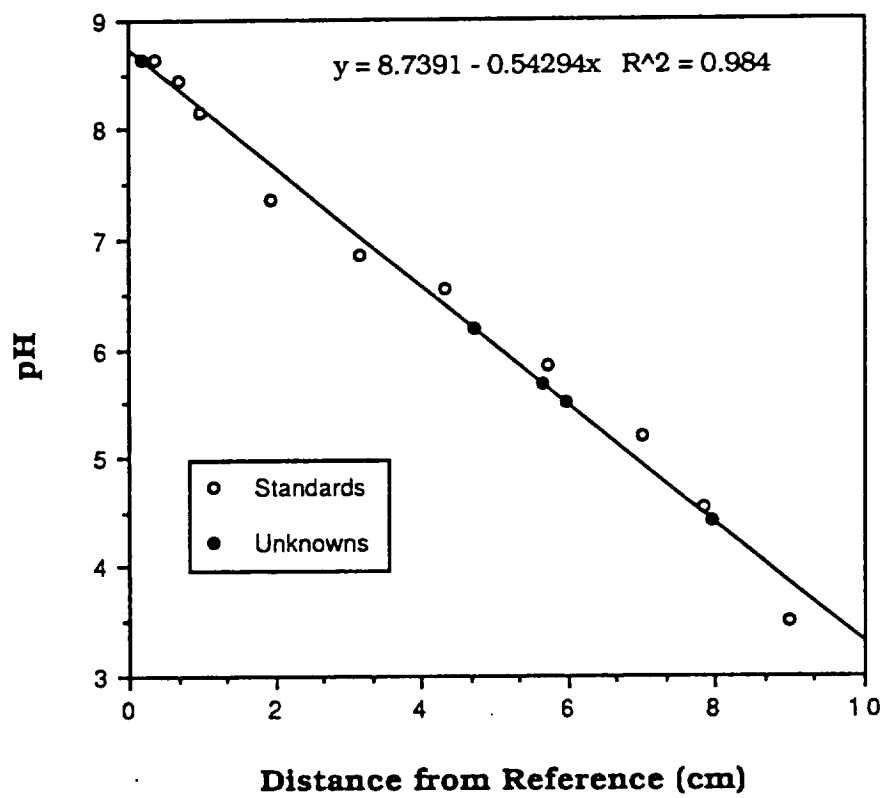




Isoelectric Focusing. Samples dissolved in 0.01M phosphate buffer, pH 8.00 to a total protein concentration of 2.0 mg/mL.

(1) Pharmacia's Broad pI Calibration Standards; see Table 4. (2) (3) Sigma lysozyme with impurities. (4) (5) Sigma lysozyme purified. (6) Standards.

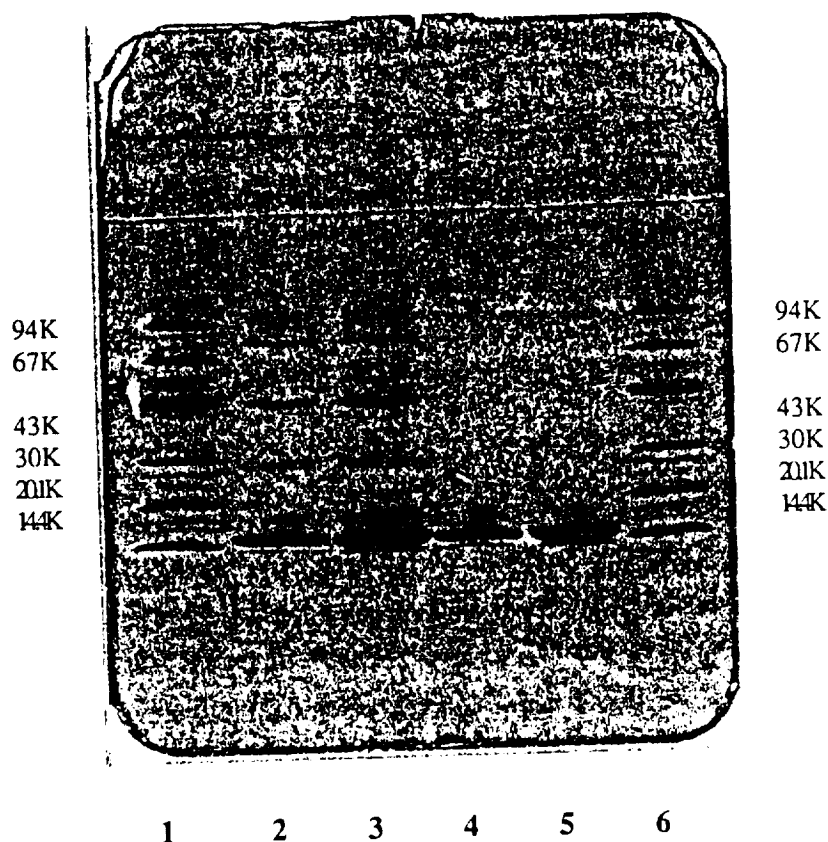
Figure 30. Separation of Sigma lysozyme and unknowns with isoelectric focusing using the PhastSystem and PhastGel 3-9..



PhastSystem. However, it was possible to determine if all the bands seen on SDS-Page had the same isoelectric pH. It was found that the high MW proteins had different isoelectric points than lysozyme (Figure 30 and Figure 31). This suggests that the unknown bands are due to other protein impurities. However, it is difficult to know whether the different isoelectric pH's are due to different types of protein components or the result of chemical modification of the same protein.

The manufacturer's recommended scale up procedures were used to scale up from the HR 5/5 to the HR 10/10. Resolution was retained up to 40 mg of lysozyme injected. While this is excellent for most protein samples it still required 25 runs to get 1 gram of protein. Since several grams of lysozyme were needed a new procedure was developed that required less time.

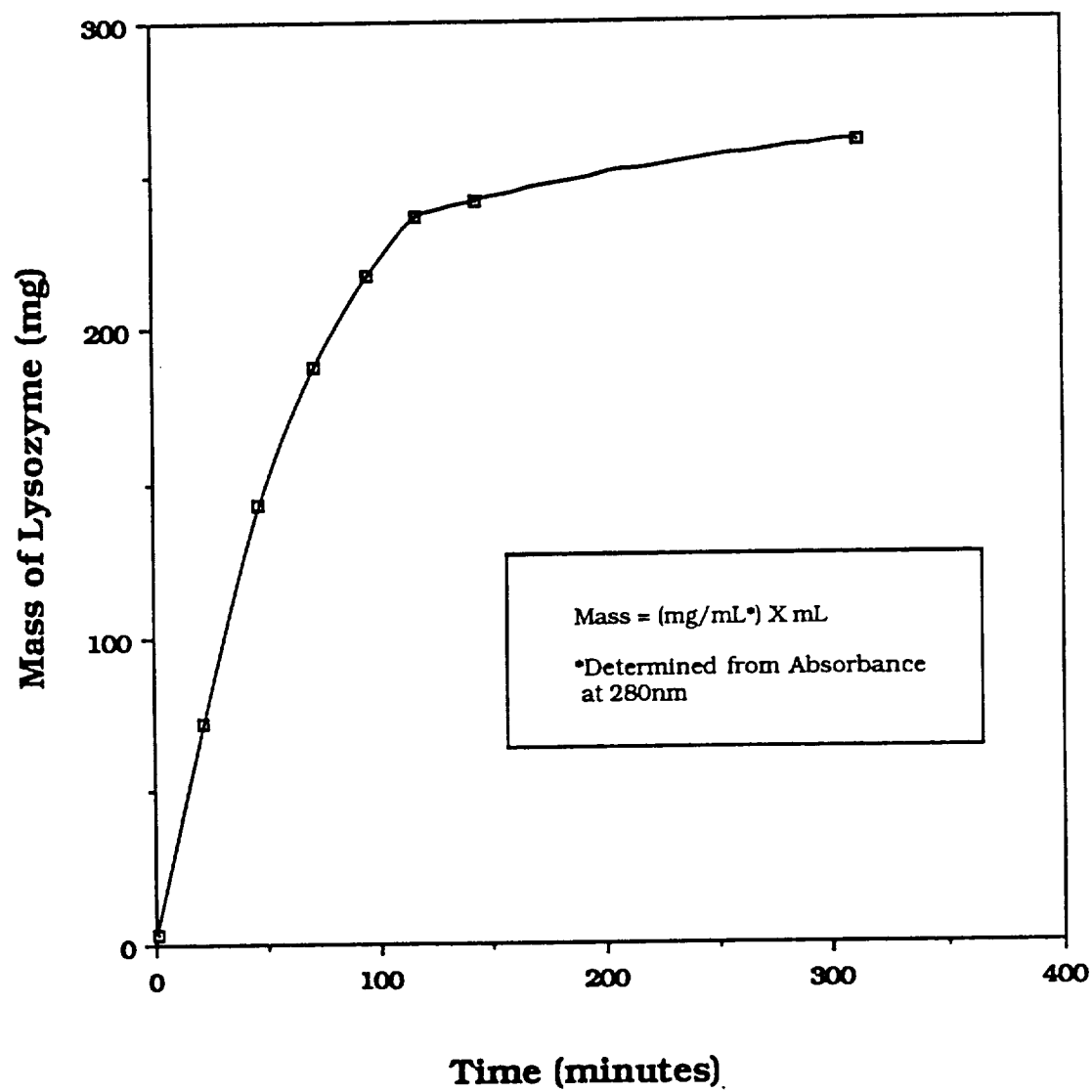
The impurities are all of a higher molecular weight than lysozyme so they can be trapped by a membrane with 15,000 MWCO. Lysozyme should traverse the membrane and be trapped in the outer bag. Analysis of the solution in the outer bag by SDS-PAGE with silver stain (Figure 32) showed only the lysozyme band. The silver stain procedure was found to have a sensitivity of 10 ng per band of protein. Since the most concentrated band (lane 1) shows no higher molecular weight impurities, the amount of impurities in the sample is less than 1.25%. The solution in the inner bag was found to contain lysozyme and the four protein impurities (Figure 32).



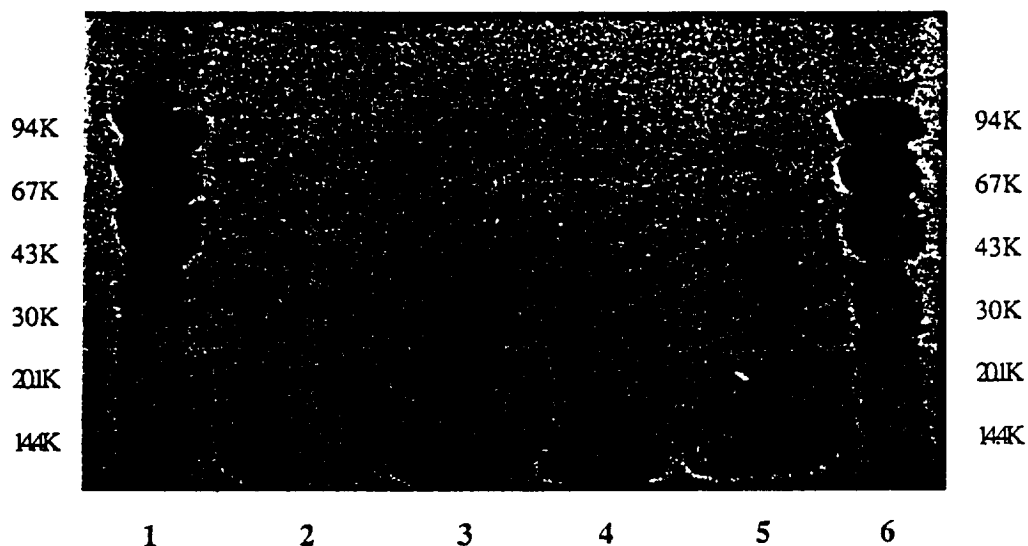
SDS-PAGE. Samples dissolved in 10mM Tris (HCl), pH 8.00, with 1mM EDTA, 2.5% (w/v) SDS and 2.5% 1,4 dithiothreitol. Heated at 100 °C for 5 minutes. Silver Stain Development described in Figure 21.

(1) Pharmacia Low MW Standards (2) Inner bag 100 ng total protein (3) Inner bag 50 ng total protein (4) outer bag 100 ng total protein (5) outer bag 50 ng total protein (6) Pharmacia Low MW Standards.

Figure 32. SDS-PAGE on solution from outer bag and inner bag after membrane separation.



ORIGINAL PAGE IS
OF POOR QUALITY



SDS-PAGE. Samples dissolved in 10mM Tris (HCl), pH 8.00, with 1mM EDTA, 2.5% (w/v) SDS and 2.5% 1,4 dithiothreitol. Heated at 100 °C for 5 minutes. Comassie Blue Development.

(1) Pharmacia Low MW Standards (2) Sigma Lysozyme Lot 46F-8060 ~ 12,000ng (3) Sigma Lysozyme Lot 46F-8060 ~ 6,000ng (4) Sigma Lysozyme Lot 46F-80602 ~ 12,000ng (5) Sigma Lysozyme Lot 46F-80602 ~ 6,000ng (6) Pharmacia Low MW Standards.

Figure 34. Comparison of different lot numbers of Sigma lysozyme with SDS-PAGE.

Monitoring the absorbance of the solution in the outer bag showed that the exchange process took 5-10 days (Figure 33). To speed up this process the 15,000 MWCO containing unpurified lysozyme was placed in the reservoir container of an Amicon Stirred Cell concentrator with a 10,000 MWCO Millipore membrane. Fresh water was added to the reservoir periodically so that the rate of the exchange process would remain high. After several changes of water the solution was concentrated down to just a few milliliters. Using the Amicon in this manner allows one to desalt, purify and concentrate in one step.

Conclusions and Recommendations

From these studies on the purity of commercially available lysozyme it is evident that care should be taken to purify or at least test the purity of commercial sources of proteins. SDS-PAGE on different lot numbers of Sigma lysozyme showed a different distribution of impurities (Figure 34). This inconsistency contributes to the difficulty in reproducing crystal growth conditions. The impurities in the Sigma lysozyme are thought to be different types of proteins rather than modifications of lysozyme. However, to be completely certain of this it would be necessary to do a specific detection technique after separation such as western blotting.

SELECTED REFERENCES

- [1] CRC Handbook of Biochemistry and Molecular Biology (1976)
Proteins, **2**, 468.

CHAPTER IV

HANGING DROP VAPOR DIFFUSION STUDIES ON THE CRYSTALLIZATION OF LYSOZYME

Introduction

Crystals of hen egg white lysozyme were grown using the hanging drop vapor diffusion method in Linbro plates. The conditions for crystallization were optimized according to pH, salt concentration and protein concentration. Several different conditions were then used to vary the quality of the crystals. These crystals were used as the initial starting conditions for the gas equilibration method of growing protein crystals. The crystals grown with the hanging drop vapor diffusion method were also used as control experiments to evaluate the gas equilibration method. Since the gas equilibration method required that no volatile solution components be used it was necessary to develop new conditions for crystallization than those used in the past. Efforts were made to evaluate the quality of the crystals grown under the new conditions and explain the results in terms of the crystal growth mechanism of lysozyme. Studies were also done to determine if the conductance monitoring technique described in Chapter 2 interfered with the crystal growth process.

Materials and Methods

NaCl was Baker Analyzed Reagent grade. Deionized water (Barnstead Nanopure II), 0.2 μm filtered, was used for all solutions. pH buffers were Fisher (± 0.01). Sodium acetate and ammonium sulfate were Fisher reagent grade. All other buffers and salts were Fisher. Linbro plates were purchased from Flow Laboratories and glass microscope coverslips were from Fisher. Sealing grease was either Apiezon L or Dow Corning High Vacuum grease.

Lysozyme Crystal Growth

Acetate Buffer. Conditions were optimized by simultaneously varying the protein and salt concentration at pH 4.00 and pH 4.70 (see Table 6 and Table 7). The crystal appearance quality was estimated (see Visual Inspection) and plotted against the salt and protein concentration in either a 3-D surface or contour graph. The optimum conditions were then selected from the maximums on these graphs. The optimum conditions were repeated to ensure reproducibility. Crystals were grown in 0.1M sodium acetate buffer adjusted to pH 4.00 and 4.70 with 6N NaOH and 6N HCl. [1]. NaCl concentrations were 5-10% (w/v) NaCl in the buffer. Protein concentrations were ranged from 10.0 to 50.0 mg/mL buffer. The protein solution was made to approximate concentration by weighing out the lyophilized protein and dissolving it in the buffer solution. The solution was adjusted to

50mg/mL by measuring A_{280} and using $A^{1\%}$ of 26.5 [2]. Reservoir solutions were 1.0 mL of the NaCl solution. Drop solutions were made up of 10 μ L of reservoir solution and 10 μ L of protein dissolved in the buffer. Drops were deployed using Drummond Fixed Volume Micropipets which had a precision rating of 1%. Microscope coverslips were silanized using the procedure in Appendix 3. The coverslips were sealed to each well with Dow Corning High Vacuum grease. The Linbro boxes were placed in styrofoam boxes and maintained at room temperature. The room temperature was estimated to be 23 \pm 4° C.

Citrate Buffer. Crystals were grown with 0.1M citrate buffer at pH 4.00 [3]. NaCl concentrations were 1-5% (w/v) NaCl in the buffer. The conditions were not optimized for citrate buffer with the procedure described above. Protein concentrations were prepared the same as with the acetate buffer. Reservoir solutions were 1.0 mL of the NaCl solution. Drop solutions were made up of 10 μ L of reservoir solution and 10 μ L of protein dissolved in the buffer. The coverslips were sealed to each well with Dow Corning High Vacuum grease.

Continuous Conductance Monitoring

The conditions for crystallization in sodium acetate buffer (above) were used to attempt to grow crystals while monitoring conductance.

At the same time, control experiments were run at the same conditions with the drop placed on silanized microscope coverslips instead of on the electrodes.

Solubility Determination

To measure the solubility of lysozyme under different conditions 2 μ L aliquots of the mother liquor were removed from drops containing crystals. To ensure that the system was in equilibrium the measurements were taken at least 1 month after the drops were set up. The aliquots were diluted into 1.0 mL of the appropriate buffer and the absorbance of this solution was measured at 280 nm using an $A^{1\%}$ of 26.5.

Visual Analysis

A polarizing microscope (Zeiss, West Germany) with camera attachment was used to study crystal appearance quality. The appearance of the crystals at a particular condition were assigned a Response Code according to Table 5. Pictures of the crystals were taken using a 35mm camera to microscope attachment with either Kodacolor ISO 400, Ektachrome ISO 400 Daylight or Ektachrome ISO 160 Tungsten balanced.

Table 5. Estimation of Crystal Quality by Visual Inspection.

Response Code	Appearance Quality
0	evaporated or destroyed
1	clear, no crystals
2	precipitate, non-crystalline
3	many small crystals
4	few large crystals

Diffraction Analysis

The crystals were characterized using a Buerger Precession Camera (The Charles Supper Company) and later with a Huber Precession Camera. X-Rays of $\lambda = 1.54\text{\AA}$ were produced from a Cu Rotating Anode Generator (Rigaku) operated at 40 kV and 50 mA and Ni-filtered. Reflections were captured either on Polaroid XR-7 3000 speed film or Kodak X-ray film (crystal-to-film distance = 75mm or 100mm). The crystals were mounted in glass capillary tubes and sealed with epoxy. The crystals were mounted with their crystallographic c axis oriented parallel to the capillary axis. Once mounted, the crystals were first optically positioned and then aligned to the X-Ray beam following the manufacturer's recommendations. Two of unit cell parameters were determined by measuring the spacing between zero level reflections off of a photograph. The crystal was then rotated 90° to measure the third axis.

Table 6. Optimization of crystallization conditions for lysozyme at pH 4.00.

Number	% NaCl (w/v)	[Protein] (mg/mL)	Quality (0-4)
1	3.0	10.0	1
2	3.0	10.0	1
3	3.0	10.0	1
4	3.0	25.0	2
5	3.0	25.0	2
6	3.0	25.0	2
7	3.0	43.0	0
8	3.0	43.0	2
9	3.0	43.0	2
10	4.0	10.0	2
11	4.0	10.0	2
12	4.0	10.0	2
13	4.0	25.0	2
14	4.0	25.0	2
15	4.0	25.0	2
16	4.0	43.0	4
17	4.0	43.0	4
18	4.0	43.0	4
19	4.0	43.0	3
20	4.0	43.0	3
21	5.0	10.0	1
22	5.0	10.0	1
23	5.0	25.0	3
24	5.0	25.0	3
25	5.0	43.0	4
26	5.0	43.0	4
27	5.0	43.0	4
28	5.0	43.0	4
29	5.0	43.0	4
30	5.0	43.0	4

Table 7. Optimization of crystallization conditions for lysozyme at pH 4.70.

Number	% NaCl (w/v)	[Protein] (mg/mL)	Quality (0-4)
1	3.0	10.0	2
2	3.0	10.0	2
3	4.0	10.0	2
4	4.0	10.0	2
5	5.0	10.0	2
6	5.0	10.0	2
7	3.0	25.0	2
8	3.0	25.0	2
9	4.0	25.0	2
10	4.0	25.0	2
11	5.0	25.0	2
12	5.0	25.0	3
13	3.0	43.0	2
14	3.0	43.0	2
15	4.0	43.0	2
16	4.0	43.0	2
17	5.0	43.0	3
18	5.0	43.0	3

SDS-PAGE on Crystals

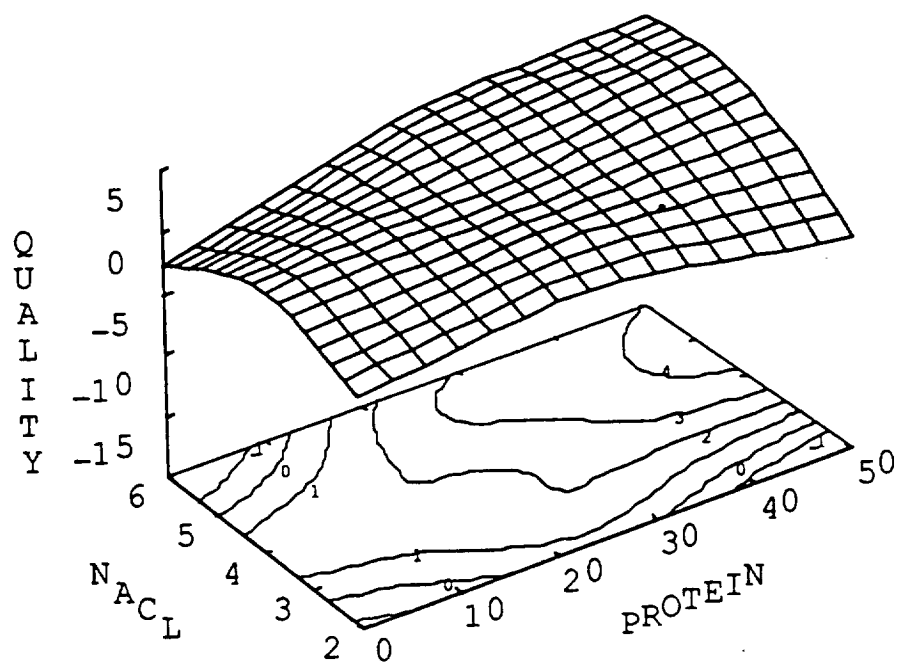
To determine the protein composition of crystals they were sampled from the mother liquor and dissolved in SDS buffer. To retrieve the crystals the entire drop was pulled into a disposable glass pipet using suction. The mother liquor was expelled into a 1.8 mL centrifuge tube and 500 μ L of SDS buffer was added. The crystals adhered to the glass in the pipet and were washed into a centrifuge tube with 100 μ L of SDS buffer. These samples were prepared for SDS-PAGE by heating at 90°C for 5 minutes. Separation and silver stain development were carried out with the PhastSystem as in Chapter 3.

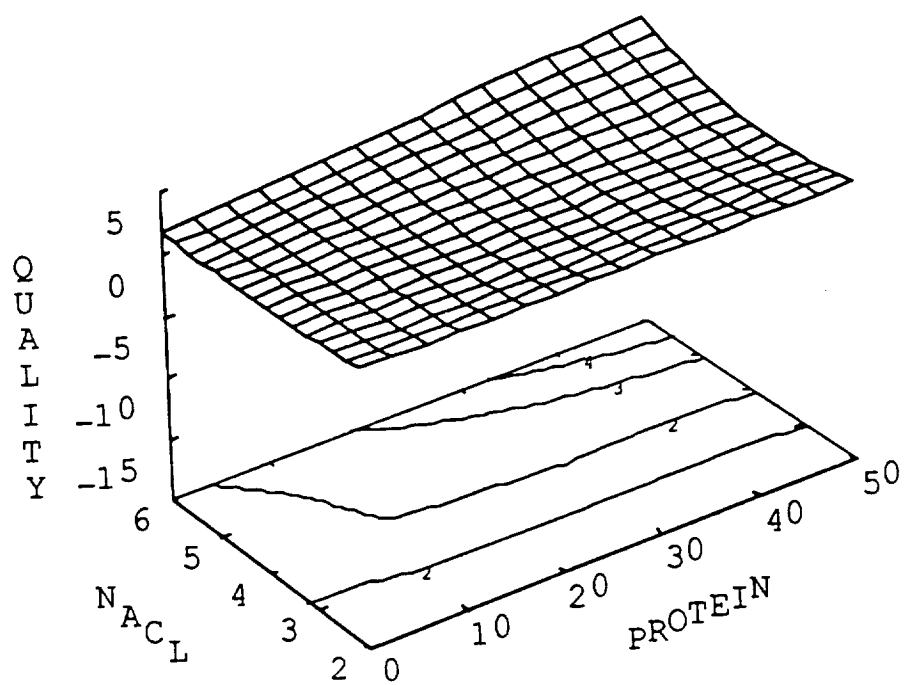
Results and Discussion

Since many factors can influence protein crystal growth a large number of conditions must be scanned to determine the most important factors and to provide the best conditions for crystal growth. To deal with the large number of screening experiments automated devices have been developed and used to develop effective search strategies to determine how a parameter influences protein crystal growth [4]. This is a costly and time consuming effort which requires several hundred separate experiments to optimize 4 or 5 parameters. Another approach has been to use a statistical factorial design [5] which can reduce the number of experiments into the

range of 20 - 30 to optimize 6 parameters. For lysozyme crystal growth enough information was available in the scientific literature to reduce the parameters to be optimized to pH, protein and salt concentration. The conditions for crystallization of hen egg white lysozyme in acetate buffer were determined using a 3^2 factorial design where two factors (protein and salt concentration) were evaluated at three levels (see Tables 6 and 7). This was done for pH 4.00 and pH 4.70. The response curve for both of these sets of experiments are shown in Figure 35 and Figure 36. At pH 4.00 maximum crystal quality was found to be at 50 mg/mL lysozyme concentration (concentrations are before dilution) and 5% NaCl concentration. This would give a drop concentration of 25 mg/mL lysozyme and 2.5% NaCl. At pH 4.70 the response curve was flat when compared to the response curve of pH 4.00 and the maximum appeared to be out of the range of conditions. The best crystals (level 3) obtained at pH 4.70 were at protein concentrations of 40-50 mg/mL and salt concentrations of 5-6% NaCl. Since pH 4.00 gave the best crystals these conditions were selected for crystal growth studies.

The crystals grown in acetate buffer, pH 4.00, at a lysozyme concentration of 25 mg/mL and salt concentration of 2.5% (w/v), were large tetragonal crystals with well defined edges. The average area of the crystals grown under these conditions was measured by the procedure illustrated in Figure 37) and was found to be 0.396 mm² (Table 8). These crystals were mounted onto the diffractometer and were found to give rise to diffraction spots (See Figure 38). The space





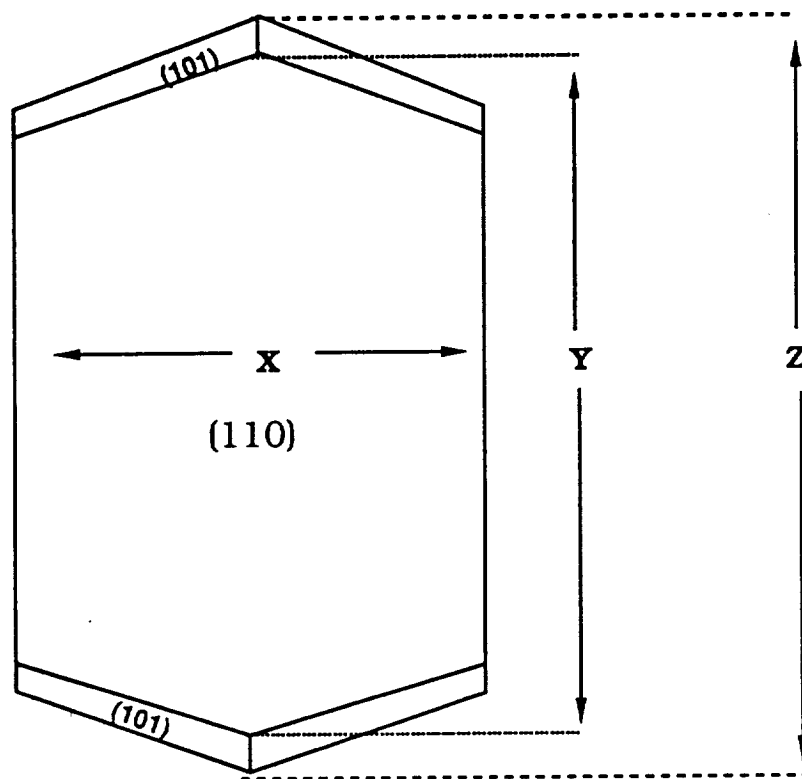


Figure 37. Procedure for measurement of the crystal area. Crystals were magnified and photographed. Length X and Z were measured either off of the photographs with a precision micrometer ($\pm 0.05\text{mm}$) or with a micrometer eyepiece ($\pm 0.10\text{mm}$). The area was calculated by multiplying X by Z and dividing by the magnification.

Table 8. Size and Number of Lysozyme Crystals Grown in Linbro Wells and Acetate Buffer

Linbro Well Number	Number of Crystals	Average Area of Crystals ^(a) (mm ²)
A1	3	0.356
A2	2	0.343
A3	2	0.528
A4	1	0.400
A5	2	0.643
A6	2	0.486
B1	1	0.659
AVERAGE AREA (mm²)		0.396 ± 0.065

(a) Measured after crystals stopped growing as determined by visual inspection.

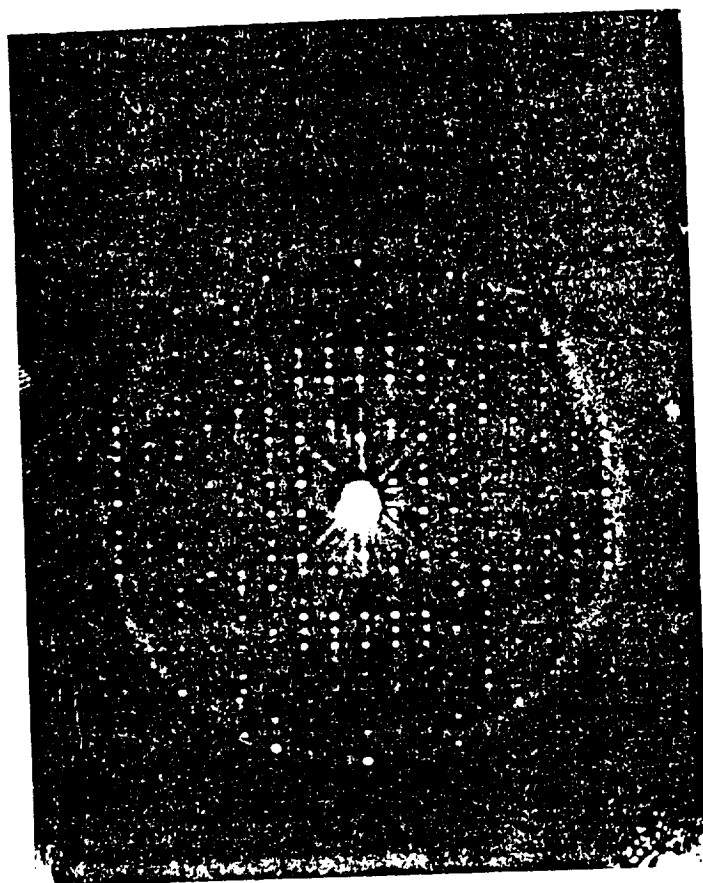


Figure 38. 100° precession photograph of a lysozyme crystal grown in 0.1M acetate buffer, pH 4.00, at a lysozyme concentration of 25 mg/mL and salt concentration of 2.5% (w/v). From this and an identical photograph obtained from rotating the crystal 90°, unit cell parameters were found to be $a=b=78.7$ and $c=38.2$.

group was determined to be $P4_32_12$ with unit cell parameters $a=b=78.7$ and $c=38.2$. These crystals are similar in size and number to crystals obtained by other investigators using the same conditions [6].

A large variation in the quality, number and size of crystals was found between those grown in acetate and those grown in citrate buffers (Figure 39). The crystals grown in citrate were of the same morphology as the ones grown in acetate, however there were more crystals per well and they were much smaller (Table 9). The solubility of lysozyme in citrate buffer at pH 4.00, 2.5% NaCl and room temperature was determined to be $8.41 \text{ mg/mL} \pm 0.02 \text{ mg/mL}$. This is a smaller value than the solubility of lysozyme in acetate buffer under the same conditions (12.20 mg/mL) as measured by Pusey [7]. From this, it follows that lysozyme is less soluble in citrate buffer than in acetate. This is in agreement with crystallization attempts carried out in acetate buffer using ammonium acetate and ammonium citrate as precipitating agents [8]. The lower solubility could encourage more nuclei to form. Since there is only a limited amount of protein which must be shared with all nuclei then each crystal will grow to a smaller size. Because of the volatility of the acetate buffer, it was necessary to crystallize lysozyme in a buffer that was involatile for the gas controlled technique. That is why, even though the acetate buffer gave larger and more symmetrical crystals, most of the gas experiments were done in the citrate buffer.

Table 9. Size and Number of Lysozyme Crystals Grown in Linbro Wells and Citrate Buffer

Linbro Well Number	Number of Crystals (Approximate)	Average Area of Crystals ^(a) (mm ²)
A1	29	0.153
A2	30	0.118
A3	>35	0.104
A4	24	0.161
A5	>35	0.066
A6	>25	0.088
B1	>25	0.070
AVERAGE AREA (mm²)		0.109 ± 0.038

(a) Measured after crystals stopped growing as determined by visual inspection.

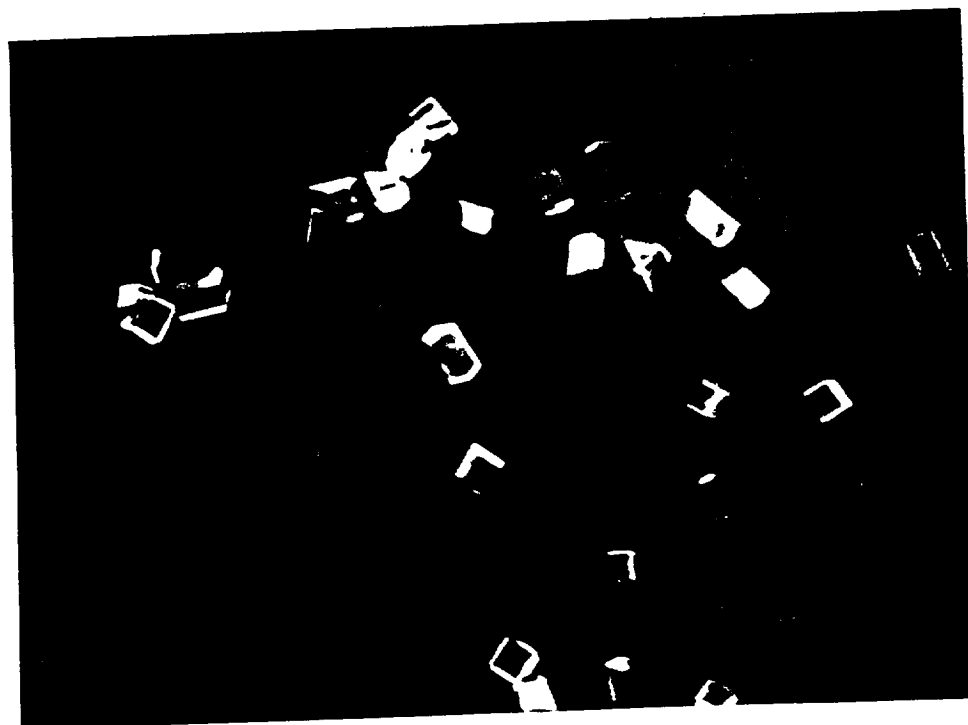


Figure 39. Hen egg white lysozyme crystals grown in 0.1M acetate and 0.1M citrate buffers at equal salt and protein concentrations.

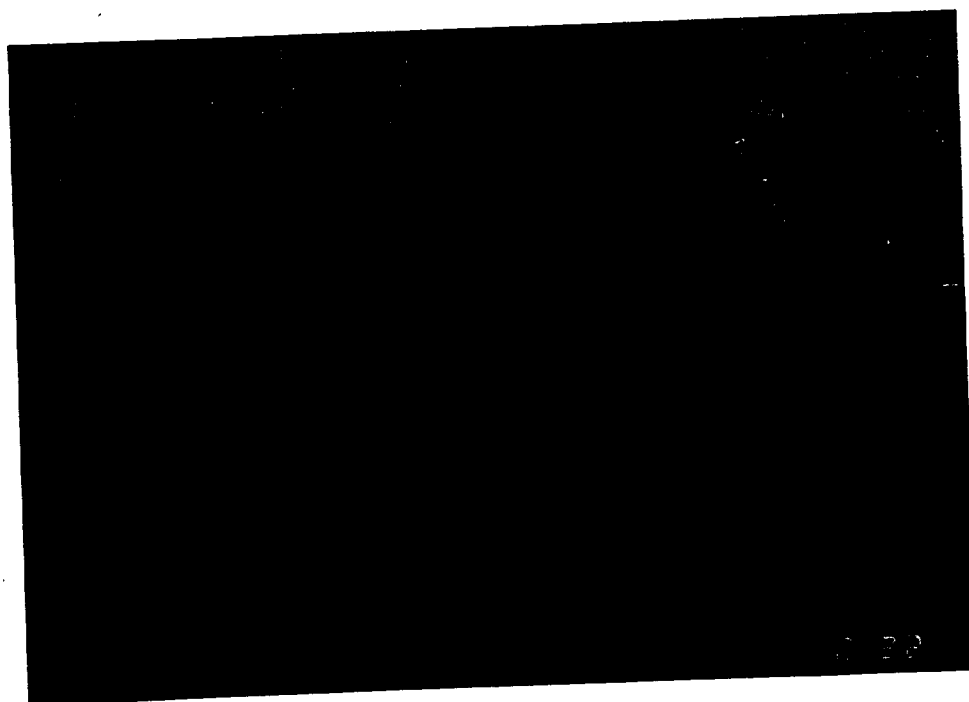
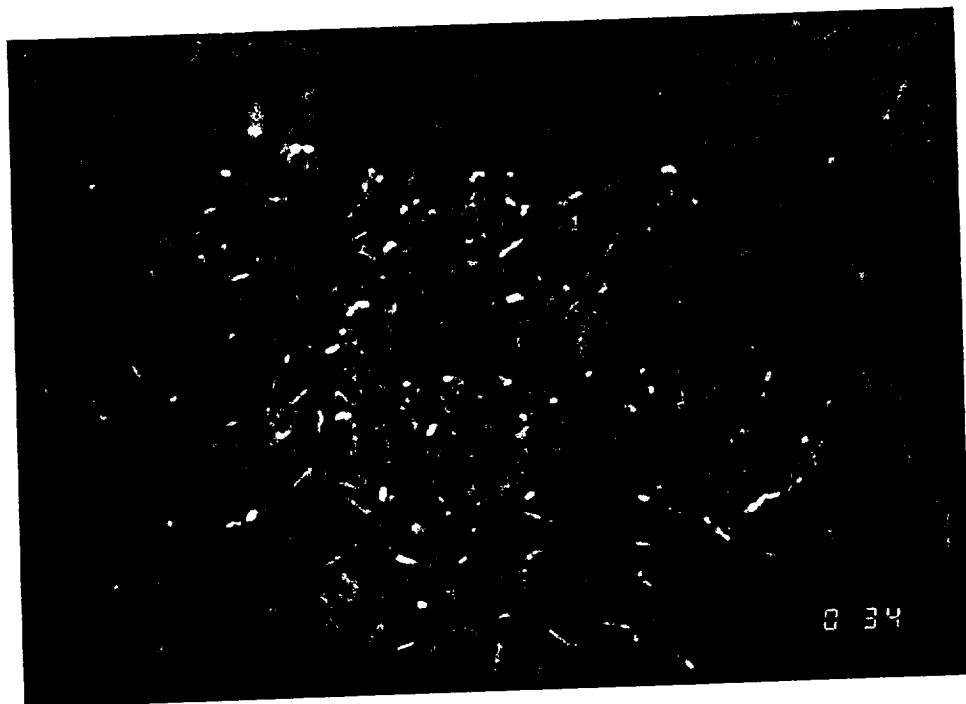


Figure 40. Crystals grown from purified lysozyme in citrate buffer at conditions mentioned in text. Compare these crystals with those grown in citrate and unpurified lysozyme (Figure 39, lower photo).

The largest difference observed was between that of the crystals grown from the purified and unpurified Sigma lysozyme in citrate buffer (Figure 40). Here the morphology changed from 3-dimensional tetragonal seen with unpurified lysozyme to 2-dimensional needle crystals when the purified form was used. This morphology change did not occur under the same conditions in acetate buffer. Under closer observation, it can be seen that these needle crystals are indeed tetragonal with unequal growth of the 110 face (Figure 37 length Y). One of these crystals was mounted on the diffractometer and the unit cell parameters were found to be $a=b=78.6 \text{ \AA}$ and $c=38.1 \text{ \AA}$ (Figure 41). Since this is equal within experimental error to the unit cell parameters of the symmetrical tetragonal crystals, then the needle crystals are also tetragonal. This form of lysozyme crystal has been reported by Durbin and Feher at low supersaturation in acetate buffer [9]. In fact, their recent electron microscope experiments showed a different growth mechanism with the symmetrical tetragonal than with the elongated tetragonal needle crystals [10].

Since the unpurified form of Sigma lysozyme contains unknown protein impurities that also absorb light at 280 nm it is difficult to make the lysozyme concentration equal in the two solutions. It is possible that the different crystal morphologies observed could be due to the different lysozyme concentrations. To determine if this was the case, the concentration of purified lysozyme was scanned from 94.5 mg/mL to 12.5 mg/mL in citrate buffer. At all concentrations the needle crystals were present, often mixed with the symmetrical

ORIGINAL PAGE IS
OF POOR QUALITY

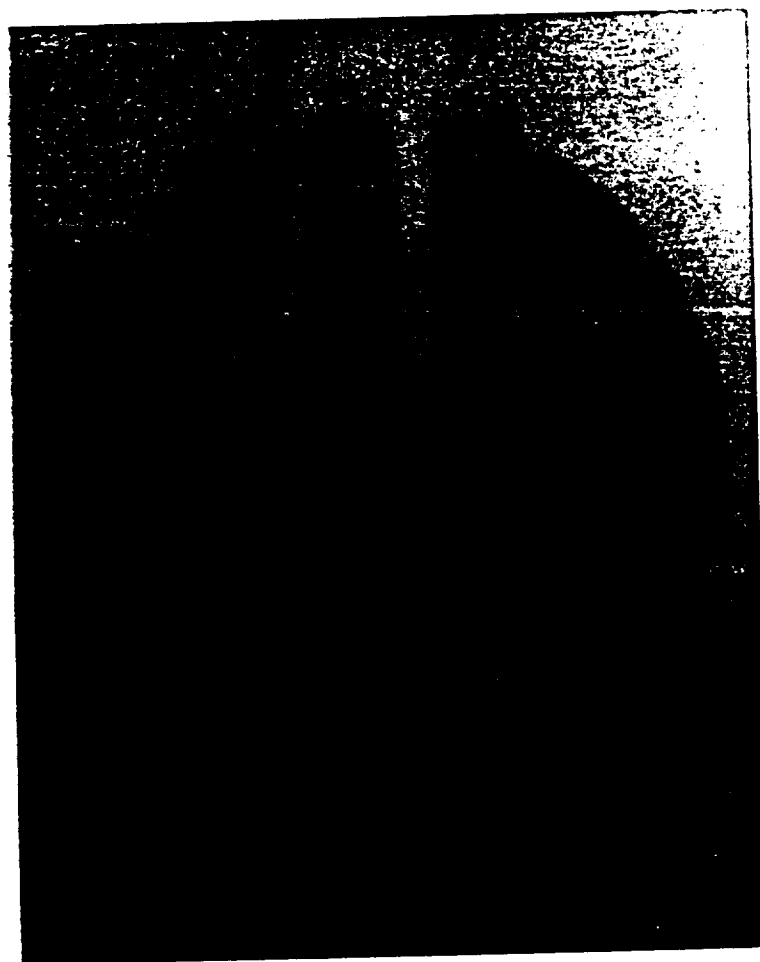
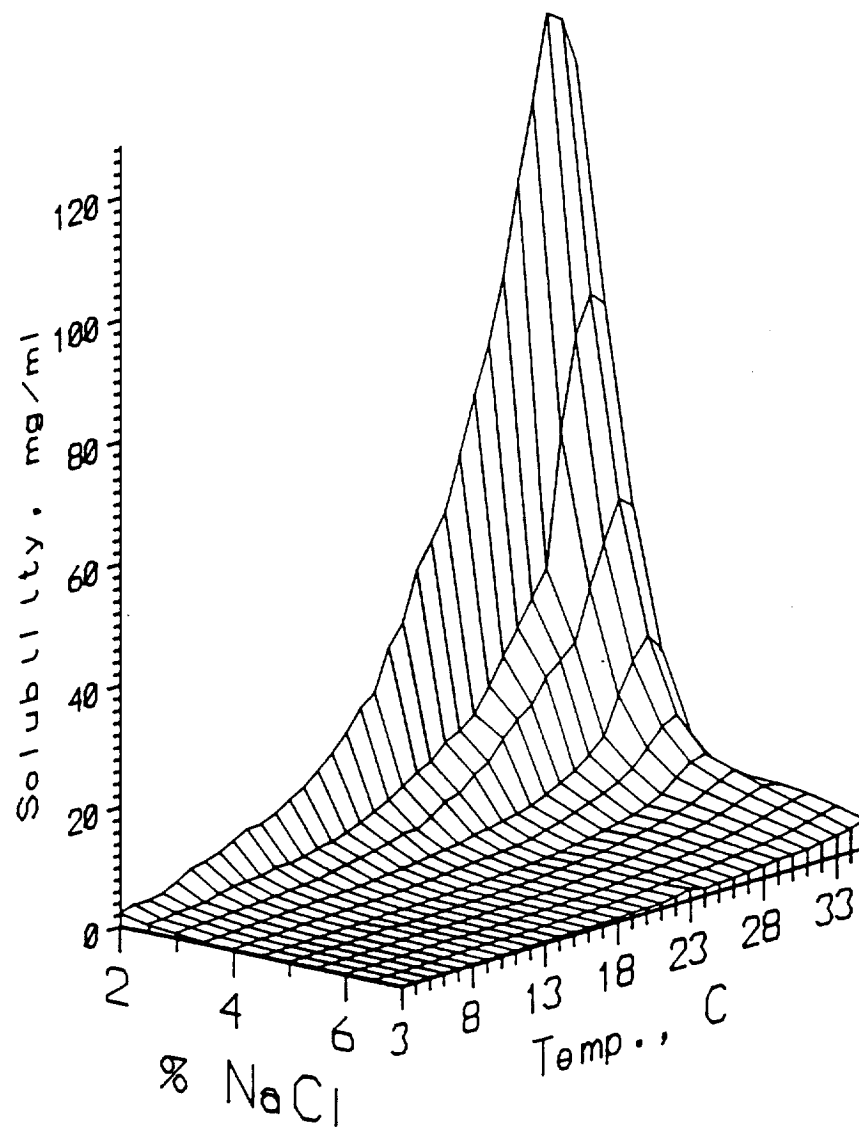


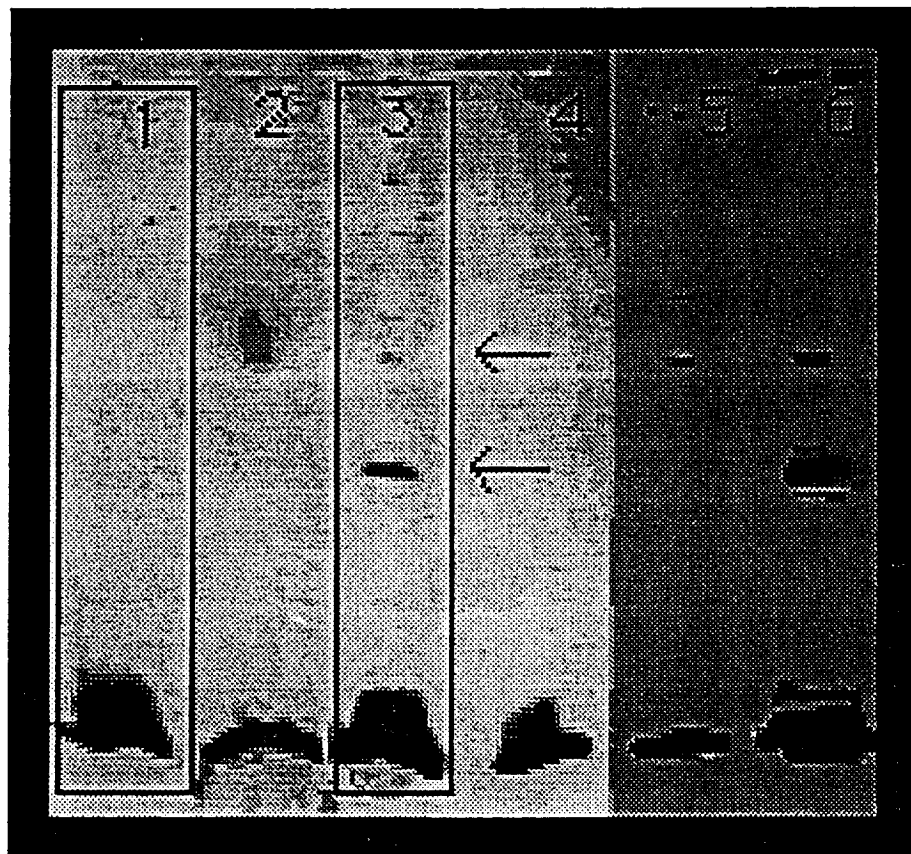
Figure 41. 10° precession photograph of a lysozyme crystal grown in 0.1M citrate buffer, pH 4.00, at a supposed purified lysozyme concentration of 25 mg/mL and salt concentration of 1.0% (w/v). From this, unit cell parameters were found to be $a=b=78.6 \text{ \AA}$ and $c=38.1 \text{ \AA}$.

tetragonal crystals. This seems to suggest that the elongation of the 110 face is not solely due to growth at low supersaturation conditions as was observed by Durbin and Feher but that other factors are also influencing the crystal shape. Further evidence of this is that there was no difference in the crystals grown with the purified and unpurified forms in the acetate buffer. If one looks at the phase diagram for lysozyme in acetate buffer (Figure 42) the region of interest (pH=4.00, temperature=23°C and [salt]=2.5%) is relatively flat. This can be interpreted as small changes in the conditions (such as unequal protein concentrations) will have very little effect on the final crystal forms. However, the the phase diagram for lysozyme in citrate buffer is unknown and it is expected that it would not have the same shape as the one in acetate buffer since lysozyme is less soluble in citrate than in acetate. It is likely then that the region of interest could be quite steep and that small changes in the conditions would yield large changes in the crystal appearance.

In an effort to understand the reason for the different crystal forms, the crystal growth of unpurified lysozyme was followed with SDS-PAGE. Both the mother liquor and the crystal were run on a gel with SDS-PAGE (Figure 43). After silver stain development it was apparent that there were no high molecular weight impurities in the crystals but they were present in the mother liquor. This is logical since it would be difficult for these components to fit into the crystalline lattice. Whether or not the impurities are involved in the crystal growth mechanism is still unknown.

Tet. Lysozyme, pH 4.0





SDS-PAGE. Samples dissolved in 10 mM Tris (HCl), pH 8.00, with 1mM EDTA, 2.5% (w/v) SDS and 2.5% dithiothreitol. Heated at 100oC for 5 min. Silver Stain Development. Lanes 5 and 6 background smoothed.

(1) Dissolved lysozyme crystal (2) Mother liquor (3) Mother liquor (4) Dissolved lysozyme crystal (5) Mother liquor (6) Mother liquor. See text for details.

Figure 43. SDS-PAGE with silver stain development on a solution of dissolved lysozyme crystal and diluted mother liquor.

Continuous Conductance Monitoring

In order for the flat conductance cell to be of use for monitoring solution conditions it must not interfere with the crystal growth process. To investigate this, a drop was placed over the electrodes containing lysozyme at the conditions for crystallization in acetate buffer. The conductance coverslip was then inverted over a reservoir solution that was twice the concentration of NaCl as the drop. The system was sealed with grease and the electrodes were energized continuously. After 24 hours the drop was observed under a microscope. The solution was brown in color and no crystals were observed. The control experiments remained clear and colorless for 6 days. Crystals were observed in the control experiments on the seventh day. Since the continuous energizing of the electrodes interferes with the crystal growth process, possibly by denaturing the protein, the flat conductance cell used in this manner is only useful for determining the evaporation curve before biological components are added. To overcome this problem, the electrodes could be energized when an optically isolated relay on the external module board activates a double throw relay which connects the conductivity meter to the electrodes. Crystals of lysozyme were grown with this arrangement by Bray [11].

Conclusions and Recommendations

The success of the development of the gas equilibration technique was dependent upon having the best conditions for lysozyme crystal growth. It was necessary that the conditions be reproducible so that any variation in crystal quality could be interpreted in terms of the type of equilibration and not variations in initial conditions. The importance of this was recognized early on and much effort was put into establishing protocols for delivering initial starting conditions that were exactly the same as those used in Linbro well hanging drop vapor diffusion studies. It was also important to establish the best crystals obtained in hanging drop vapor diffusion at a number of different starting conditions. These crystals were used to compare the crystals grown with different equilibration profiles using the gas equilibration technique. Furthermore, it must be known that any monitoring techniques used were not interfering with the crystal growth process. Since the flat conductance cell was found to interfere with the crystal solution when left energized continuously, it was used primarily for quantification of the equilibration curves. It was not used on samples that were to produce crystals.

SELECTED REFERENCES

- [1] CRC Handbook of Biochemistry and Molecular Biology (1976), Vol 1, 372.
- [2] CRC Handbook of Biochemistry and Molecular Biology (1976), Vol 2, 468.
- [3] CRC Handbook of Biochemistry and Molecular Biology (1976), Vol 1, 372.
- [4] Cox, Jane and Patricia C. Weber (1988) J. Crystal Growth, **90**, 318-324.
- [5] Carter, Charles W. , Eric T. Baldwin and Lloyd Frick (1988) J. Crystal Growth, **90**, 60-73.
- [6] Ataka, Mitsuo and Shoji Tanaka (1986) Biopolymers, **25**, 337-350.
- [7] Pusey, Marc, J. (1990) J. Crystal Growth, in press.
- [8] Ries-Krautt, Madeleine and Arnaud F. Ducruix (1989), J. Biol. Chem., **264**, 745-748.
- [9] Durbin, S.D. and G. Feher (1986) J. Crystal Growth, **76**, 583-592.
- [10] S. D. Durbin and G. Feher (1990) J. Mol. Biol. **212**, 763-774.
- [11] Bray, T.L. (1990) Masters Thesis, School of Chemistry and Biochemistry, Georgia Institute of Technology, Atlanta, GA.

CHAPTER V

pH CONTROL OF SUPERSATURATION

Introduction

Crystallization of proteins by pH equilibration has become a popular technique [1]. The ability to control the pH of a drop will expand the pH equilibration profiles available to protein crystal growers. The objective of the pH experiments described in this chapter was two-fold: (1) Determine the rate of pH equilibration in a hanging drop vapor diffusion crystallization experiment; (2) Determine if it was possible to computer control the pH of a small drop (10-30 μ L) with purges of acetic acid or water-saturated nitrogen gas. Once the pH equilibration within a Linbro well was known, efforts were made to slow down that equilibration with the added control of the gas system.

Materials and Methods

pH calibration buffers were 0.05M Fisher certified accurate to \pm 0.01 at 25° C. Deionized water (Barnstead Nanopure II), 0.2 μ m filtered, was used for all solutions. pH buffers were Fisher (\pm 0.01). Sodium acetate and ammonium sulfate were Fisher reagent grade.

Buffers and salts were all Fisher. All pH control experiments were carried out with 30 μ L drops of deionized water.

pH Equilibration

The sitting drop arrangement was used to monitor the pH equilibration in vapor diffusion crystal growth. No biological components were present in the drop. The pH was adjusted so that there was at least a 2 pH unit difference between the drops and reservoirs. For the reservoirs, a solution of 1.0 M sodium acetate (NaOAc) was adjusted to a pH of 5.32 with 6N HCl and a 1.0M ammonium sulfate $((\text{NH}_4)_2\text{SO}_4)$ was adjusted to a pH of 7.95 with 6N NaOH. For the drops, a 0.5M sodium acetate solution was adjusted to a pH of 7.48 with the NaOH and a 0.5M ammonium sulfate solution was adjusted to a pH of 5.22 with the HCl. The solutions were set up in a Linbro box with inverted beakers purchased from Fisher (Figure 32). Depressions were made in the beakers by heating them until soft and depressing the flat surface with a curved rod. They were then silanized using the procedure in Appendix 3 and sealed to the bottom of each well with silicone rubber sealant (Elmers). 1.0 mL of the 1.0M solutions was placed into the reservoir with a 1.0 mL eppendorf pipet. A 30 μ L drop of the 0.5M solutions was placed onto each miniature beaker with an eppendorf pipet. This was repeated for all 24 wells so that 12 wells were set up for NaOAc and 12 were set up for $(\text{NH}_4)_2\text{SO}_4$. The initial pH of both the drop and reservoir were

recorded. Each well was sealed with vacuum grease. At random, a well was selected for $(\text{NH}_4)_2\text{SO}_4$ and NaOAc and the time and pH of both the drop and reservoir were recorded. The well was marked so that no well was measured twice. The pH was monitored in this manner until the pH no longer changed from its previous value. Two trials were run for each salt.

Calibration

pH. The voltage response from the recorder output of the pH meter was converted to pH by a calibration relationship that was determined by measuring the response of three pH buffers (4.00, 7.00 and 10.00 pH units). The response was averaged over the time period that each buffer was measured and was plotted against the appropriate pH value. The relationship was entered into the LabTECH program so that conversion to pH was made as the readings were taken from the pH meter.

Gas Flow Rate. The flow rate of the gas stream was monitored by two rotameters, one for flow rates on the order of 0-8.0 mL/sec and one for flow rates ranging from 0 to 1.5 mL/sec. Both had to be field calibrated for N_2 (g). This was done using a soap bubble flow meter which was made from a 50.0 mL buret and a suction bulb.

pH Control

First, the gas bubblers were filled, one with 20.0 mL of deionized water and one 20.0 mL 2.04M acetic acid. The gas flow was monitored both out of each bubbler and out of the cell with the low flow rotameter. The flow was found to be equal at all three locations and was constant at 0.45 mL/sec. A 30 μ L drop of deionized water was suspended from the micro pH electrode with a 50 μ L Hamilton syringe. The control program described in Chapter 2 was executed and the pH, time and temperature was monitored at a rate of 1 Hz. There was no temperature control for these experiments so the temperature was monitored and the pH had to be corrected for any temperature change.

Results and Discussion

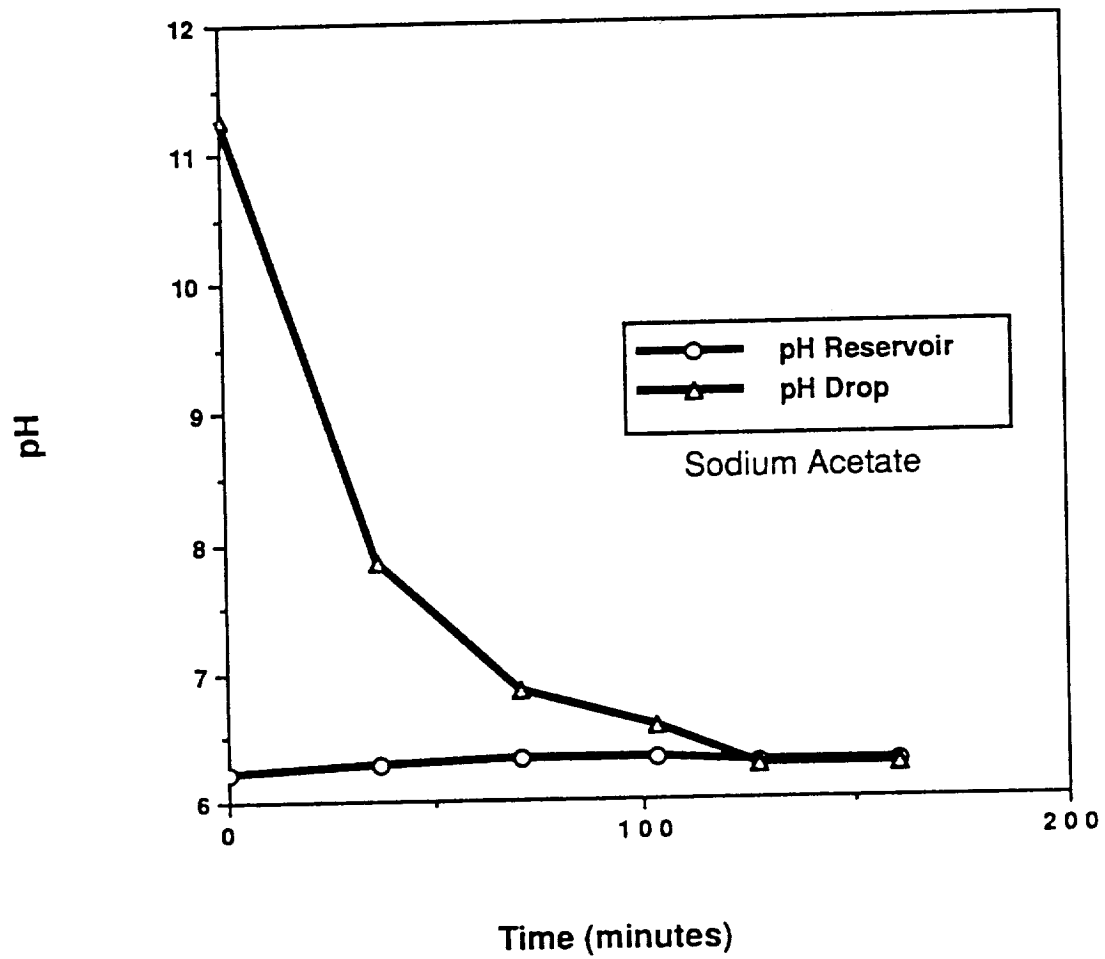
At a fundamental level, pH measurement involves some uncertainty. pH measurement by an electrode measures the activity of the hydrogen ion or a_{H^+} . The relationship is known to be:

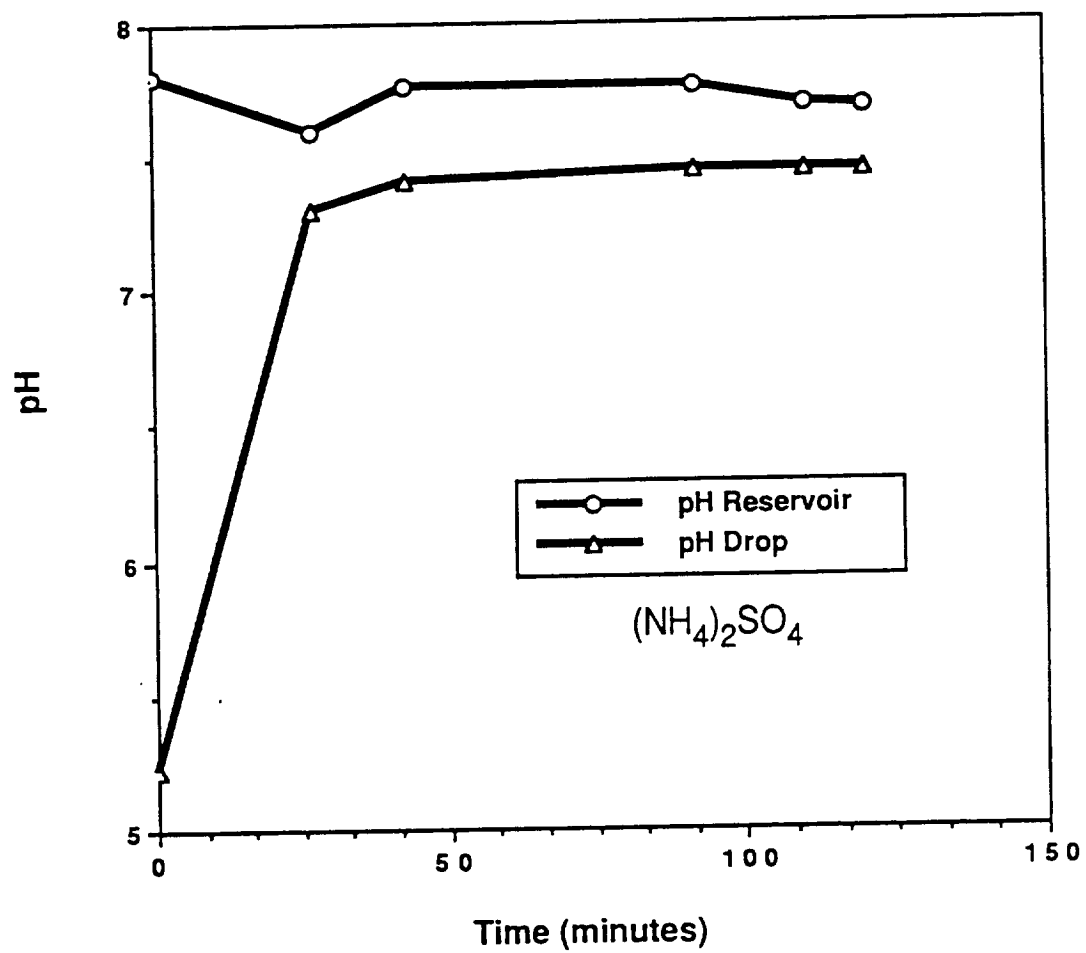
$$pH = -\log a_{H^+} = \frac{E_{cell} - E_{o'} - E_j}{S}$$

where $E_{o'}$ is a constant from the reference half-cell, E_{cell} is the electrical potential of the electrochemical cell and E_j is the junction potential which must be known in order to measure pH. Since it is

not possible to measure E_j with complete accuracy, the pH scale was established by reference to a standard buffer with a given pH value [2]. The pH of the unknown solution is measured by comparing the potential of an electrode in the unknown with the potential in a standard buffer. However, E_j may change from sample to sample especially in the case of samples with different ionic strengths. Illingworth [3] reported large pH errors in samples with different ionic strengths. For the pH control experiments carried out on hanging drops, the ionic strength of the solutions was kept constant by using deionized water. Since deionized water is low ionic strength it can cause problems with pH measurement such as errors in the junction potential and sluggish response. To minimize these errors, an electrode was chosen that was micro in size and had a design which minimized electrode junction potential errors. This same electrode was used for pH equilibration experiments.

The pH equilibration rates in Linbro wells for both ammonium sulfate and sodium acetate were determined and are shown in Figures 44 and 45 respectively. The change in pH represents the transfer of volatile ammonium and acetate ions between the drop and the reservoir. The time scale for this transfer is on the order of 2 hours for both salts. Mikol and Giege also determined the pH equilibration of a drop of ammonium sulfate to be about 2 hours [4]. The pH of the reservoir tends to determine the final pH of the drop. Because this is a rapid process, in crystallizations the rate of approach to the final supersaturation level will be very fast. This should affect the final size



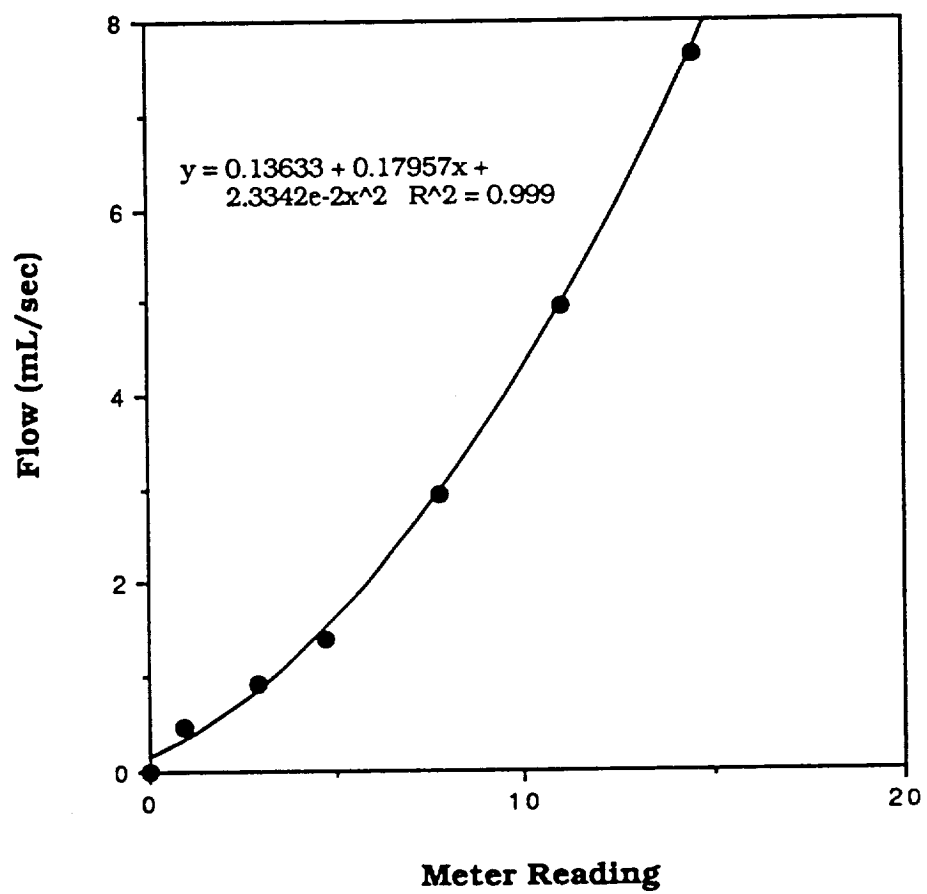


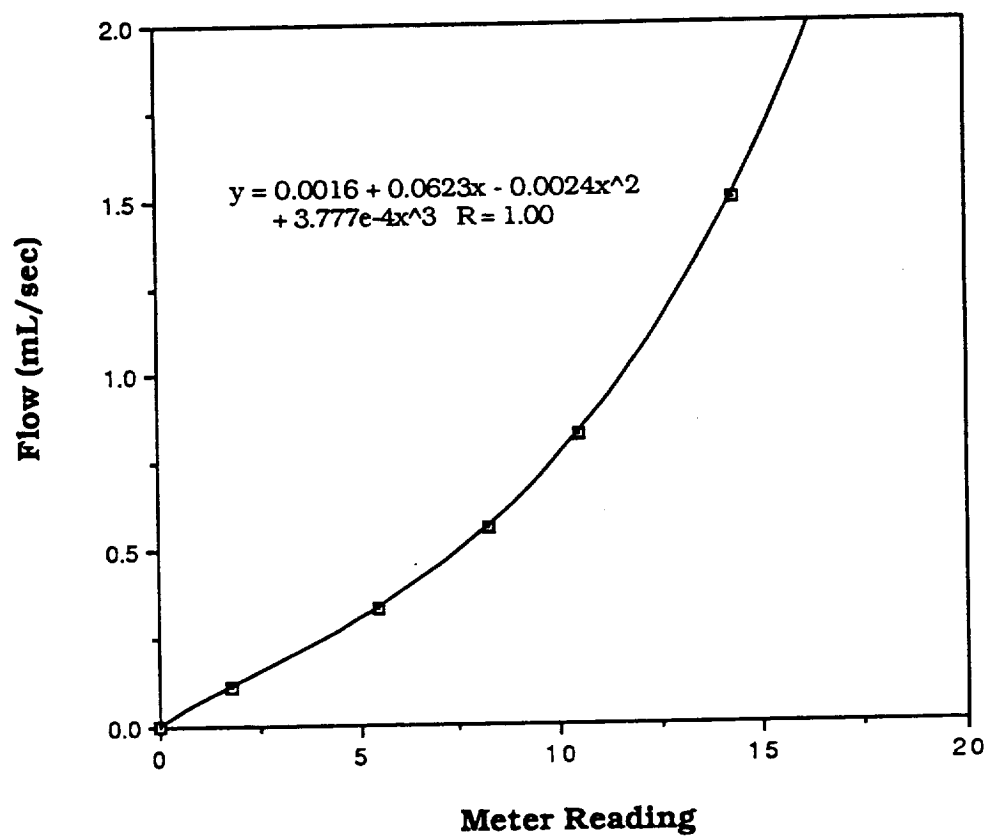
and number of crystals. It would be of some benefit for crystal growers to have the ability to very slowly approach the final pH by using acetic acid or ammonia saturated nitrogen gas.

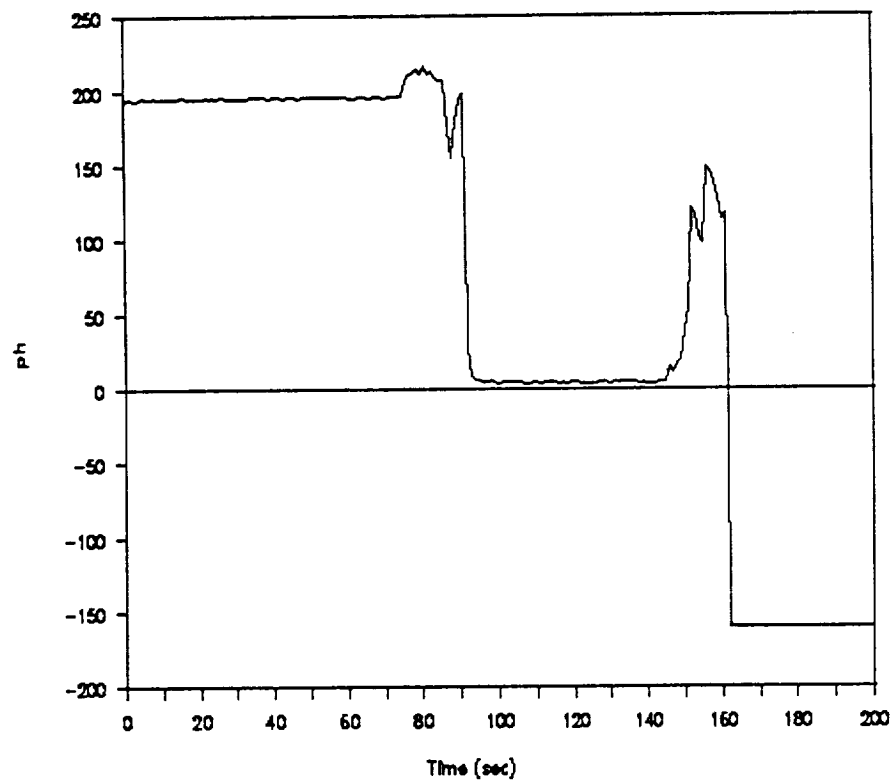
The first step in the pH control experiments was to calibrate the rotameters and the computer program. Figure 46 and Figure 47 show the results of the calibration of the high and low flow rotameters respectively. Figure 48 shows data output from the computer program for the pH measurement of the three calibration buffers. When the voltage response was plotted against the pH values (Figure 49) a straight line with a correlation of 1.00 was obtained.

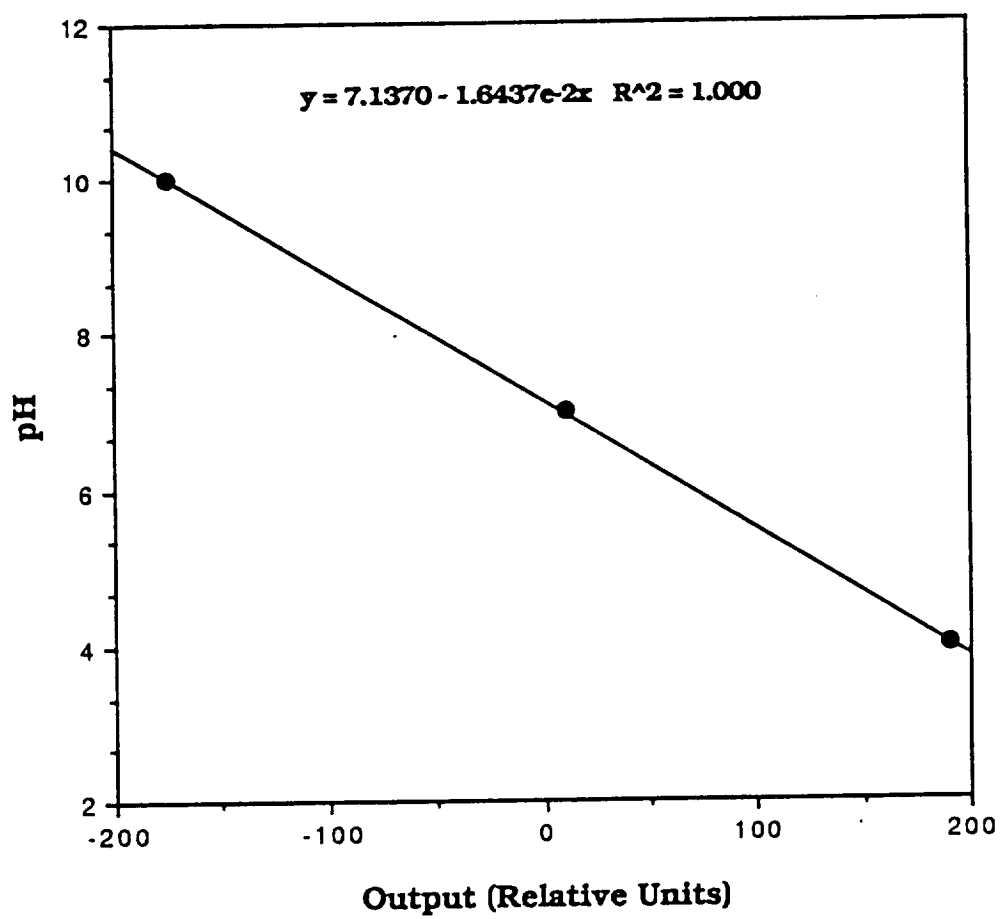
The first experiment performed was to open the valve to the acetic acid bubbler and see if any pH change could be detected in the drop after a significant amount of time (45 minutes). As can be seen in Figure 50, the pH of the drop changed from 5.9 to 4.1 in a matter of seconds so that the rate of change was equal to $-1.91\text{E-}2$ pH units/sec. After the acetic acid saturated gas had been purging the cell for 15 minutes the pH finally equilibrated at about 4.1. The "hill" occurring after the large pH drop is most likely due to pH gradients within the drop created as the acetic acid is taken into the drop at the gas/liquid interface and then must diffuse through the liquid to the electrode. It is understandable that this diffusion process would be on the order of several minutes since the ionic strength of the drop is low and therefore, the free electrolyte diffusion would be slow.

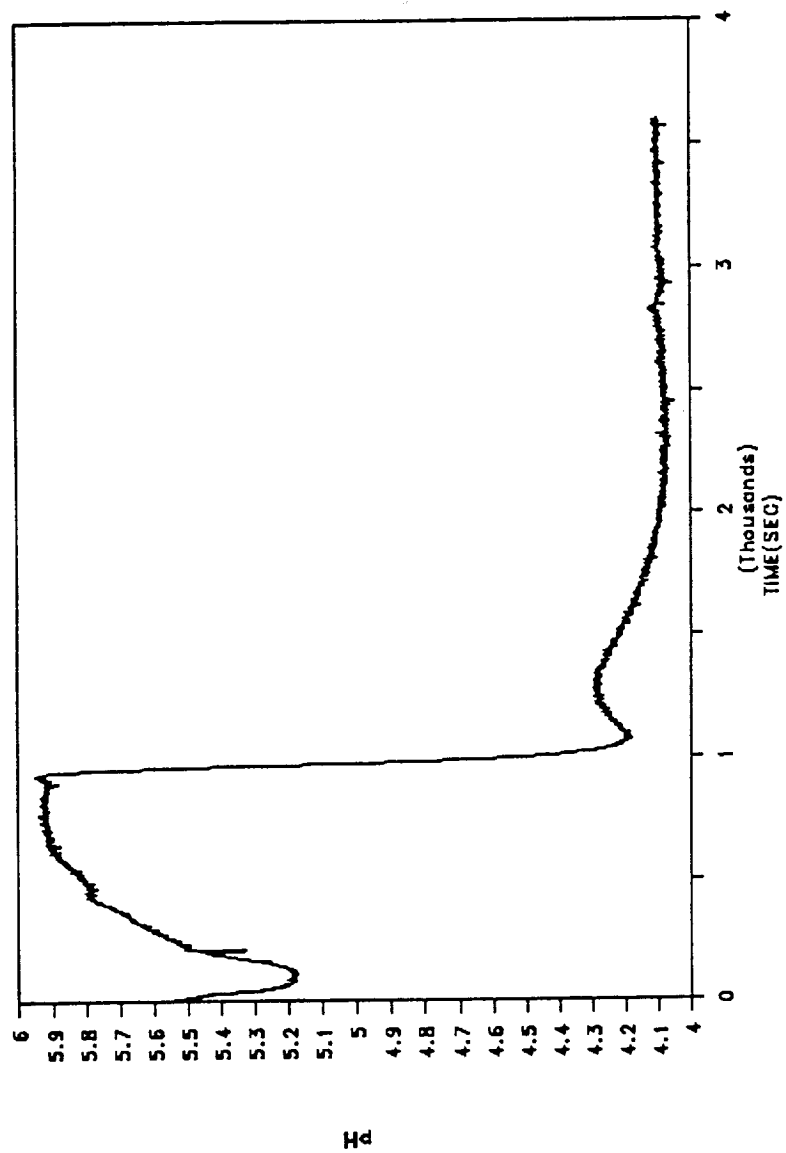
To slow the pH change rate the acetic acid saturated gas was added to the cell in 10 second purges, followed by an off period of 10





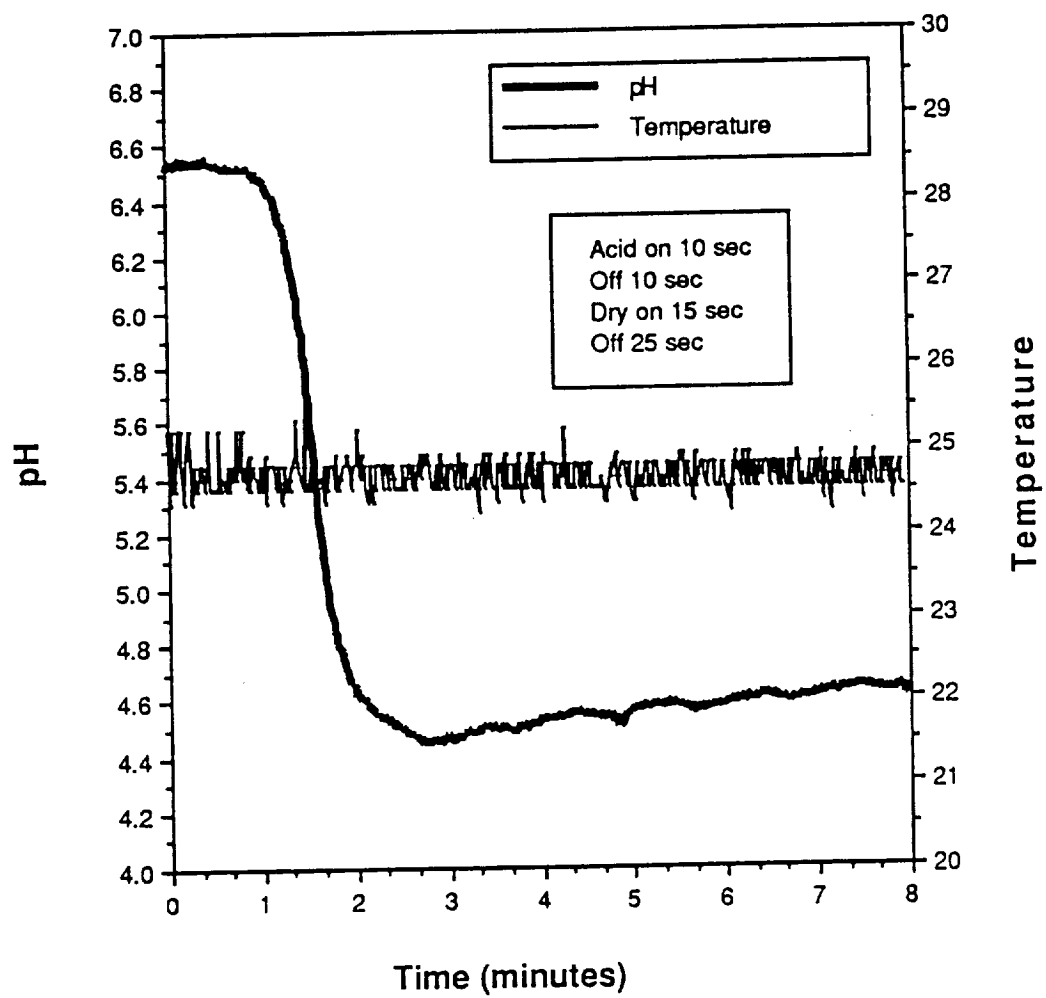






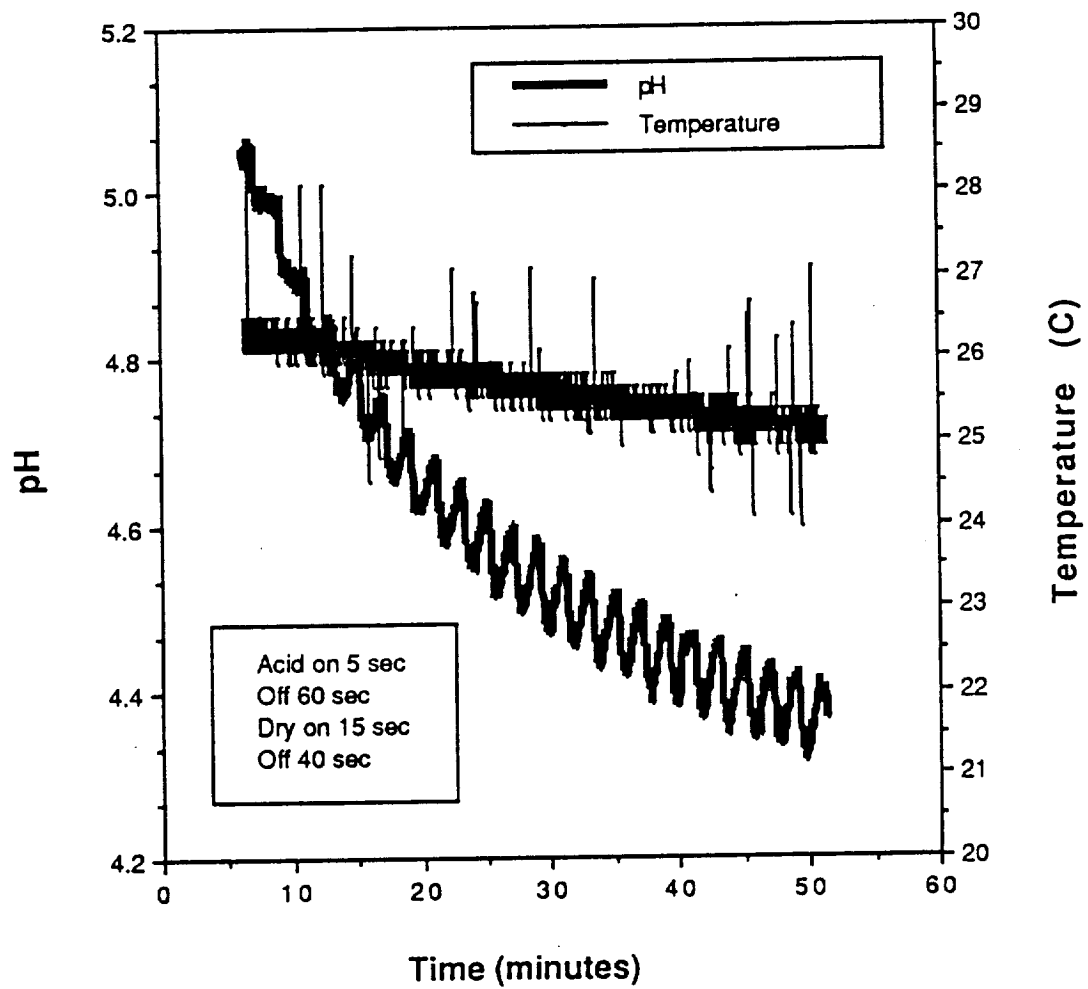
seconds to allow some time for uptake of the acetic acid into the drop. Dry nitrogen gas was then passed through the cell for 15 seconds to remove the material not absorbed into the drop. After 25 seconds the above cycle was repeated until the program was terminated. With this valve arrangement the pH of the drop changed from 6.52 to 4.44 in a period of 104 seconds or a rate of change of $-2.00\text{E-}2$ pH units/sec (Figure 51). While this is an improvement the pH is still changing rapidly and the goal of this technique is to very slowly change the pH. To slow down the pH change, the off interval between the acid valve opening and the dry gas valve opening was increased from 10 seconds to 60 seconds and the final off interval was increased from 25 seconds to 40 seconds. This caused the pH to decrease at a much slower rate ($-2.89\text{E-}4$ pH units/ sec) (Figure 52). However, after the first 7 minutes, the pH began to oscillate up and down between 0.1 pH units with an overall decrease in pH. The oscillations were in sync with the opening and closing sequence of the valves and it was thought that they were due to the removal of acetic acid from the drop and the cell with the purges of dry gas. This is an excellent picture of the removal and replacement of volatile solution components from the drop. Therefore, it is important that care be taken when volatile buffers and precipitating agents are used. It is possible to replace these components by saturating the gas and purging the cell.

Figure 53 shows the pH change with the addition of a purge of water-saturated gas. With this arrangement there are now two factors



which determine the pH change within the drop, the addition of acetic acid and the dilution of the drop with water. Initially, there is decrease in the pH from the addition of acetic acid. There is a shift in the direction of pH change at about 5 minutes when the dilution effect begins to overcome the acetic acid addition effect. This experiment was repeated to determine if the pH change was reproducible and the duplicate experiment is shown in Figure 54. Once again there is a quick decrease in the pH until the pH begins to first level and then rise after 5 minutes. The overall shape of the curve was similar to the previous experiment. The differences that do exist are thought to be due to the difference in temperature between the two experiments. It has been reported that pH values can differ as much as 0.2 pH units/ °C [5]. It was desirable to be able to control both the dilution and acid addition so that a slow stepwise control of the pH was possible.

To determine the relative strengths of the two effects, both the water and the acid intervals were made equal (10 seconds). As seen in Figure 55, the acid addition effect is dominant in the early stages and then the dilution effect is dominant in the later stages. Since the water addition is the most dominant effect, its interval was reduced to 5 seconds while the acid addition interval remained at 10 seconds. This resulted in a small pH decrease initially (0.5 pH units) followed by a stepwise increase in the pH (Figure 56). While this is more controlled, it was desired that the dilution effect be further minimized. Therefore, the water-saturated gas was mixed with dry gas



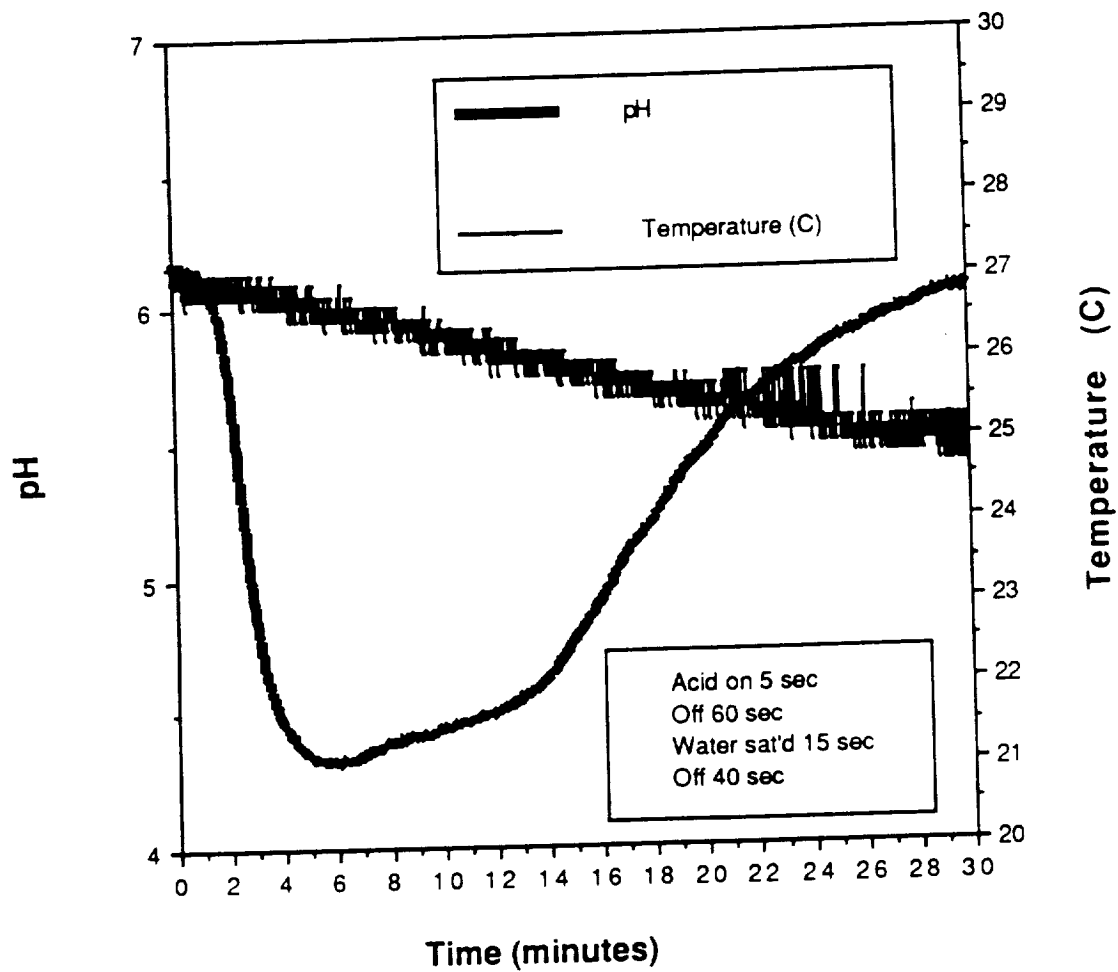
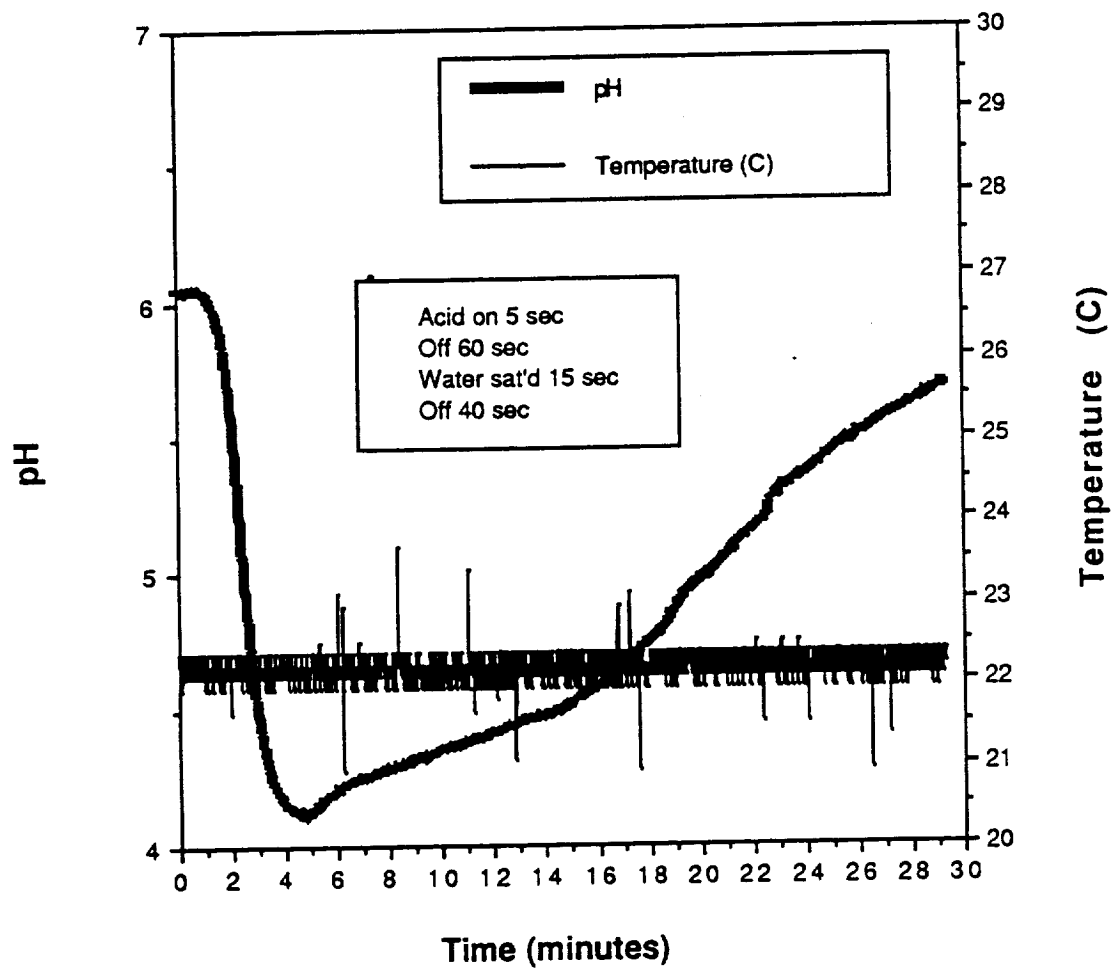


Figure 53. Results of pH4EXP. Dry gas purged replaced with water-saturated gas purge.

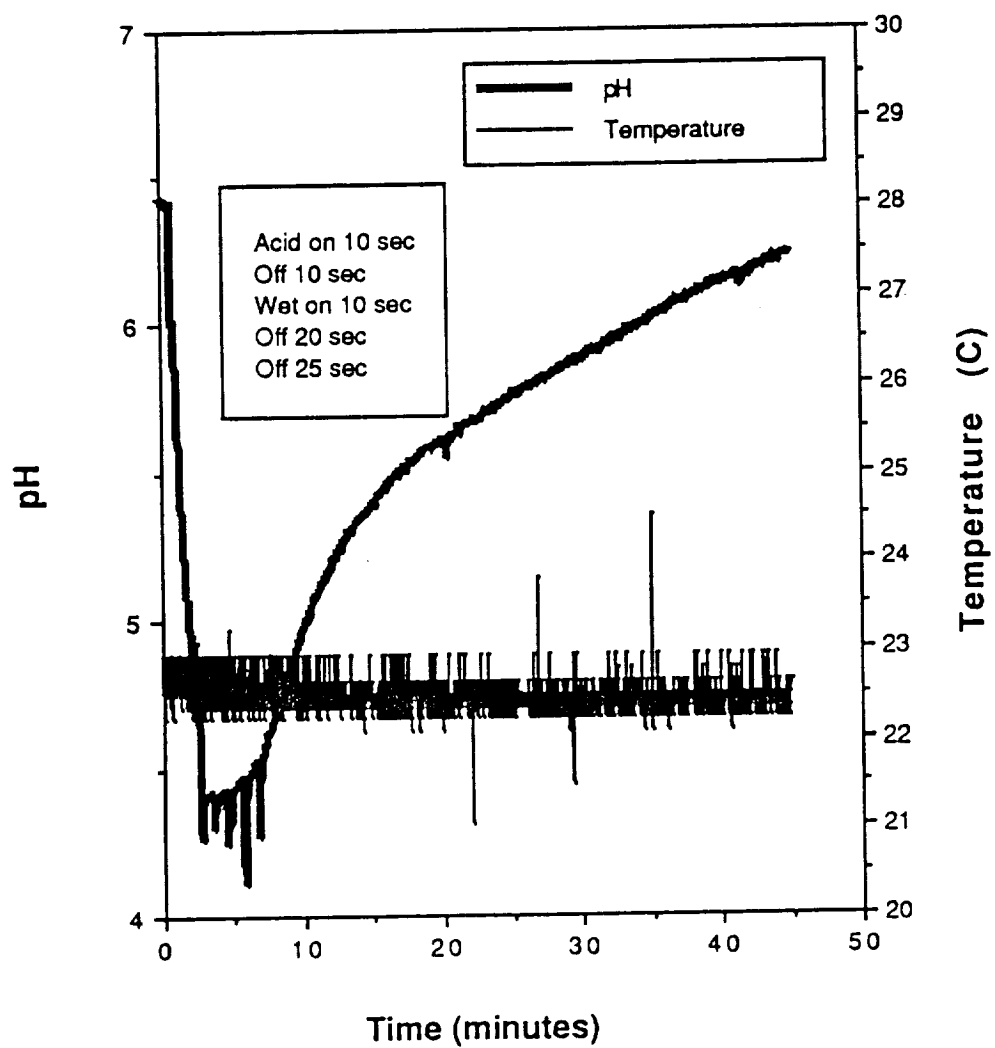


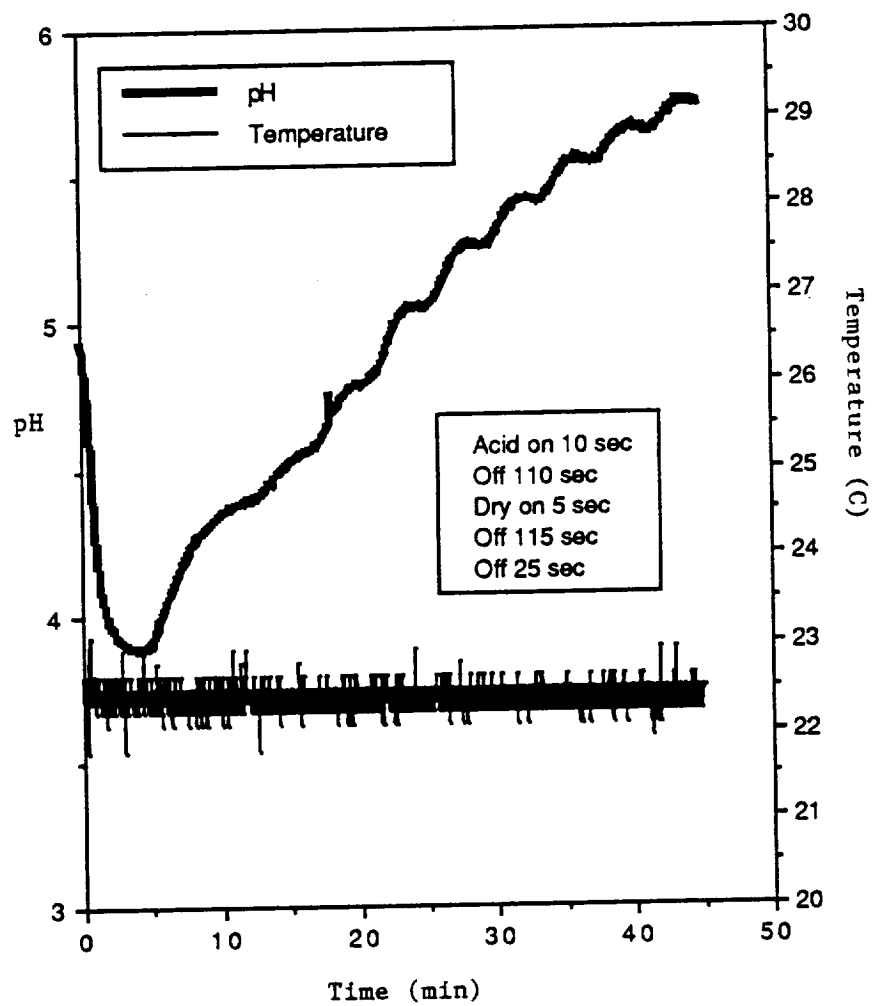
before it entered the cell. This should reduce the water content of the gas and thereby reduce the dilution of the drop. The acid interval was also increased to 15 seconds while the water-saturated/dry gas purge time was kept at 5 seconds. As can be seen from Figure 57, this slowed down the dilution of the drop so that there was a stepwise decrease in the pH of the drop. The rate of change in pH was -1.84×10^{-4} pH units/sec and finally levels to approximately a zero slope.

Table 10 compares the slopes for the various experiments reported above. The addition of the water-saturated/dry gas allowed for the slowest decrease in pH. Also, in almost every experiment there was an initial dip in pH that was on the order of -1×10^{-2} pH units/sec. These dips are likely due to the very fast incorporation of acetic acid into the drop with the first purge. The rate of change for pH1EXP is of a similar magnitude where the pH change is due only to one continuous acetic acid purge.

Conclusions and Recommendations

From this series of experiments it has been shown that the pH of a hanging drop can be controlled with purges of acetic acid saturated nitrogen gas coupled with purges of water-saturated and dry nitrogen gas. It is recommended that more experiments be carried out to determine what effect the oscillations have on protein crystal growth. It may be possible that since the oscillations are for short periods of time (10 seconds) and small in amplitude (0.1 pH units) they will not





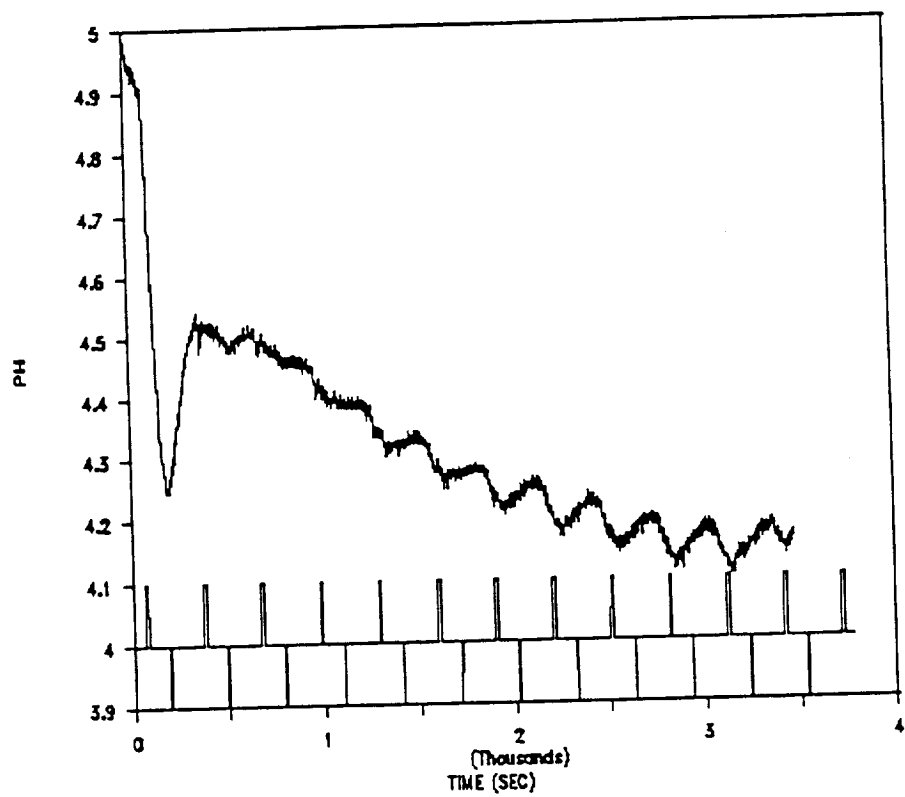


Table 10. Comparison of rate of pH change.

Experiment Title	Initial Region Rate ^a pH units/sec	Second Region Rate ^b pH units/sec	Third Region Rate ^c pH units/sec
pH1EXP	-3.45E-2	-1.91E-2	N/A
pH2EXP	N/A	-2.00E-2	N/A
pH3EXP	N/A	-2.89E-4	N/A
pH4EXP	-1.25E-2	+6.80E-4	+1.33E-3
pH5EXP	-6.50E-3	+5.20E-4	+1.89E-3
pH6EXP	-2.05E-2	+1.86E-3	+4.35E-4
pH7EXP	-5.04E-3	Not Measured	Not Measured
pH8EXP	-3.65E-3	-1.84E-4	~0

^aCalculated from initial pH to the pH at which slope first changes direction.

^bCalculated from the last point used in (a) to the pH at the second slope change.

^cCalculated from the last point used in (b) to the final pH.

interfere with the crystal growth process. Otherwise, it is possible that they could be eliminated by very short (1 second) purges of both acid and water-saturated gas or with the use of buffered solutions. Since acetic acid is only useful in the pH range of 4-6., it may be necessary to use other volatile acids and bases to provide more control over the pH. The final test of this technique is the growth of crystals by pH equilibration and the evaluation of the crystals grown with different pH equilibration profiles.

SELECTED REFERENCES

- [1] McPherson, A. Jr., *Preparation and Analysis of Protein Crystals* (Wiley, New York, 1982).
- [2] Bates, R.G. (1973) *Determination of pH, Theory and Practice*, 2nd Edition, (Wiley New York, NY).
- [3] Illingworth, J.A. (1981) *Biochem. J.*, **195**, 259-262.
- [4] Mikol, V., J.L. Rodeau and R. Giege (1989) *J. Appl. Cryst.*, **22**, 155-161.
- [5] Brezinski, S.P. (1983) *Analyst*, **108**, 425-442.

CHAPTER VI

EVAPORATION CONTROL OF SUPERSATURATION

Introduction

It is expected that the kinetics of supersaturation, which is directly related to solvent evaporation, will affect protein crystal growth and nucleation and accordingly determine the quality, number, size and morphology of the crystals. Before it was possible to dynamically control the supersaturation of a hanging drop with $N_2(g)$ it was necessary to determine the vapor equilibration occurring in a traditional hanging drop vapor diffusion crystallization experiment. Once this processes was understood it was possible to mimic the evaporation with the $N_2(g)$ equilibration and then improve upon it with the added control provided by the gas equilibration system.

Materials and Methods

Calibration

Flat Conductance Cell Calibration. The coverslip was calibrated with NaCl standards. 20 μ L drops were placed onto the electrodes

and monitoring the response from the conductance meter with the computer and with a digital voltmeter.

Thermal Conductivity Detector Calibration. The TCD was calibrated by placing drops of deionized water with accurate volumes onto a coverslip. The well was sealed with grease. The computer program was started and allowed to run until the drop evaporated. The peaks from the detector were integrated and the areas were summed. Once the drop had evaporated to dryness, the value of the summed peak areas was plotted against the volume of the drop. The drop volumes used were 5 μL , 10 μL and 20 μL drops.

Thermocouple Calibration. The T-type thermal couples were calibrated by placing the temperature sensitive junction into the Lauda circulating water bath at temperatures ranging from 18° C to 26° C and recording the voltage response with the computer. Each reading was repeated three times.

Vapor Equilibration in Linbro Wells

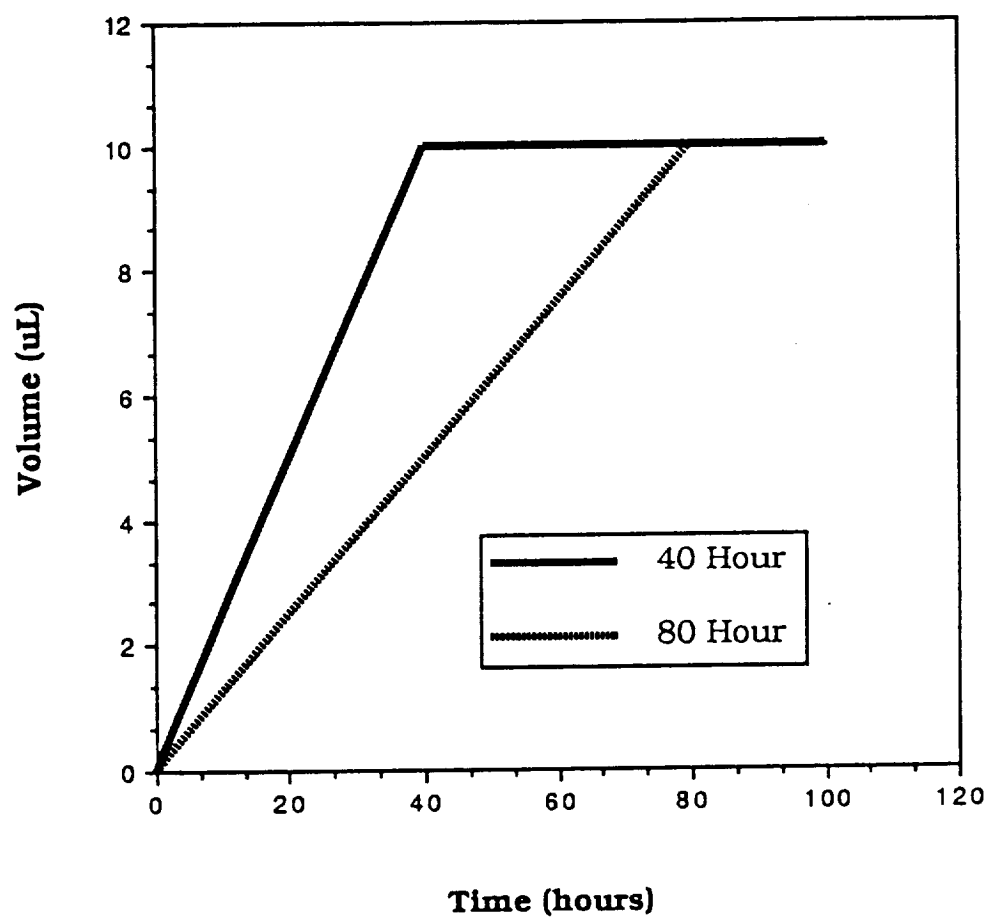
For quantification of the evaporation in a Linbro well no biological components were used. The conductance coverslip described in Chapter 2 was used to monitor the evaporation of 20 μL drop of NaCl over a reservoir of twice the NaCl concentration. For evaporation measurements, 1.0 mL of a 0.1M NaCl solution was placed into a

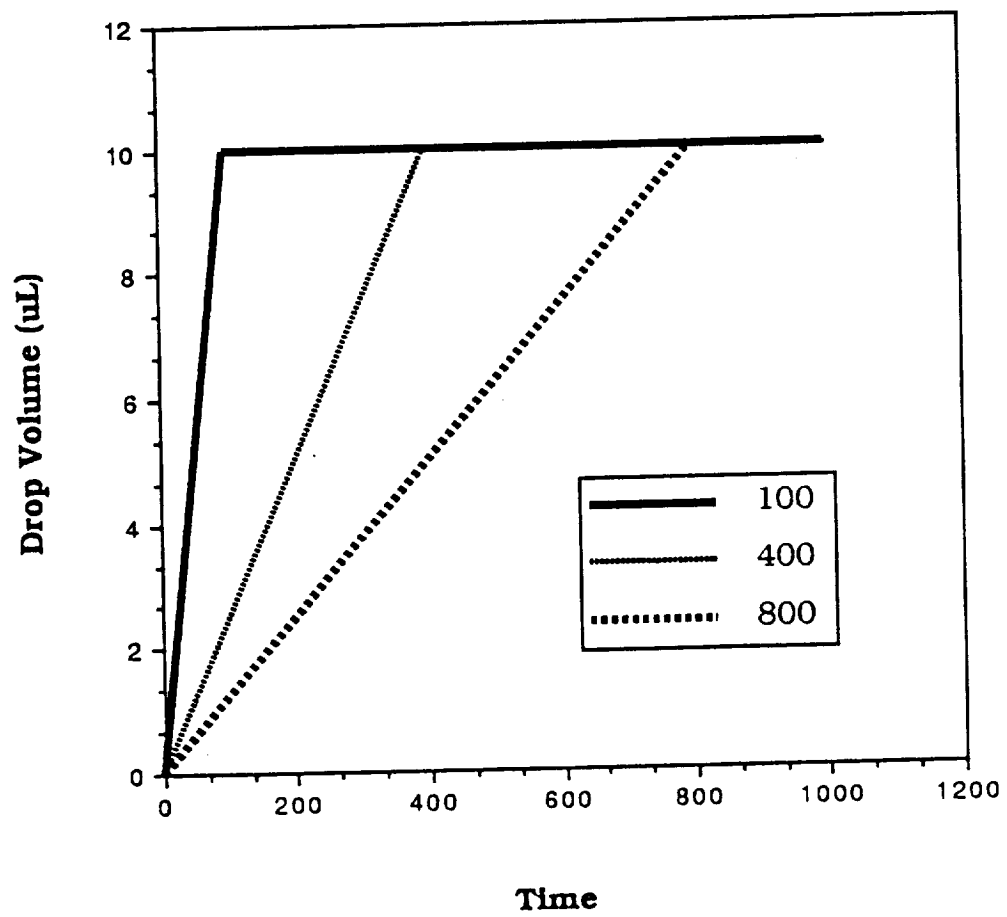
Linbro well. 10 μ L of the reservoir solution was placed on the electrodes and 10 μ L of deionized water was added so that the final concentration of the drop was 0.05M NaCl. The coverslip was inverted and sealed to the well with Dow Corning vacuum grease. The computer program was started and both conductance and temperature were monitored until there was no more change in conductance.

Evaporation Control

Initial Conditions. The initial starting conditions for protein and salt concentrations were the same as those developed in Chapter 4. The protein used is specified and was either Sigma in its purified or unpurified form (see Chapter 3). The four conditions used were: (1) Purified lysozyme (23.2 mg/mL), pH 4.00, 0.1M citrate buffer, 1% NaCl. (2) Purified lysozyme (23.2 mg/mL), pH 4.00, 0.1M citrate buffer, 0.5 % NaCl. (3) Purified lysozyme (25.9 mg/mL), pH 4.00, 0.1M acetate buffer, 5% NaCl (4) Unpurified lysozyme (23.2 mg/mL), pH 4.00, 0.1M acetate buffer 5% NaCl.

Evaporation Curves. Different evaporation curves were followed and their effect on the crystals was studied. Two different series were run. The first was a series of short term evaporation curves (<100 hours) which are shown in Figure 58. The second set of curves were long term evaporation (< 1000 hours) and are shown in Figure 58. The desired curve was entered into the program in terms of volume



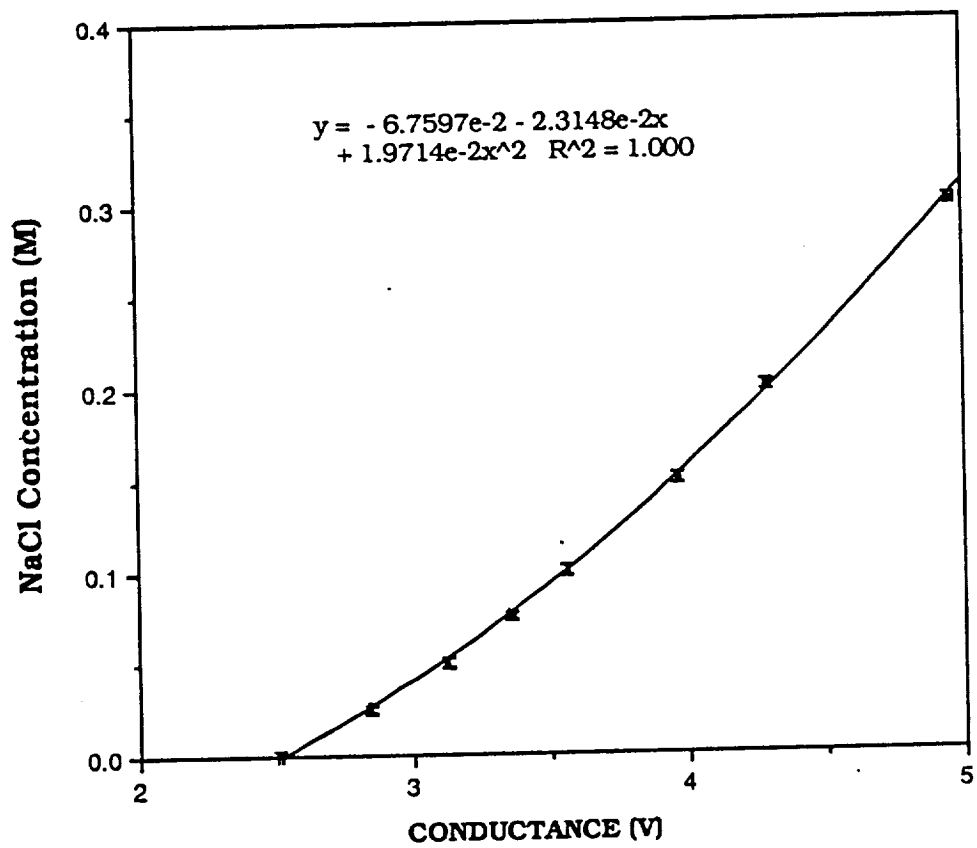


evaporated over time where volume was in μL and time in seconds. The initial volume of all of the drops were $20\ \mu\text{L}$ where $10\ \mu\text{L}$ came from the protein solution and $10\ \mu\text{L}$ was from the salt solution. Since the $10\ \mu\text{L}$ dispenser had a precision of 1% (full scale) the initial volume of the drops were $20\ \mu\text{L} \pm 0.2\ \mu\text{L}$. Upon termination of the experiment, the coverslips were transferred to an empty Linbro well and sealed with grease. The crystals were photographed periodically until they ceased to grow.

Results and Discussion

Calibration

Flat Conductance Cell Calibration. The flat conductance cell was calibrated with solutions of known NaCl concentrations (Figure 60). The calibration response curve was linear at NaCl concentrations below 0.1M and then exponential above 0.1M. A linear relationship exists between the conductance response and the square root of concentration. This is to be expected since NaCl is a strong electrolyte [1]. The calibration relationship was used in the computer to convert the voltage response of the conductance meter to NaCl concentration. In order to stay within the linear range of the flat conductance cell very dilute concentrations of NaCl ($< 0.1\text{M}$) had to be used.



CALIBRATION OF TCD
FLOW=7.5 TEMP=20.5

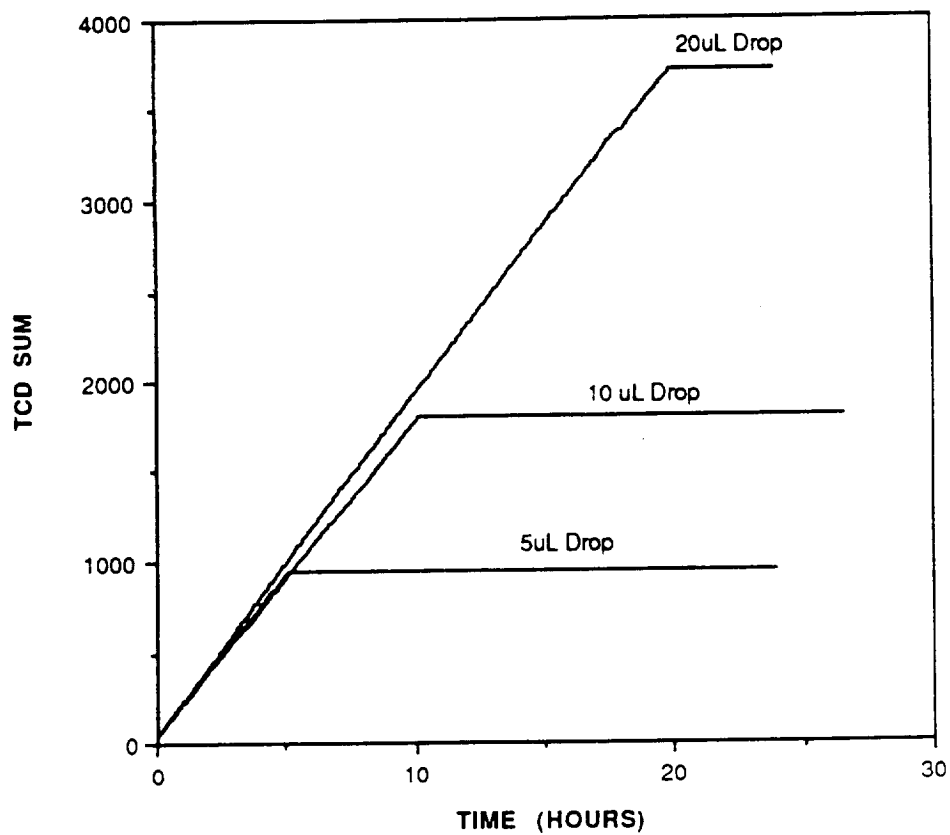
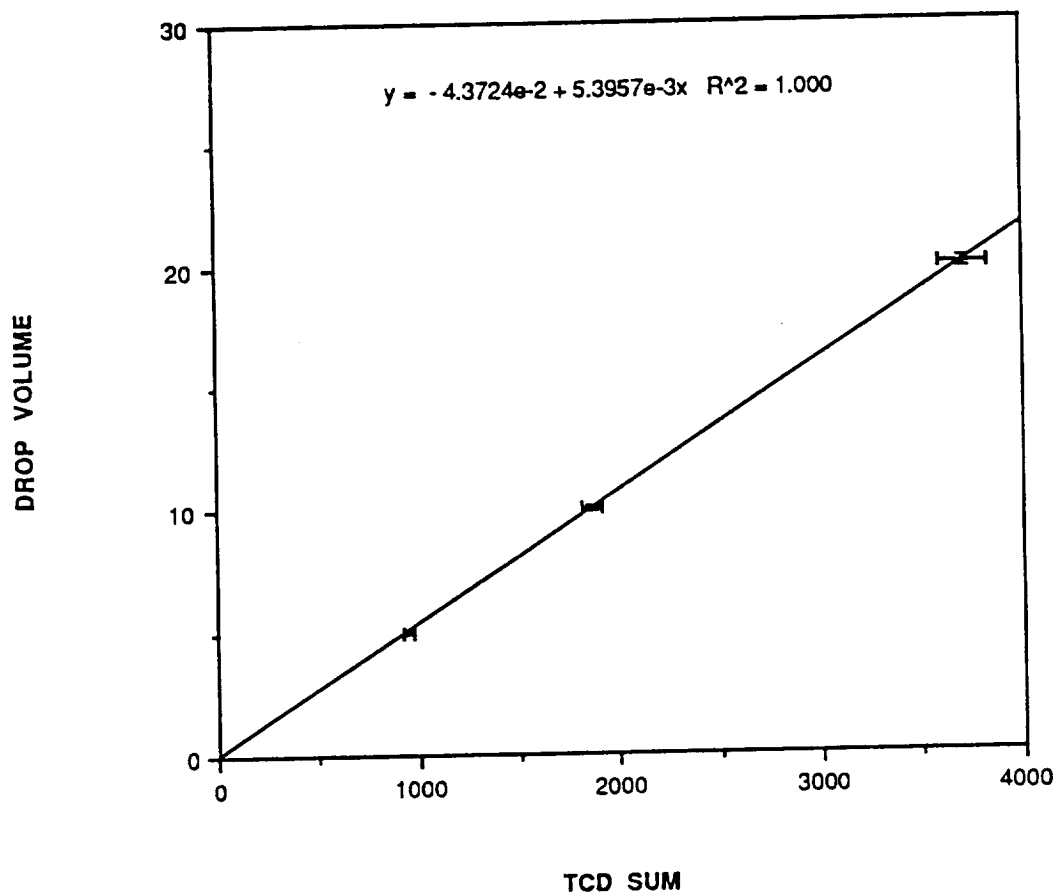
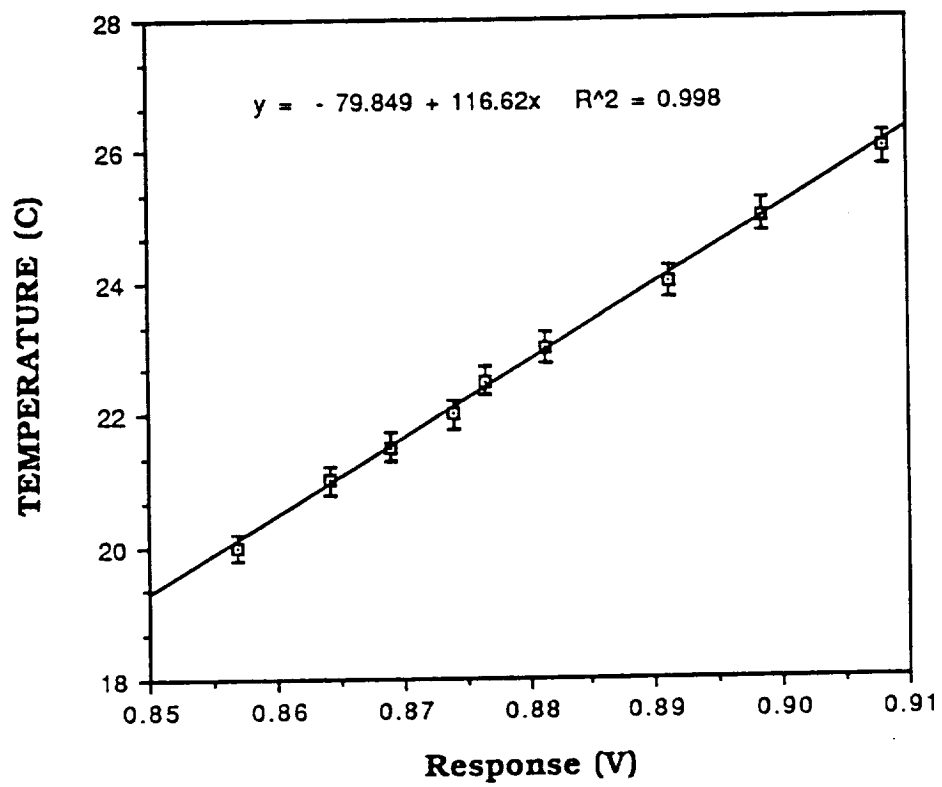


Figure 61. Evaporation to dryness of a 5 µL, 10 µL and 20 µL drop as monitored by the TCD.





Thermal Conductivity Detector Calibration. Each drop of deionized water was evaporated to dryness as shown in Figure 61. The integrated sum was plotted against the drop volume and a direct relationship was obtained (Figure 62). This relationship was entered into the computer program.

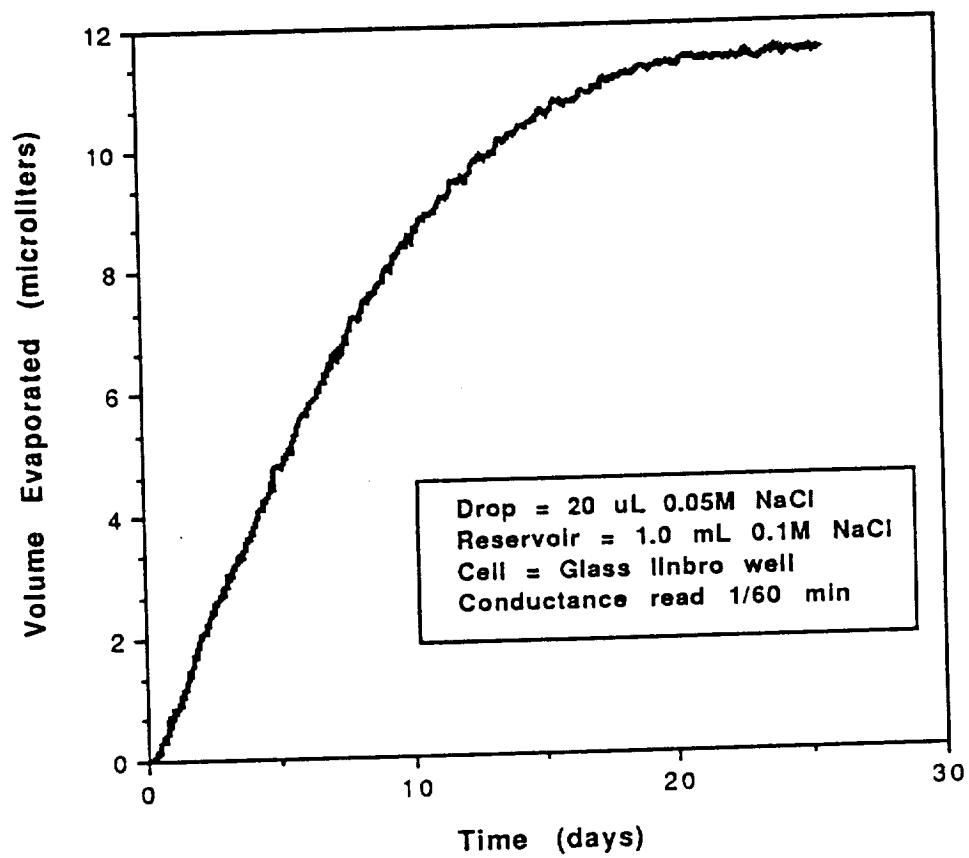
Thermal Couple Calibration. A straight line relationship was obtained between the temperature of the water bath and the voltage response of the thermal couple (Figure 63). The linear correlation coefficient was $R^2 = 0.998$. This relationship was entered into the computer program to convert voltage to temperature in degrees Celsius.

Vapor Equilibration in Linbro Wells

A few studies have been devoted to understanding the parameters which govern the evaporation of water and volatile solution components in Linbro wells [2] [3]. However, these studies were done on measurements of hanging drops by sacrificing one drop out of a series of drops and measuring the change in refractive index, which is proportional to the salt concentration within the drop. While this can be related back to volume evaporated from the drop, it assumes that each drop equilibrates at the same rate. Furthermore, there are more sensitive techniques for determining salt concentration than changes in refractive index. In fact, the errors involved in the refractive index

measurement have an uncertainty in estimating the change in volume of a 30 μL drop of $\pm 2.0 \mu\text{L}$. This means that the refractive index procedure is only useful for detecting volume changes greater than 2.0 μL . A more sensitive technique for determining salt concentration in a drop is measuring solution conductivity since the conductance of a solution is directly related to the concentration of salt in that solution. Another advantage to using the flat conductance cell described in Chapter 2 is that it allows the monitoring to be done on a single drop so that a dynamic picture of solvent evaporation is obtained.

By monitoring the conductance of a dilute NaCl drop, the evaporation profile of vapor diffusion from the drop to the reservoir was determined (Figure 64). From this it was found that the time to reach equilibrium was 20 days (Figure 65) and the final volume reached was just over one half of the initial drop volume. The shape of the evaporation curve was linear for the first 15 days and then curved asymptotic to the final drop volume. Since the crystallization conditions for lysozyme in NaCl are at much higher NaCl concentrations (1-5% NaCl) the time required to reach equilibrium should be much shorter. However, the shape of the equilibrium curve should be similar. In fact, similar experiments using refractive index have shown that equilibrium can take anywhere from 24 hours to 25 days and that the shape and time are determined by the initial solute concentrations, the difference in the equilibrium vapor pressure of the



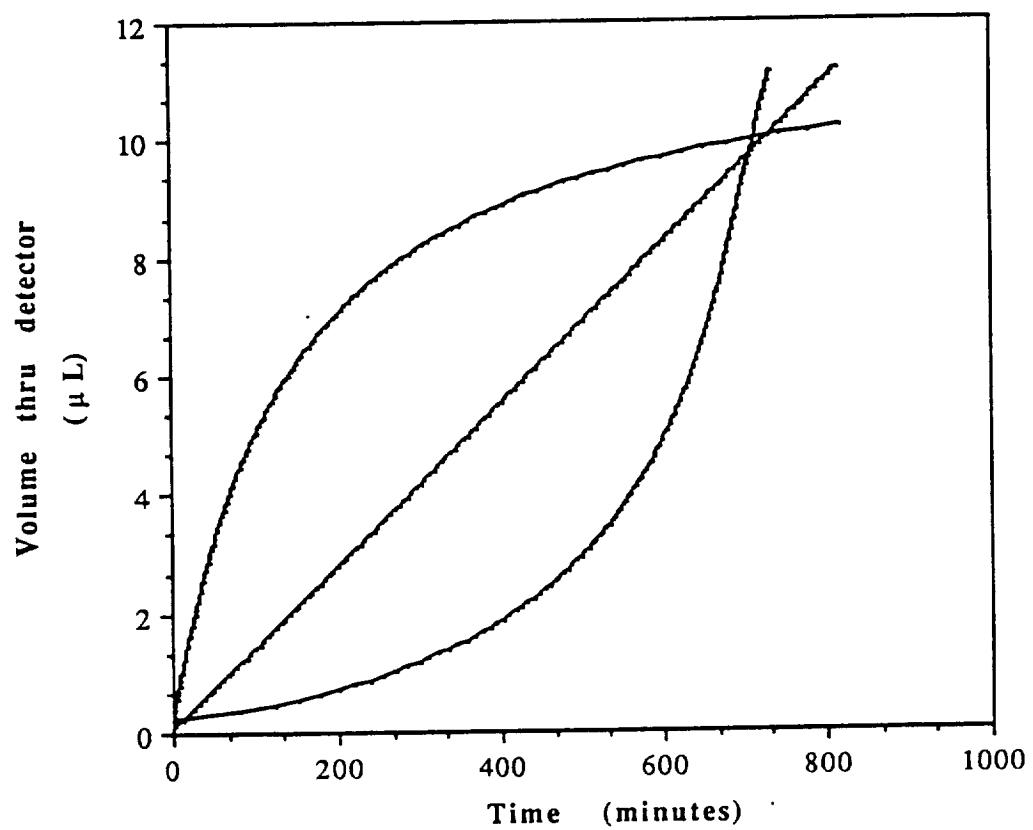
drop and reservoir, temperature and the diffusion path of the vapor [4].

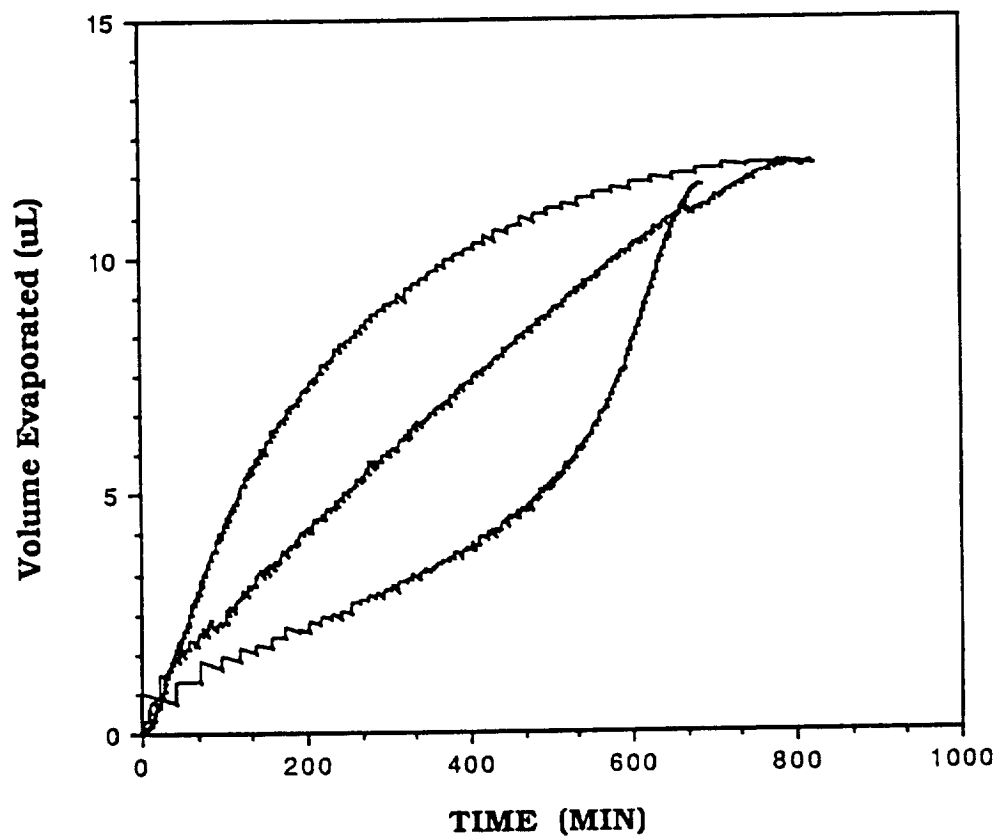
Evaporation Control

The general shape of the equilibration curve in Linbro wells was recognized to be similar to the Michelis-Menton binding curve which has the general form

$$y = \frac{nAx}{1 + Ax}$$

By adjusting the coefficients n and A , an equation was developed for a curve which approached half the drop (10 μ L) volume in about 25 hours. This equation was used to investigate the ability of the instrument to control evaporation of a 20 mL drop (Chapter V). Two other curves were also developed. One was the inverse of the first equation and the third a linear equation. These three equations were entered into the computer program and the response of both the TCD and the conductance of the drop were monitored. Figure 65 shows the detection of moisture in the gas stream by the thermal conductivity detector. These curves are in exact agreement with the theoretical equations followed by the computer program. During the same set of experiments the conductance of the drop was measured at 5 minute intervals and the result is shown in Figure 66. While the





shapes of these curves are similar to the theoretical curves there are differences which are most likely due to concentration gradients within the drop created by localized evaporation of solvent at the surface of the drop.

The first test of the ability of this device to grow crystals was a study where the conditions for crystallization of unpurified lysozyme in acetate buffer at pH 4.7 were used (condition (4)). Two linear curves were followed that evaporated 10 μ L from a 20 μ L drop in 40 hours and 80 hours. The results of the crystals obtained with these equilibration curves are shown in Tables 11 and 12. Not only did the controlled evaporation curves yield crystals but they were of comparable size and number to those grown under the same conditions as those grown in the Linbro wells (see Table 8, Chapter 4). The average number of those grown with the 80 hour (4.4 ± 1.4) was equal within experimental error as those grown with the 40 hour (4.57 ± 0.98) equilibration. This was also true of the area of the crystals in the 80 hour ($0.39 \pm 0.11 \text{ mm}^2$) and the 40 hour ($0.37 \pm 0.05 \text{ mm}^2$). These two experiments seem to suggest that gas controlled evaporation is a viable method for growing protein crystals and that it does produce crystals that are of the same quality in terms of size and number as the crystals grown with the traditional reservoir method. However, these experiments were done with the impure lysozyme and with acetate buffer which was removed from the drop with purges of dry gas. This severely limits the chances of

Table 11. Results of crystals grown with controlled evaporation following the 40 hour evaporation curve.

Linbro Well	Number of Crystals	Average Area (mm²) ^a
C2	6	0.33
C4	4	0.32
D1	5	0.33
D2	3	0.44
D4	5	0.43
D5	5	0.35
D6	4	0.40
MEAN	4.6 ± 0.98	0.37 ± 0.05

^a Measured with the procedure shown in Figure 37.

Table 12. Results of crystals grown with controlled evaporation following the 80 hour evaporation curve.

Linbro Well	Number of Crystals	Average Area (mm²) ^a
B1	6	0.24
B2	4	0.30
B3	5	0.30
B5	5	0.50
B6	2	0.53
C1	5	0.41
C3	6	0.33
C4	4	0.37
C5	2	0.54
MEAN	4.4 ± 1.4	0.39 ± 0.11

^a Measured with the procedure shown in Figure 37.

reproducing the exact same conditions for future long term experiments. For this reason, the long term experiments were carried out using the purified lysozyme from Sigma and citrate buffer in parallel with the conditions that yielded crystals in acetate buffer.

Long Term Evaporation. The long term evaporation experiments were carried out on four different sets of conditions and three different equilibration curves for each condition. The crystals obtained with each curve were compared not only to the other curves but also to crystals grown with the hanging drop vapor equilibration method and are shown in Figures 67-68 and 71-72. In no case were the differences between the crystals large. However, there were general improvements seen with the longest curve as compared to the 100 hour curve or the traditional reservoir method with three of the four conditions.

Acetate Buffer. There were two sets of conditions made up in acetate buffer. The only difference between the two conditions were that in one the lysozyme was purified (Figure 67) and the other the lysozyme was unpurified (Figure 68). For the purified lysozyme there was a decrease in the number of crystals obtained with each curve (see Figure 69). As the equilibration time increased the number of crystals decreased. There was also an increase in the average area of the crystals with the slower evaporation rates (Figure 70). This trend was not seen with the unpurified lysozyme. In fact, the unpurified

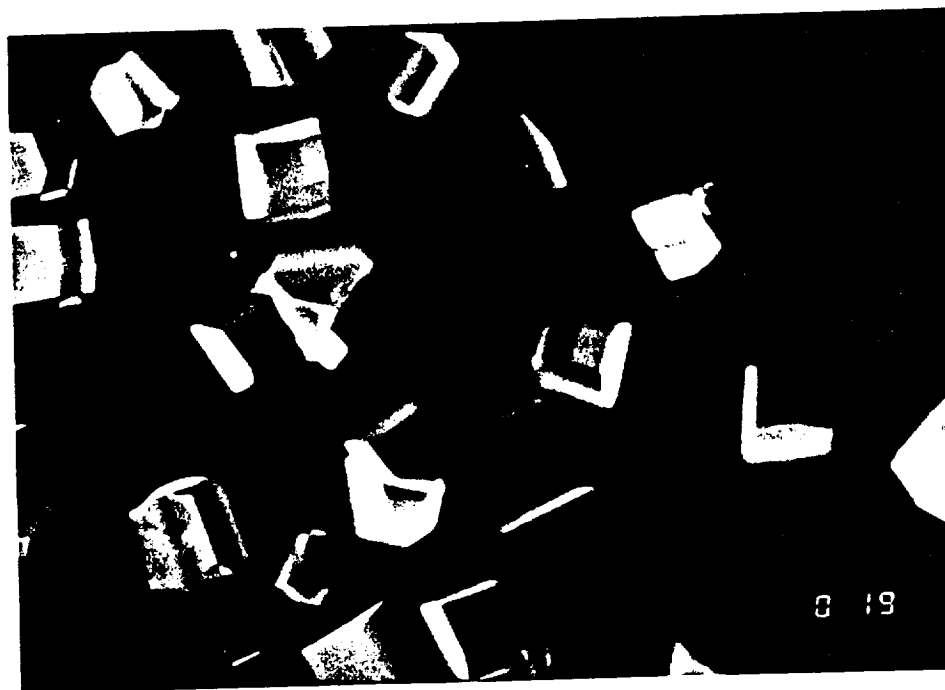
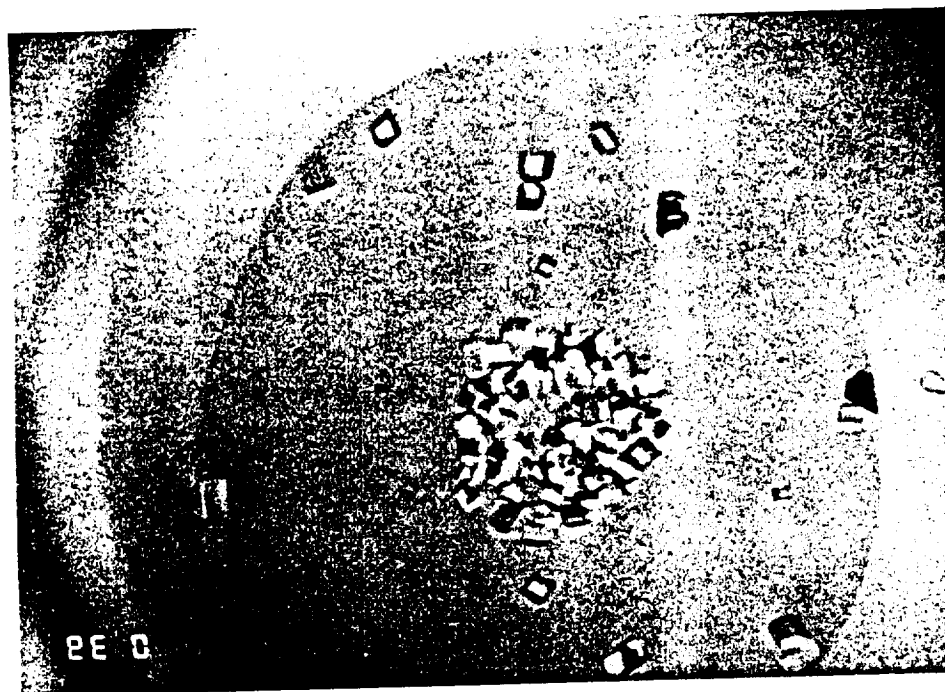


Figure 67. Purified lysozyme (25.9 mg/mL), pH 4.00, 0.1M acetate buffer, 5% NaCl (a) (above) Crystals obtained with hanging drop vapor equilibration with a reservoir. Crystals seen after 2 days (b) (lower) Crystals obtained with gas evaporation of 10 μ L in 100 hours. Crystals seen after 3 days.

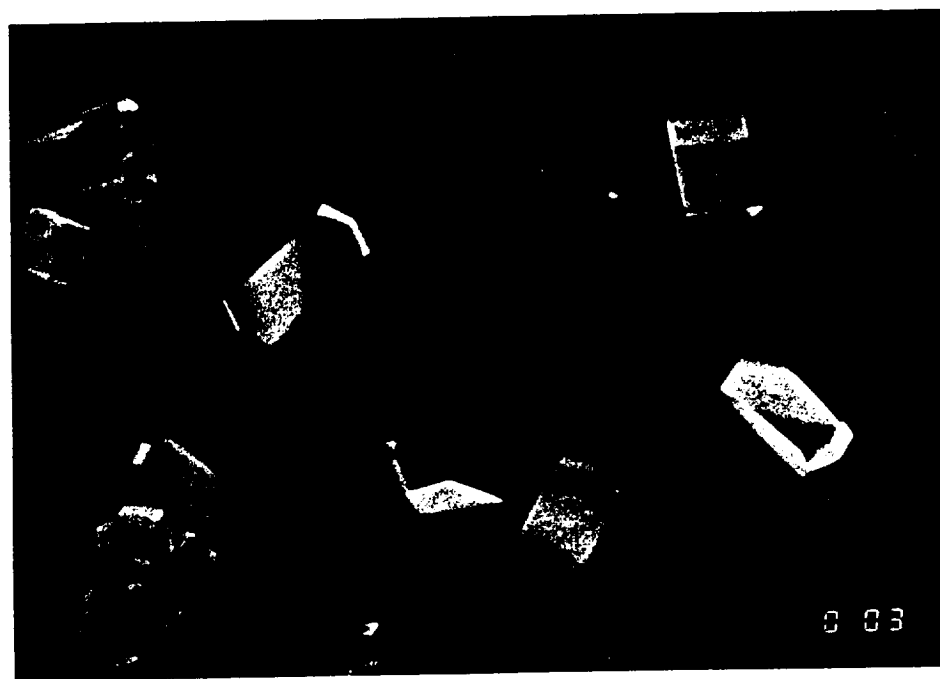


Figure 67. Purified lysozyme (25.9 mg/mL), pH 4.00, 0.1M acetate buffer, 5% NaCl (c) (above) Crystals obtained with gas equilibration curve of 400 hours. Crystals seen after 4 days (d) (lower) Crystals obtained with gas evaporation of 10 μ L in 800 hours. Crystals seen after 9 days.

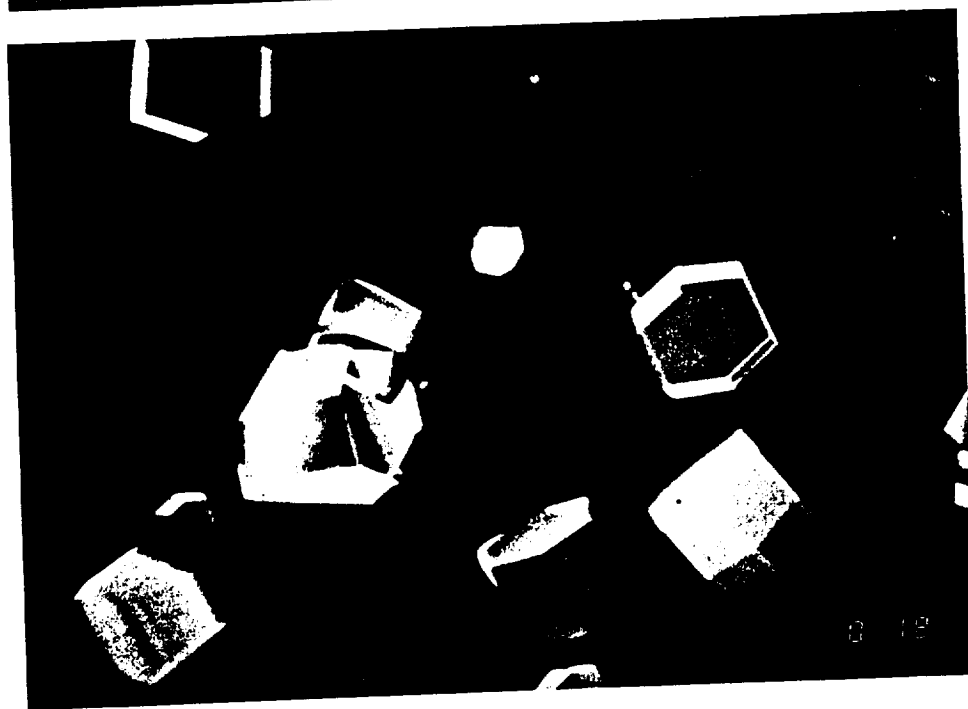
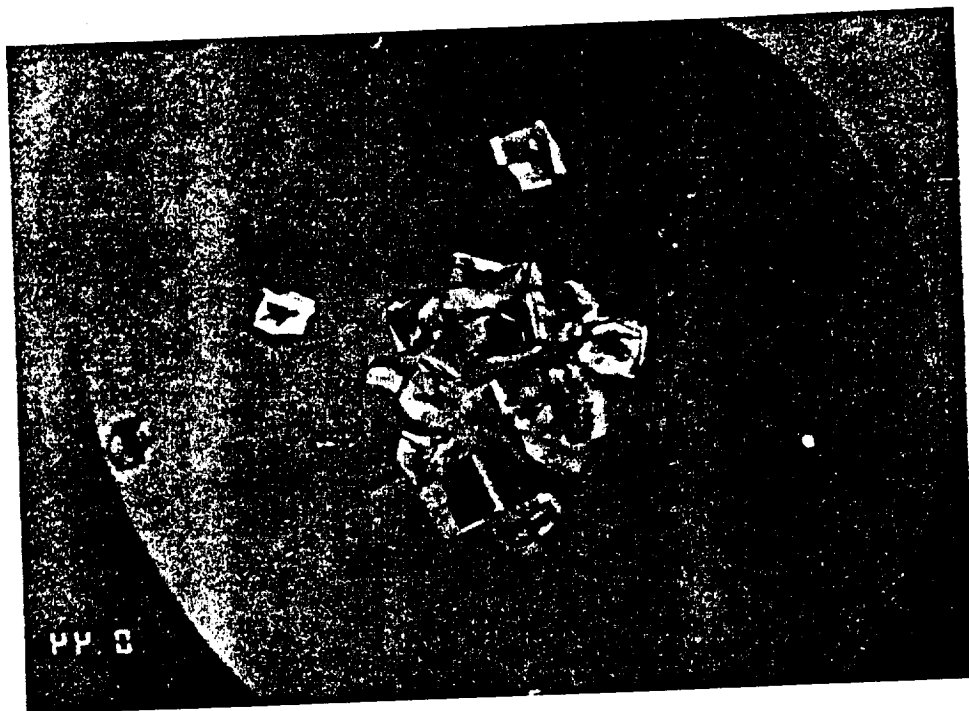


Figure 68. Unpurified lysozyme (23.2 mg/mL), pH 4.00, 0.1M acetate buffer 5% NaCl. (a) (above) Crystals obtained with hanging drop vapor equilibration with a reservoir. Crystals seen after 2 days (b) (lower) Crystals obtained with gas evaporation of 10 μ L in 100 hours. Crystals seen after 3 days.

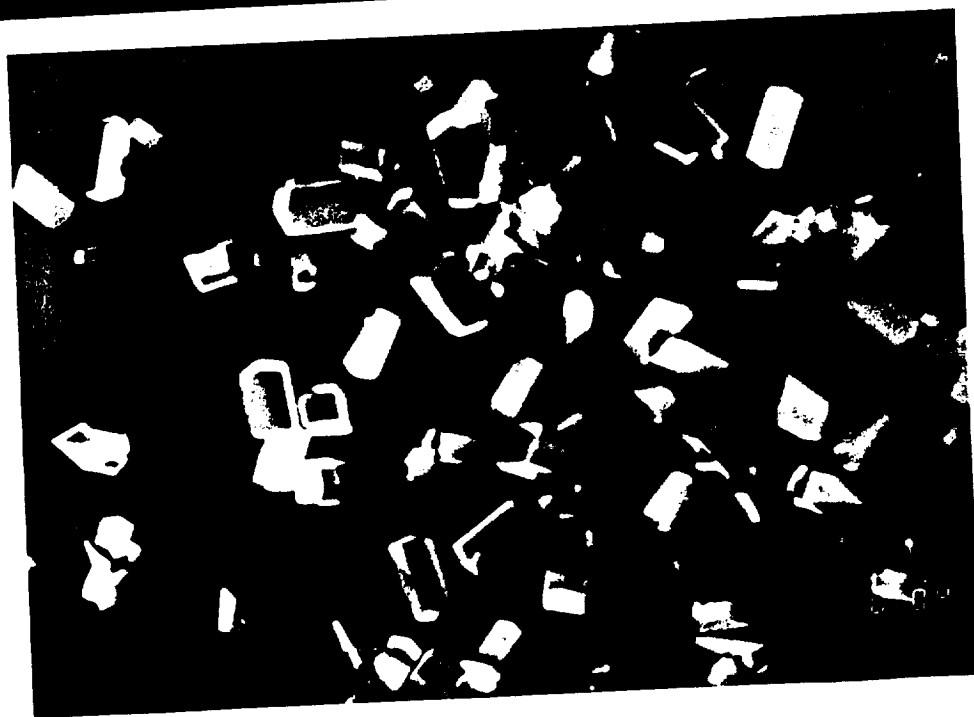
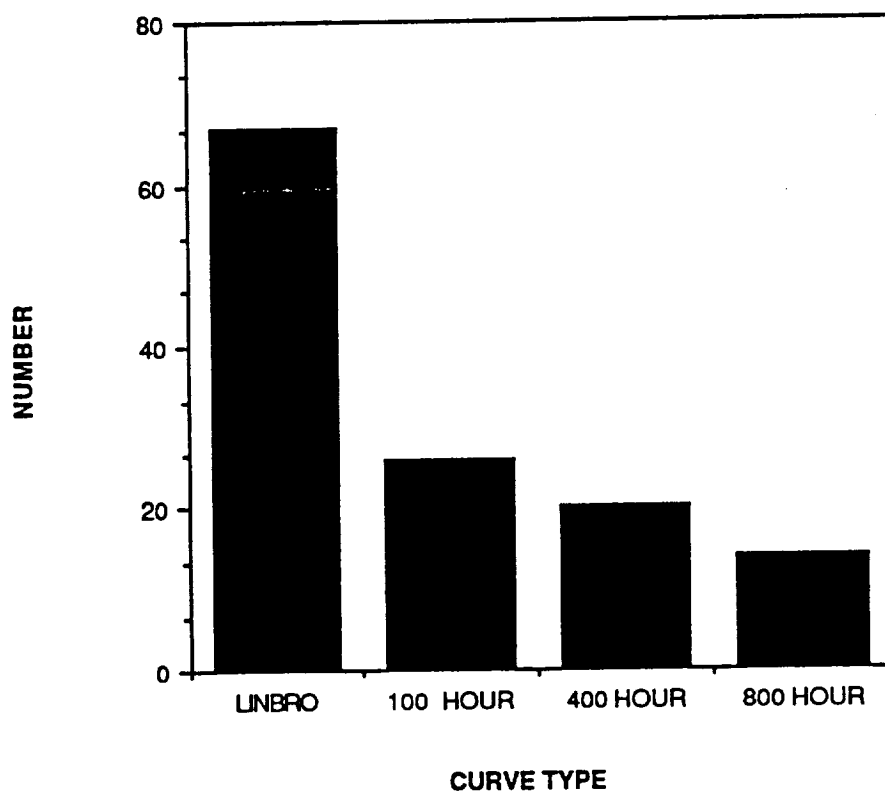
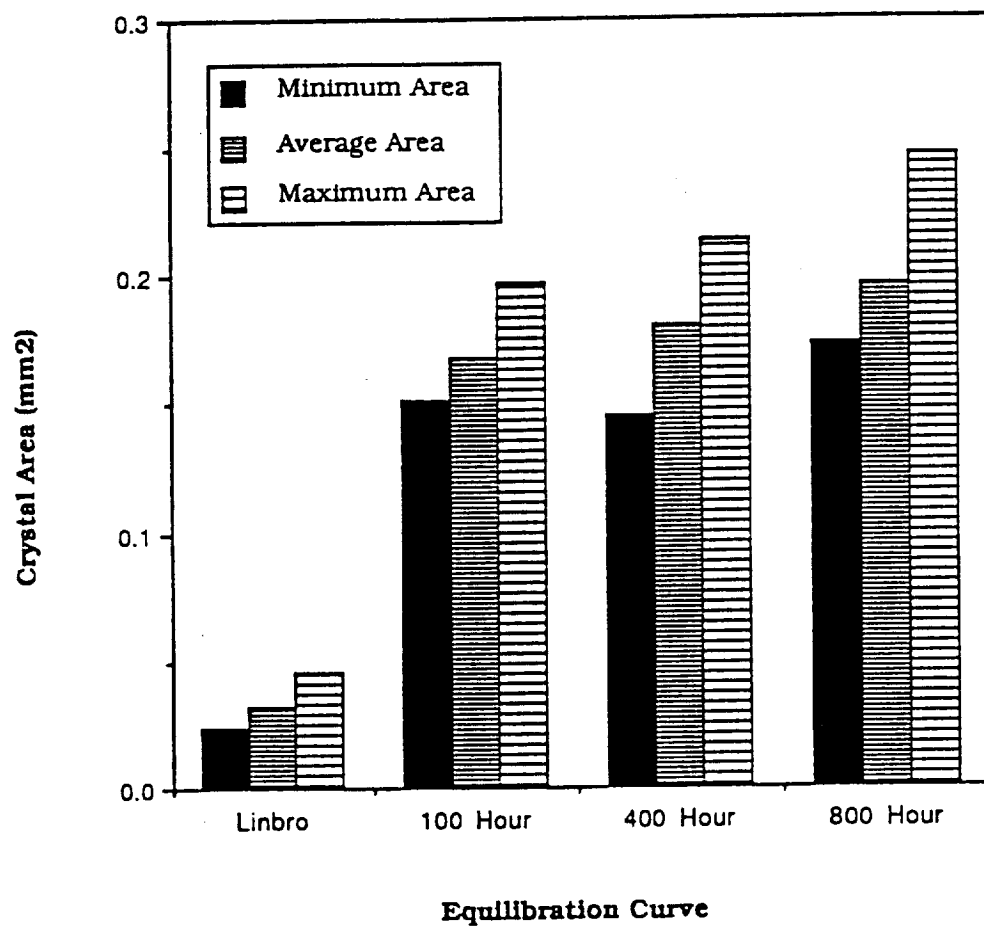


Figure 68. Unpurified lysozyme (23.2 mg/mL), pH 4.00, 0.1M acetate buffer 5% NaCl. (c) (above) Crystals obtained with gas equilibration curve of 400 hours. Crystals seen after 5 days (d) (lower) Crystals obtained with gas evaporation of 10 μ L in 800 hours. Crystals seen after 7 days.



ORIGINAL PAGE IS
OF POOR QUALITY



lysozyme showed many more crystals with the longer curve than with shorter curves. In the case of the impure lysozyme all curves were run with aliquots from the same solutions so that this difference should not be from different starting conditions. However, it is not known what effect the removal of acetate buffer with the purges of gas has on the crystals. Also, it is interesting that the larger number of crystals at the longer curves is not observed with any of the conditions which use purified lysozyme.

Citrate Buffer. In the case of the purified lysozyme in citrate buffer the most striking difference was seen at the conditions where the salt concentration was 0.5% (Figure 71). Traditional reservoir crystallization yielded a mass of precipitate that was not crystalline. When the curve was slowed to 100 hours there was still precipitant but it appeared to be crystalline. With the longer curves needle crystals were obtained and reached a significant size with the 800 hour equilibration. The appearance of the crystals with the 1% NaCl in citrate buffer (Figure 72) also improved with the longer equilibration time. The crystals changed from crystal masses in the 100 hour to separate crystals with well defined edges in the 800 hour equilibration. This difference is encouraging and seems to indicate that in this case slower equilibration is better.

Crystal Growth Time. Table 13 compares the number of days before crystals were observed at each condition for the four curves

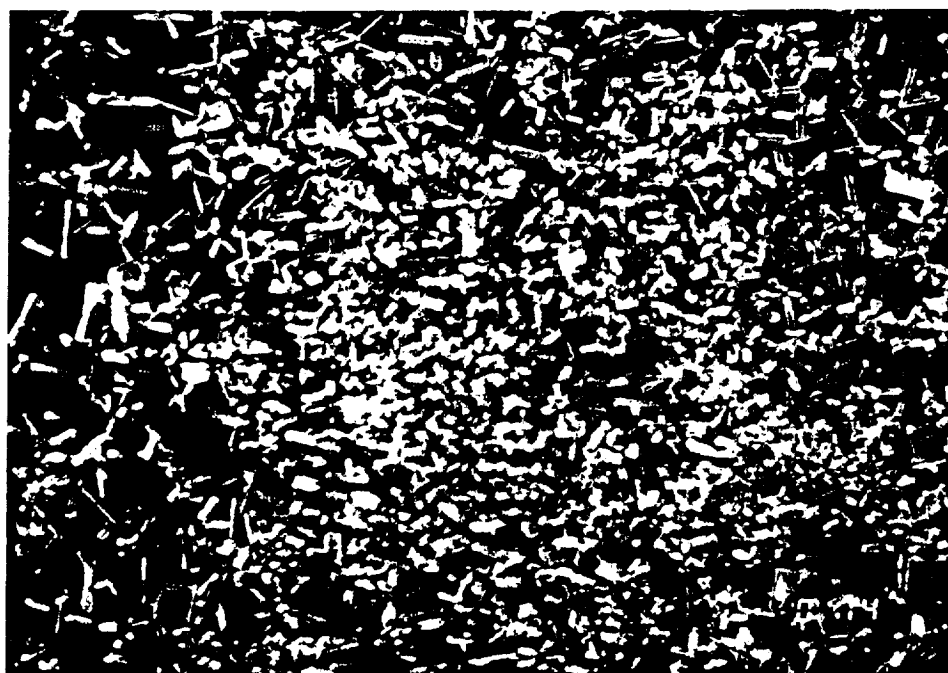
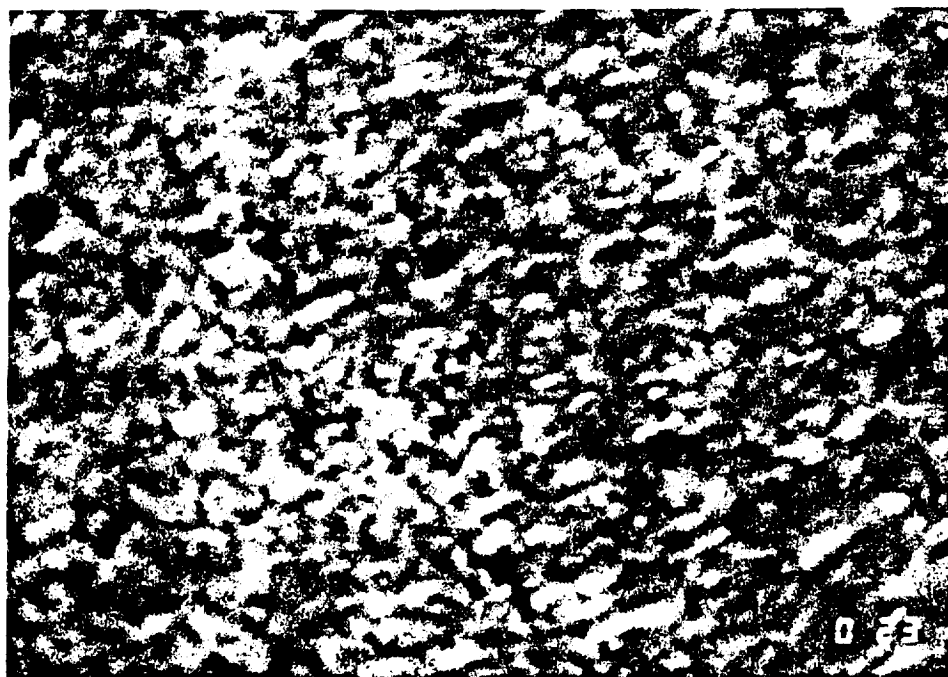


Figure 71. Purified lysozyme (23.2 mg/mL), pH 4.00, 0.1M citrate buffer, 0.5 % NaCl. (a) (above) Crystals obtained with hanging drop vapor equilibration with a reservoir. Crystals seen after 4 days (b) (lower) Crystals obtained with gas evaporation of 10 μ L in 100 hours. Crystals seen after 3 days.



Figure 71. Purified lysozyme (23.2 mg/mL), pH 4.00, 0.1M citrate buffer, 0.5 % NaCl. (c) (above) Crystals obtained with gas equilibration curve of 400 hours. Crystals seen after 5 days (d) (lower) Crystals obtained with gas evaporation of 10 μ L in 800 hours. Crystals seen after 10 days.

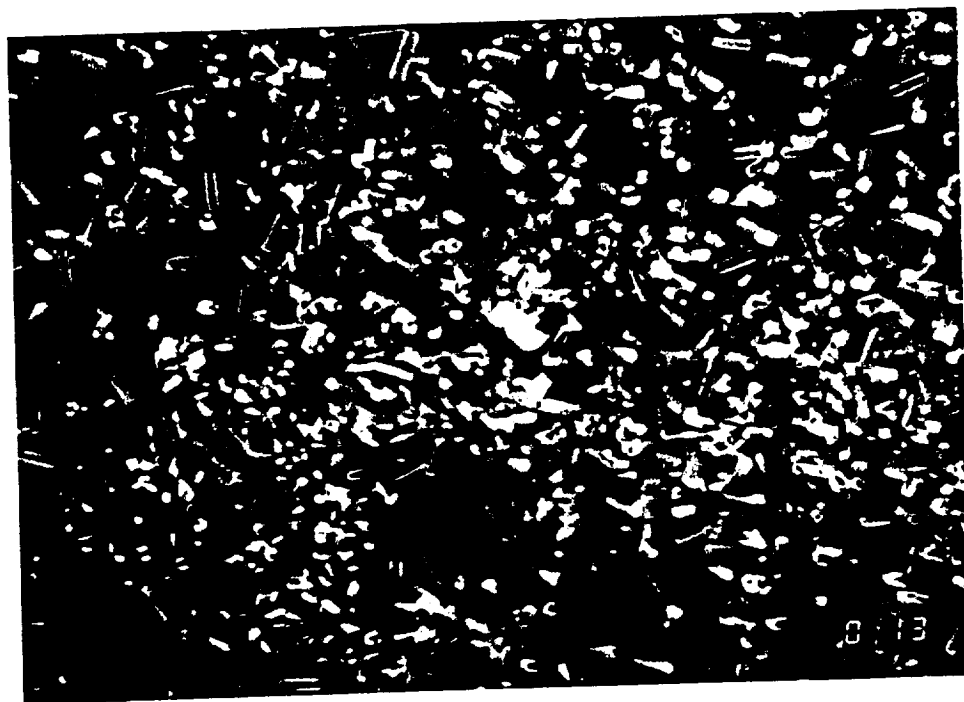


Figure 72. Purified lysozyme (23.2 mg/mL), pH 4.00, 0.1M citrate buffer, 1% NaCl. (a) (above) Crystals obtained with hanging drop vapor equilibration with a reservoir. Crystals seen after 4 days (b) (lower) Crystals obtained with gas evaporation of 10 μ L in 100 hours. Crystals seen after 3 days.

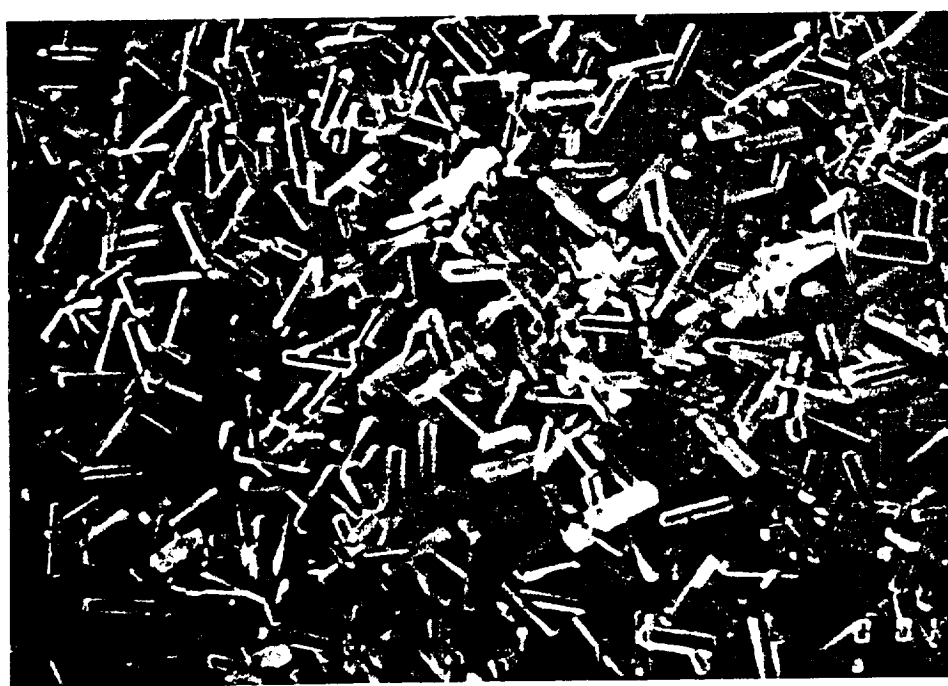
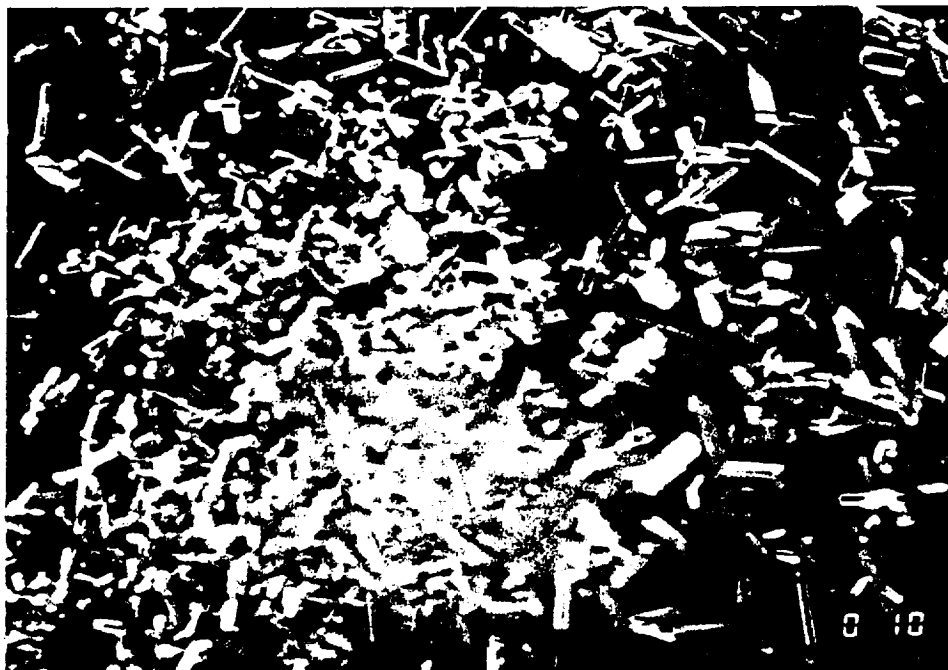


Figure 72. Purified lysozyme (23.2 mg/mL), pH 4.00, 0.1M citrate buffer, 1% NaCl. (c) (above) Crystals obtained with gas equilibration curve of 400 hours. Crystals seen after 5 days (d) (lower) Crystals obtained with gas evaporation of 10 μ L in 800 hours. Crystals seen after 11 days.

Table 13. Number of days before crystals were observed in drops.

CONDITION	LINBRO	100 HOUR	400 HOUR	800 HOUR
(1)	4	3	5	11
(2)	4	3	5	10
(3)	2	3	4	9
(4)	2	3	5	7

(1) Purified lysozyme (23.2 mg/mL), pH 4.00, 0.1M citrate buffer, 1% NaCl. (2) Purified lysozyme (23.2 mg/mL), pH 4.00, 0.1M citrate buffer, 0.5 % NaCl. (3) Purified lysozyme (25.9 mg/mL), pH 4.00, 0.1M acetate buffer, 5% NaCl (4) Unpurified lysozyme (23.2 mg/mL), pH 4.00, 0.1M acetate buffer 5% NaCl.

Table 14. Volume evaporated in microliters before crystals were observed.

CONDITION	LINBRO	100 HOUR	400 HOUR	800 HOUR
(1)	?	6.4	3.0	3.3
(2)	?	6.4	3.0	3.0
(3)	?	6.4	3.0	2.7
(4)	?	6.4	3.0	2.0

(1) Purified lysozyme (23.2 mg/mL), pH 4.00, 0.1M citrate buffer, 1% NaCl. (2) Purified lysozyme (23.2 mg/mL), pH 4.00, 0.1M citrate buffer, 0.5 % NaCl. (3) Purified lysozyme (25.9 mg/mL), pH 4.00, 0.1M acetate buffer, 5% NaCl (4) Unpurified lysozyme (23.2 mg/mL), pH 4.00, 0.1M acetate buffer 5% NaCl.

studied. The drops were studied once a day to see if crystals were present. The longer the equilibration curve the longer it took to achieve crystals. Only with the 800 hour curve was there a difference in the number of days required to achieve crystal growth with the four different conditions. Table 14 shows the volume evaporated before crystals were observed. Crystals were not obtained at the same volume, or supersaturation level, for a single set of conditions and the four curves. Nor did they grow within the same length of time. This suggests that crystal growth is not induced at a particular level of supersaturation or at a particular length of time. The shorter curves required that more solvent be evaporated to force crystal growth within a short time period. The longer curves needed less solvent evaporated but the first crystals weren't seen for many days. The fact that there is an improvement in the appearance of the crystals with the longer curves indicates that if nucleation is delayed by evaporating less solvent the chances that a protein molecule can add to the lattice in the best orientation is increased resulting in a more ordered crystal which can continue growth to a larger terminal size.

No Evaporation. In the case of hen egg white lysozyme evaporation is necessary to achieve crystal growth. This was determined by placing a drop containing lysozyme and NaCl on a coverslip and sealing it over an empty Linbro well. The conditions used were those that had yielded crystals with reservoir evaporation. After 3 days the drop contained amorphous precipitate. The main advantage of evaporation

is that it helps to bring the solution to supersaturation, forcing the protein out of solution hopefully as a crystalline solid.

Conclusions and Recommendations

The device described in Chapter 2 is able to control the relative humidity in the crystallization chamber and thus the transport of water to or from the drop. Using this, several evaporation curves were used to investigate the role of evaporation in protein crystal growth. Difference in the crystals were apparent with the different evaporation curves. At three of the four conditions for lysozyme crystal growth longer evaporation curves yielded better crystals. The only set of conditions which yielded worse crystals was that using the unpurified lysozyme. The time required to see a change in the appearance of the crystals was much longer than expected. The number of curves studied so far represent only a small fraction of the ones now available with the gas equilibration device. Additional curves need to be studied to determine the best evaporation profile for lysozyme. Once determined it is hoped that the information gained can be applied to many proteins to increase the chances that a protein can be crystallized and its three dimensional structure determined.

One of the main advantages of this technique is the ability to decouple the nucleation conditions from the growth conditions. In most circumstances the crystallization drop contains substances that lower the equilibrium vapor pressure around the drop. Thus, it is

possible to purge the volume around the drop with nitrogen in vapor equilibrium with pure water and cause an increase in the volume of the drop. This possibility opens several avenues for crystallization that are not frequently used in the more conventional methods. Proteins that are less soluble in low salt solutions can be brought to supersaturation by diluting the drop through occasional purges of the chamber with "wet" nitrogen. In many cases it would be desirable to detect the onset of nucleation and respond by slowing or reversing the evaporation rate to maintain or achieve conditions for optimal crystal growth. Coupling of this device with a nucleation detection system, such as laser light scattering, would provide feedback to the computer and allow the evaporation profile to be altered after nucleation.

Finally, recent interest in the growth of crystals under the microgravity conditions of the U.S. Space Shuttle has resulted in the development of this device which provides for control of some of the crystallization parameters. This device is more suitable for automation than the traditional techniques. Automation is desirable for the Space Shuttle experiments and for the U.S. Space Station to minimize crew interaction time, provide a common procedure for a wide variety of crystallization experiments, miniaturize the apparatus and compensate for short duration flight opportunities. The principles described in this thesis can easily be incorporated into flight hardware.

SELECTED REFERENCES

- [1] Skoog, Douglas A. (1985) *Principles of Instrumental Analysis*, (Sanders College Publishing, New York).
- [2] Mikol, Vincent, Jean-Luc Rodeau and Richard Giege (1990) *Analytical Biochemistry*, **186**, 332-339.
- [3] Fowlis, W.W., L.J. DeLucas, P.J. Twigg, S.B. Howard, E.J. Meehan, J.K. Baird (1988) *J. Crystal Growth*, **90**, 117.
- [4] Fowlis, W.W., L.J. DeLucas, P.J. Twigg, S.B. Howard, E.J. Meehan, J.K. Baird (1988) *J. Crystal Growth*, **90**, 117.

APPENDIX 1

ALTERNATIVE TECHNIQUES FOR MONITORING EVAPORATIVE WATER LOSS

<u>APPENDIX</u>	<u>TITLE</u>	<u>PAGE</u>
Appendix 1A	Conductance Monitoring with a Micro Conductance Cell.	175
Appendix 1B	Periodic Refractive Index Measurement.	177
Appendix 1C	Gravimetric Analysis of Drop Volumes.	179
Appendix 1D	Chloride Ion-selective Electrode	181

APPENDIX 1A

Conductance Monitoring with a Micro Conductance Cell.

A miniature conductance cell was designed and blown out of pyrex glass tubing (Figure 73). Two 20 gauge platinum electrodes were embedded into the glass. The electrodes were first platinized with 3% chloroplatinic acid. The total volume required for a conductance

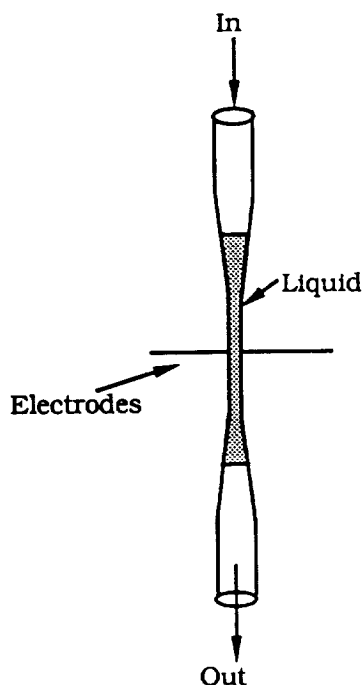


Figure 73. Micro-conductance cell.

reading was 5 μ L. The cell could be rinsed with deionized water, followed by an acetone rinse and blown dry with a dust free air blower in about 1 minute and 30 seconds. The cell was calibrated with NaCl

solutions of known concentration. It gave a linear response in the range of concentrations from .25M to 1.5M (Figure 74). The cell had a precision of < 1% in the middle concentration ranges. It was useful for calculating salt concentrations. The cell was susceptible to drafts in the room since it was not temperature controlled. Also, its main disadvantage was that it required removal of 5 μ L from a crystallization solution, thereby, interfering with the growth process.

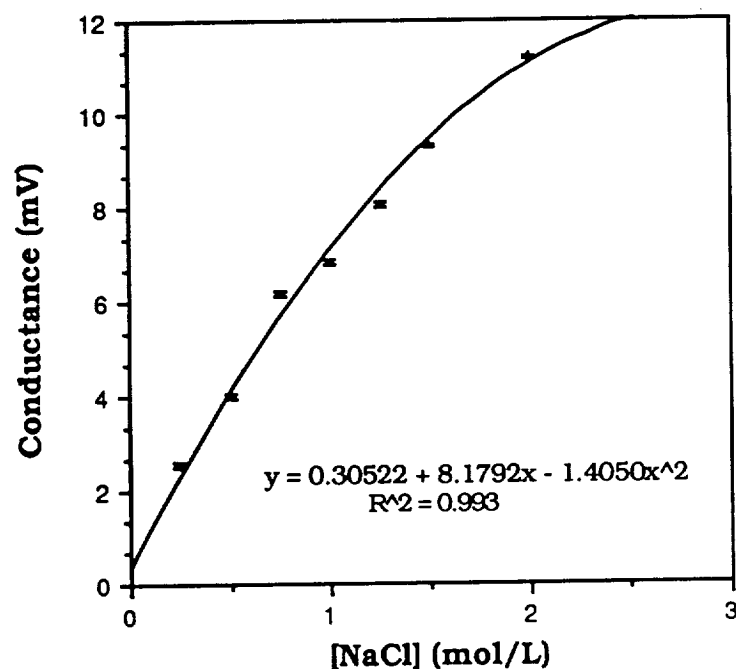


Figure 74. Calibration response curve of the micro-conductance cell. NaCl solutions made up in 0.10M Na acetate buffer, pH 4.00.

APPENDIX 1B

Periodic Refractive Index Measurement

The refractive index of a solution varies proportionally to the salt concentration. Measurement of the refractive index of a drop requires no dilution since only a small volume (1-5 μL) is required. An Erma

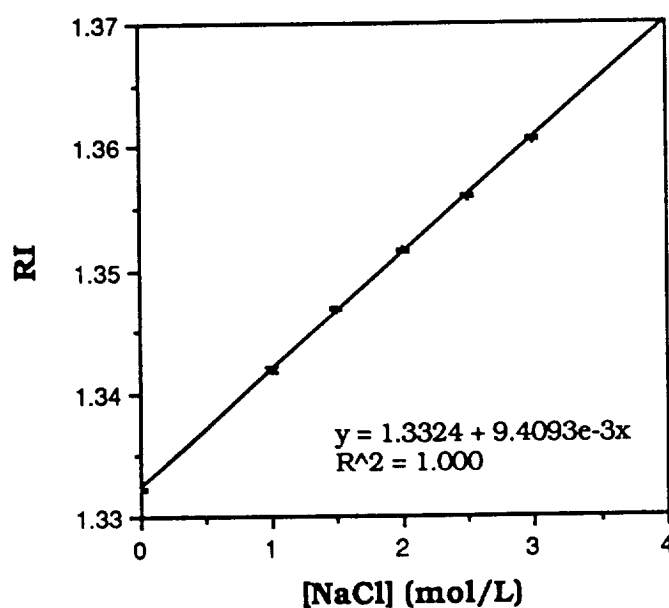


Figure 75. Calibration response of refractive index vs. NaCl concentration at 20° C.

New Abbe refractometer (Erma Optical Works, LTD) was used for the measurements according to the manufacturer's recommendations at 20.0 °C. A calibration response curve was prepared for two commonly used salts in crystallization, NaCl and $(\text{NH}_4)_2\text{SO}_4$. These curves are shown in Figure 75 and Figure 76 respectively. The main disadvantages of refractive index measurements is that it destroys the sample and that its error is high.

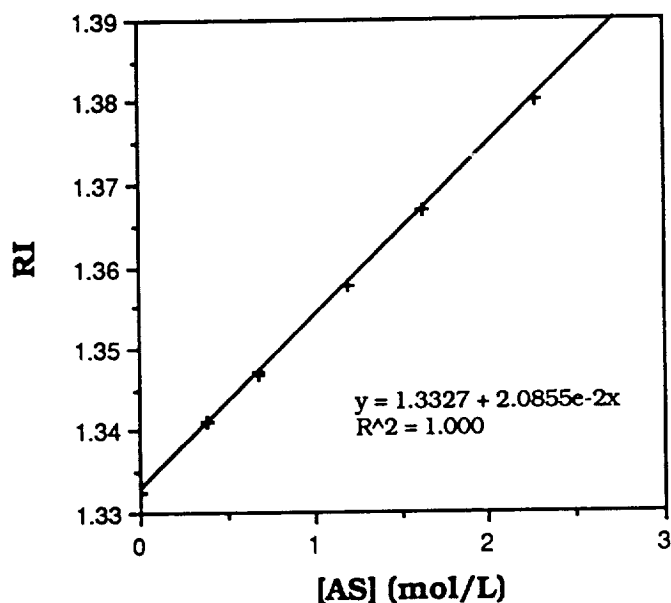


Figure 76. Calibration response of refractive index vs. $(\text{NH}_4)_2\text{SO}_4$ concentration at 20° C.

APPENDIX 1C

Gravimetric Analysis of Drop Volumes

To determine the volume of a drop of deionized water, the drop was absorbed by a slice of very absorbant glass microfibre filters (Whatman, 2.0 cm) and placed into a plastic 250 μL centrifuge tube. The entire assembly was preweighed and its mass was usually around 0.3 g. The volume of the drop was determined by difference. To determine the limit of detection of this method, five blanks were measured by preparing the assemblies and weighing twice without absorbing up a drop. The results are shown in Table 15. If a 90%

Table 15. Determination of the Limit of Detection of the Gravimetric Method.

Vial Number	Initial Mass (g)	Final Mass (g)	Δg	Volume (μL) $\rho_{25^\circ\text{C}}=0.99705$
1	0.36324	0.36321	3E-5	0.3
2	0.36229	0.36222	7E-5	0.7
3	0.36136	0.36124	12E-5	1.2
4	0.36356	0.36351	5E-5	0.5
5	0.36252	0.36250	2E-5	0.2
MEAN (μL)			0.6 \pm 0.4	

confidence level is desired then 2σ , where σ was found to be $0.6 \mu\text{L}$, gives a detection limit of $1.2 \mu\text{L}$. Or in other words, this technique can only detect a volume difference of $1.2 \mu\text{L}$.

Next, this technique was used to measure a $10 \mu\text{L}$ drop six times. The data is shown in Table 16. The mean drop volume was found to be $10.0 \pm 0.3 \mu\text{L}$. Therefore, this technique would be useful in measuring the drop volumes of water droplets. It could be used to quantify evaporation curves, however it does destroy the drop. It would not be useful for closed loop control experiments.

Table 16. Repetitive Gravimetric Measurement of a $10 \mu\text{L}$ Drop.

Vial Number	Initial Mass (g)	Final Mass (g)	Δg	Volume (μL) $\rho_{25^\circ\text{C}}=0.99705$
1	0.36321	0.37279	9.58E-3	9.6
2	0.36222	0.37205	9.83E-3	9.9
3	0.36124	0.37122	9.98E-3	10.0
4	0.36351	0.37375	10.24E-3	10.3
5	0.36250	0.37272	10.22E-3	10.2
6	0.36330	0.36250	10.34E-3	10.4
MEAN(μL)			10.0 ± 0.3	

APPENDIX 1D

Chloride Ion Selective Electrode

A chloride ion-selective electrode (Orion Research, Model 96178, Combination) was used to follow changes in the concentration of the chloride ion. Since the conditions for crystallization of hen egg-white lysozyme require NaCl as a precipitating agent it was thought that the

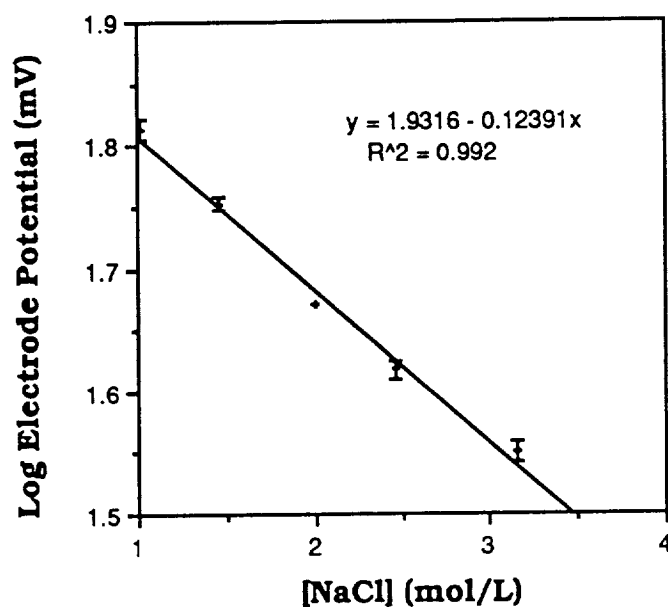


Figure 77. Calibration curve of chloride ion selective electrode.

volume change of the drop would be proportional to the change in Cl^- concentration. The electrode was calibrated with drops of known NaCl concentration. 10 μL of the standard solution was diluted to 5 mL of water to reach the required volume for measurement. 100 μL of ISA was added to adjust the ionic strength. The total volume being measured was 5.11 mL. The log of the mV response of the Orion Ionanalyzer was found to be linear to the concentration as is shown in Figure 77.

The major drawback to this measurement technique is the fact that it only works with solutions that have the Cl^- ion in them. It also requires several dilutions before measurement, which introduces error. It does destroy the sample so that it is only useful for quantifying the evaporation curves and not for measurement while growing crystals.

APPENDIX 2

Computer Programs

<u>APPENDIX</u>	<u>TITLE</u>	<u>PAGE</u>
Appendix 2A	Computer Automated Crystallization Appratus.	184
Appendix 2B	Humidity Reader	188
Appendix 2C	Conductance Reader	191

INPUT PARAMETERS

Final Vol VALUE CLOSE TIME (SEC)

 DESIRED RUN VALUE OPEN TIME (SEC)
 TIME (HRS)

EQUATION

$N = 0.00227 \cdot e^{\dots}$

EVAPORATION CURVE

FILE STORAGE

PROD DISK: C:\CA DATA

FILE NAME

PROD DISK

VALUE WRITE

CURRENT ERROR Panel

CA CA

OUTPUT PARAMETERS

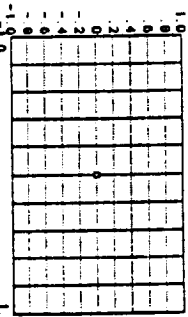
computer
simulation
crystallization
operation

TIMING:

IN PULSE MODE

PULSE TIME (ticks)

TIME (SEC) TIME (MIN)

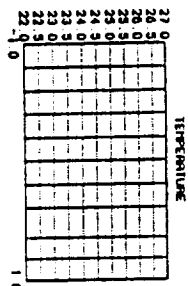


RUN TCD VOL

 EQUATION
 OUTPUT

TEMPERATURE LOOP

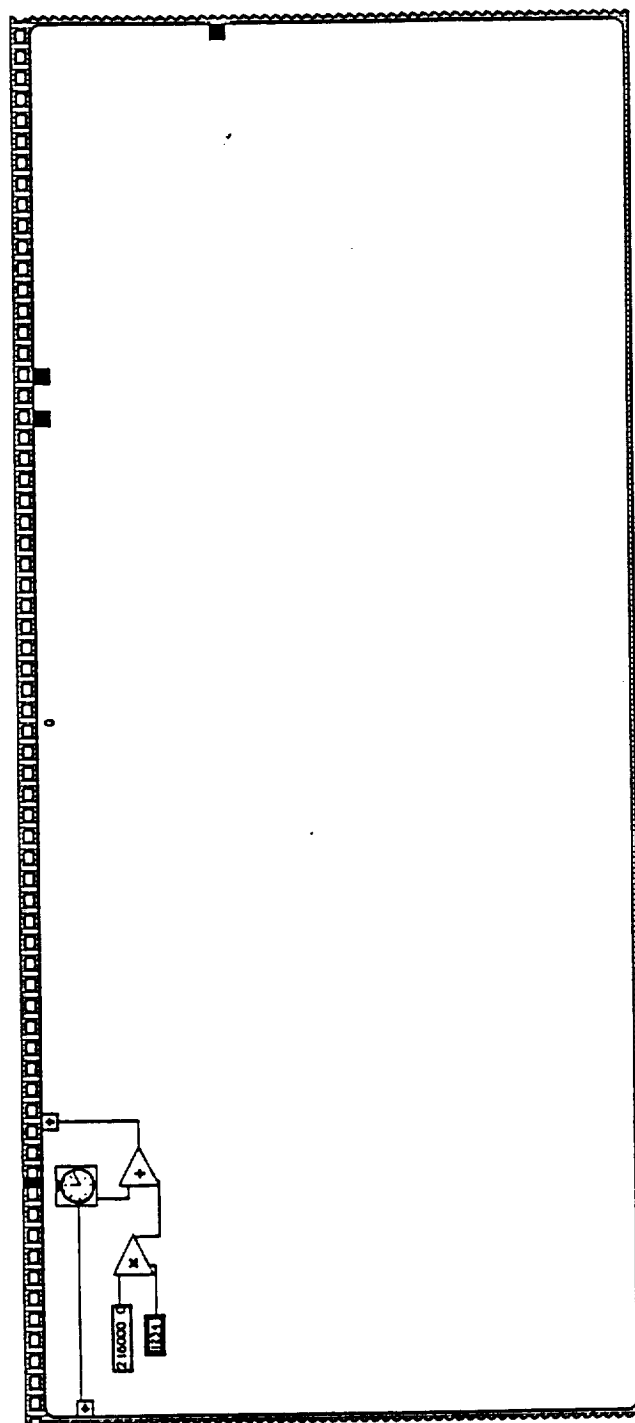
TEMPERATURE OUTPUT (V)



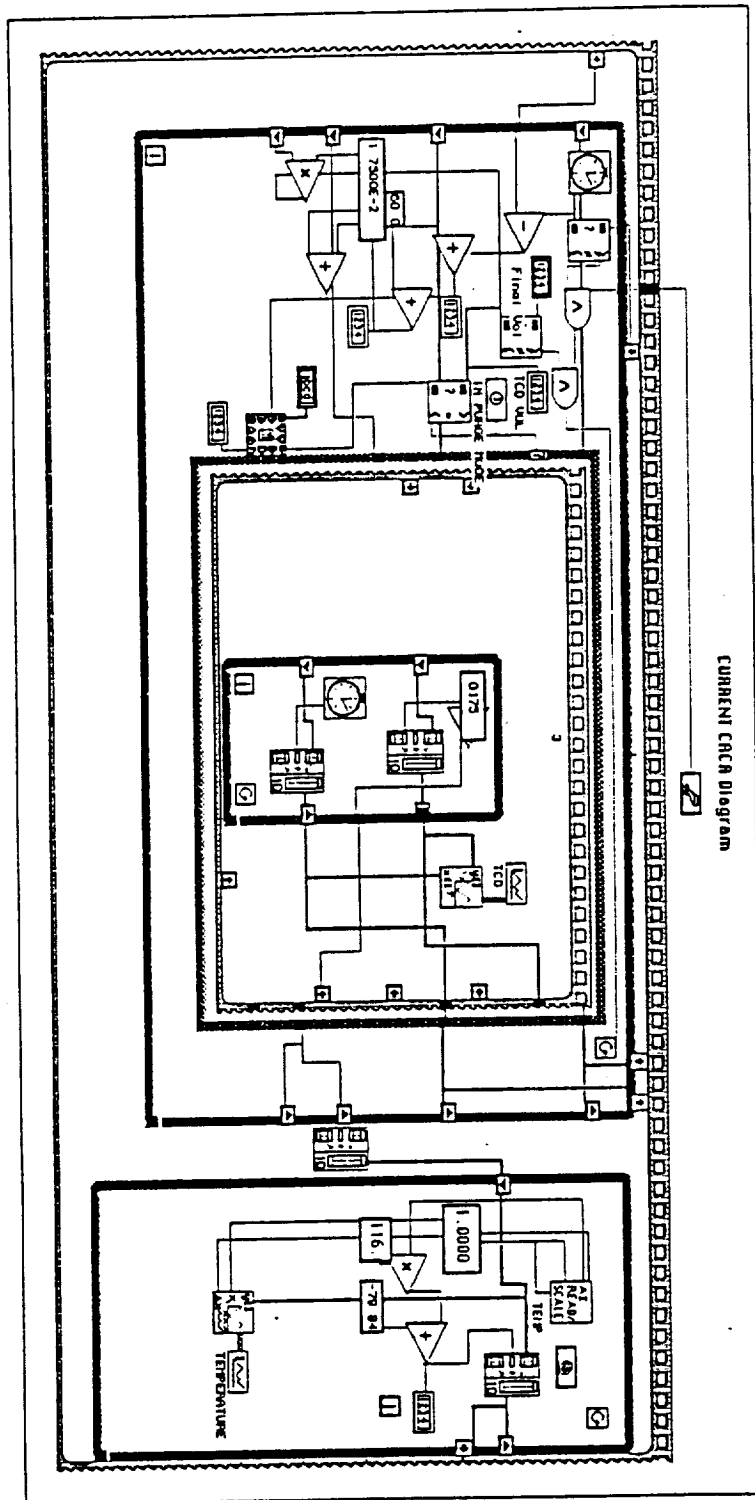
TEMPERATURE LOOP
 TEMPERATURE OUTPUT (V)

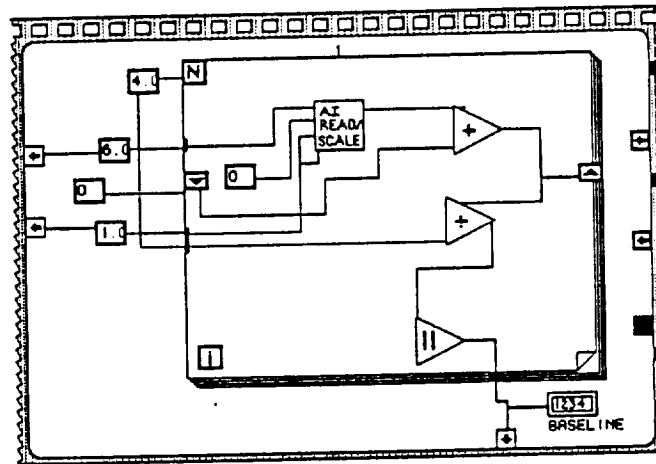
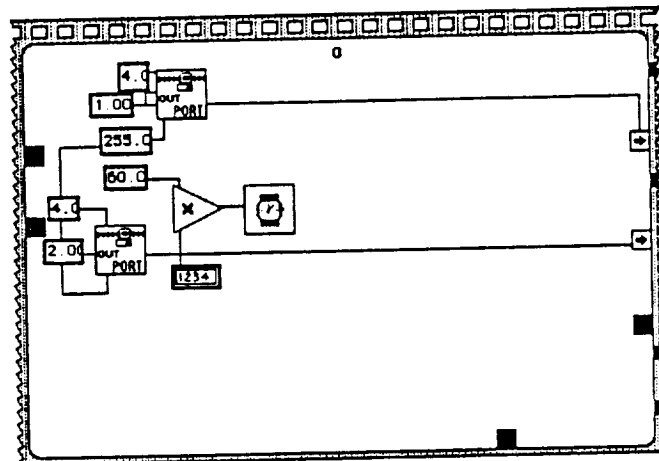
ERROR (S)

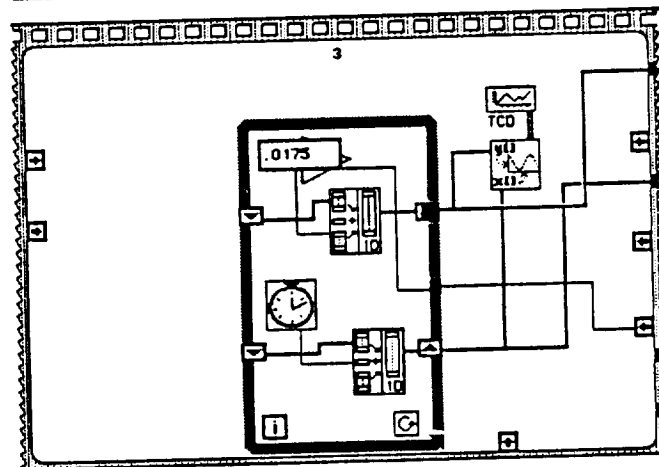
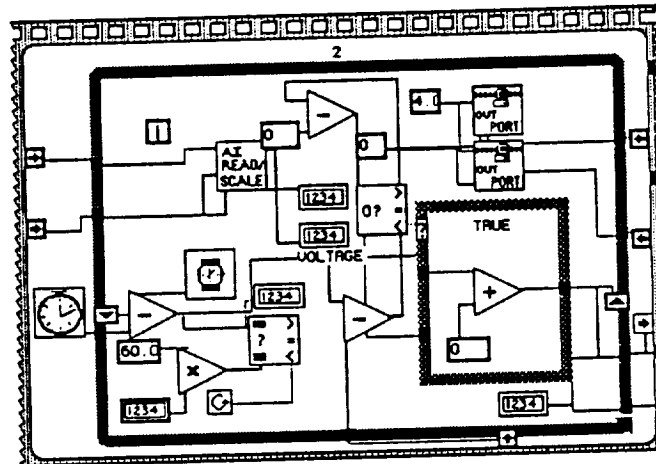
 READ
 ERROR
 FILE WRITE ERROR

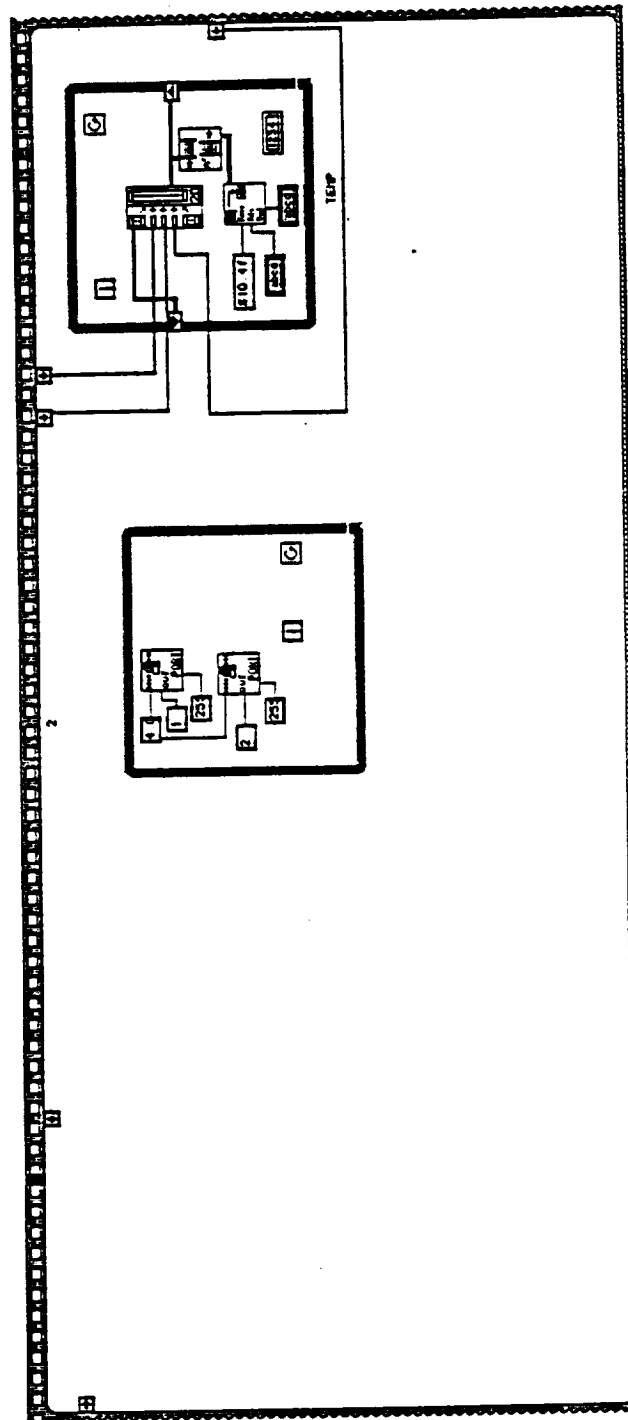


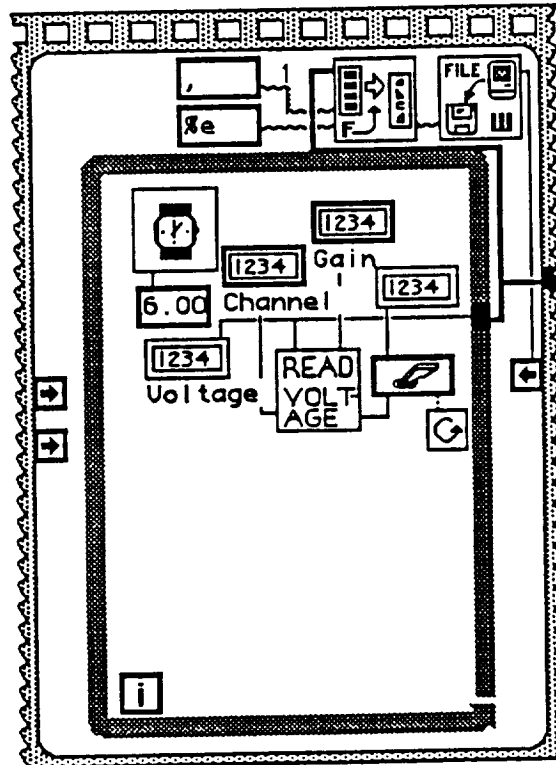
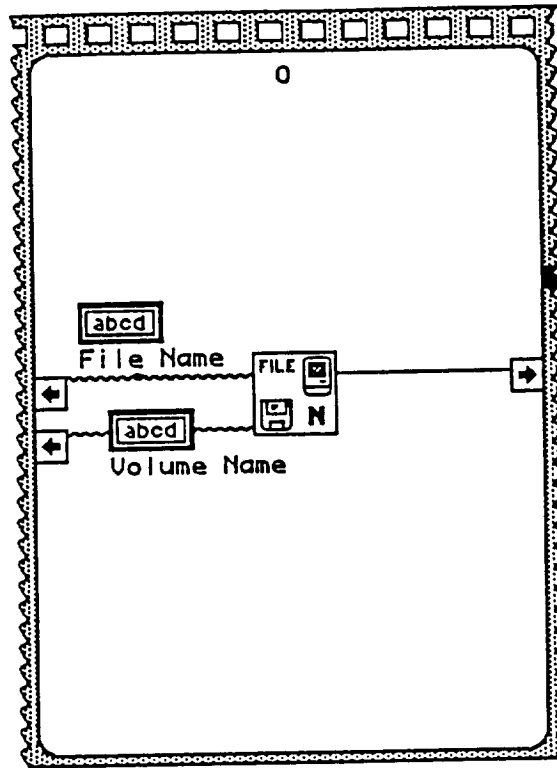
CURRENT CIRC Diagram

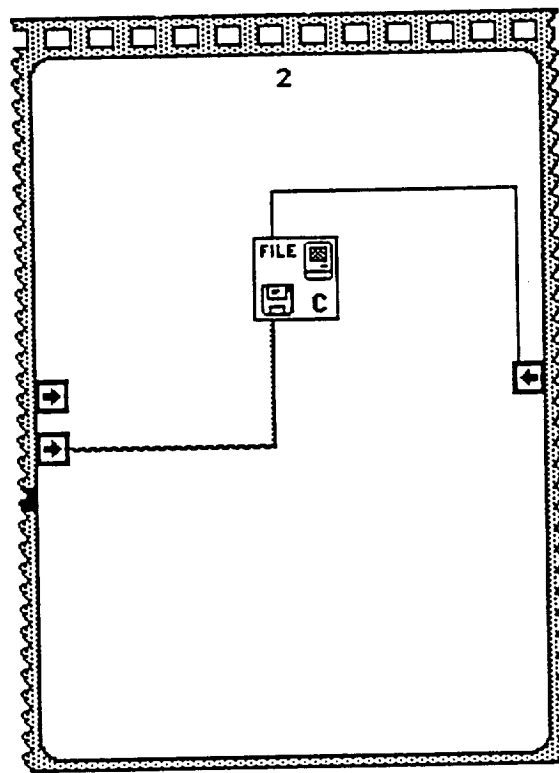










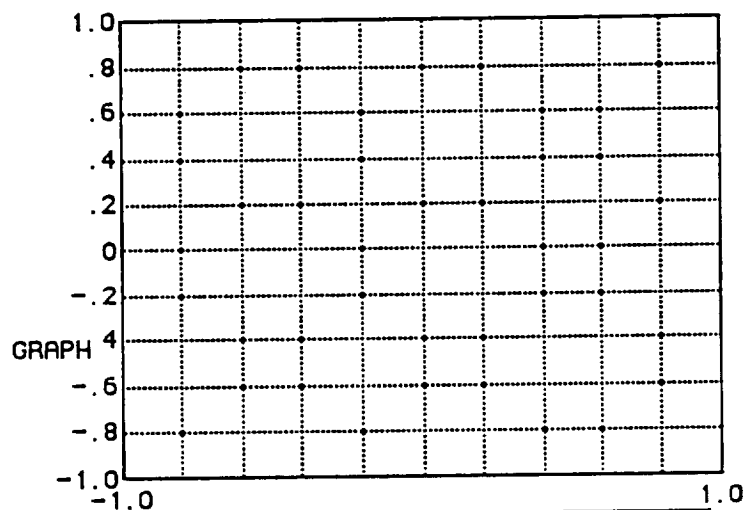


COND READER Panel

Gain



Voltage



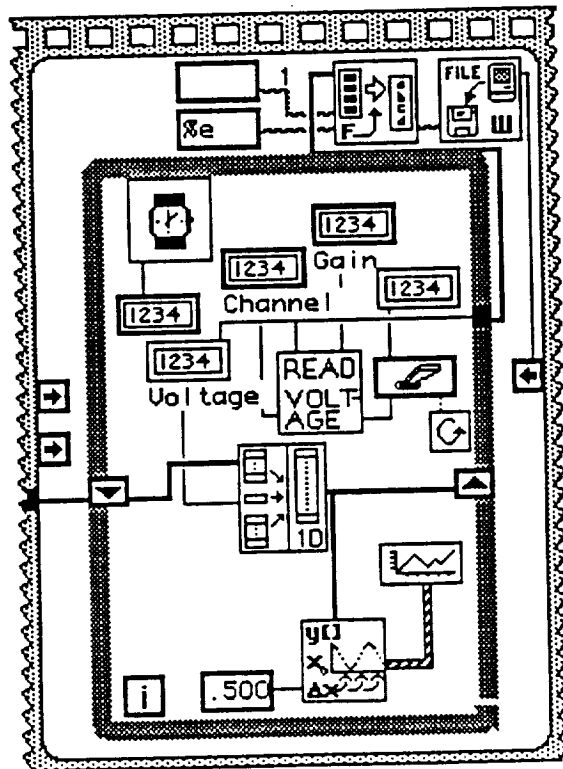
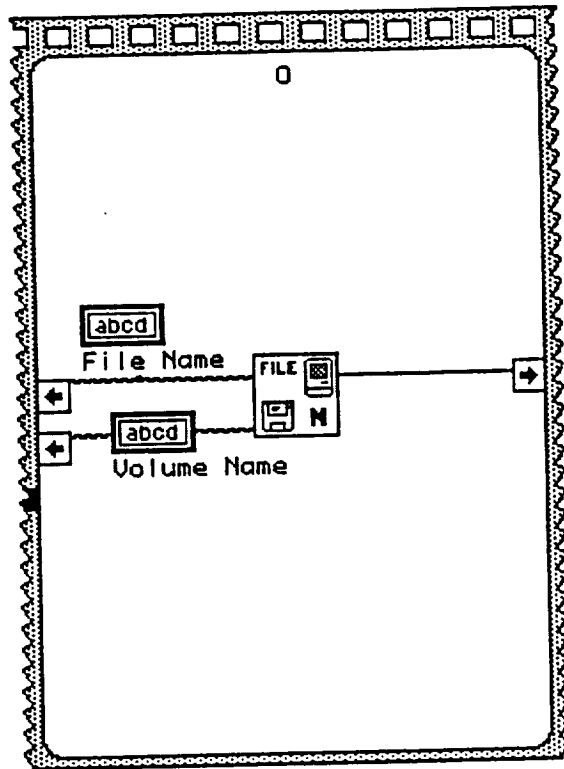
File Name

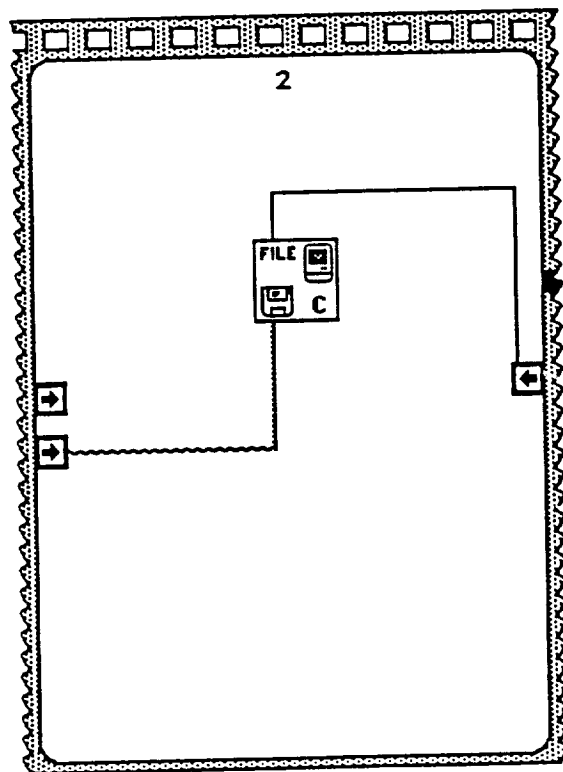
Volume Name

Channel

Sample Rate

Read Voltage Error





APPENDIX 3

Silanization of Microscope Coverslips

- 1). Sonicate coverslips in aqueous soap solution for 1 hour and rinse
with deionized water.
- 2). Dry in oven at 60°C overnight.
- 3). Dip each coverslip into a solution of 75 mL toluene and 3 mL of
1,1,1,3,3,3 hexamethyldisilane.
- 4). Cover with a dust free cloth and set out to air dry.
- 5). Rinse with deionized water.
- 6). Oven dry at 60°C overnight.

Lori J. Wilson

PERSONAL INFORMATION

Born: Gunnison, Colorado Health: Good
Date of Birth: March 12, 1964 Marital Status: Married

EDUCATIONAL BACKGROUND

1990 Ph. D. in Chemistry, Georgia Institute of Technology, Atlanta, Georgia. Major course work in Analytical Chemistry. Minor in Physical/Biochemistry. Overall G.P.A. 3.8/4.0.

1986 B. S. in Chemistry, Mercer University, Macon, Georgia. Minors in Physics and Christianity. Overall G.P.A. 3.68/4.00.

ADDITIONAL TRAINING

1986 Summer Analytical Research Participant (SARP), Packaged Soap and Detergent Division, Procter and Gamble, Cincinnati, Ohio.

1985 Summer Coca-Cola Undergraduate Research Participant (URP), Georgia Institute of Technology, Atlanta, Georgia.

1981 Summer participant in a National Science Foundation workshop entitled The Chemistry and Physiology of Over-the-counter Drugs, Georgia Southern College, Statesboro, Georgia.

WORK EXPERIENCE

1986-1990 Research Assistant, Department of Chemistry and Biochemistry, Georgia Institute of Technology; research in the area of nucleation processes of proteins; teach undergraduate chemistry laboratory.

1982-1986 Teachers Assistant, Department of Chemistry, Mercer University, Macon, Georgia; chemistry lab instructor; tutor algebra, calculus, physics and chemistry in Campus Learning Center; lab instructor in computer laboratory.

1981-1982 Drug Clerk, Eckerd Drugs, Cherokee Plaza, Atlanta, Georgia.

AWARDS

1990 National Research Council Postdoctoral Fellowship

1989 Brice-Johnston Graduate Researchers Fellowship

1987-1989 Grant Recipient, Graduate Student Researchers Program, NASA Headquarters

1986 Most Outstanding Chemistry Student, The American Institute of Chemist

1985 Outstanding Physical Chemistry Student

1983-1986 Mercer Academic Scholarship

1983-1985 Ty Cobb Educational Scholarship

1981-1986 Robert B. McCarthy Chemistry Scholarship

PROFESSIONAL ASSOCIATIONS

Toastmasters International, Georgia Tech
Blue Key National Honor Society
Gamma Sigma Epsilon, Chemistry Honor Society, President
Mercer University Student Chapter, 1985

